INVESTIGATION OF THE EFFECTS OF ANTI-INFLAMMATORY IN THE TISSUES OF GM2 GANGLIOSIDOSIS MOUSE MODEL

A Thesis Submitted to
The Graduate School of Engineering and Sciences of
İzmir Institute of Technology
in Partial Fulfilment of the Requirements for the Degree of

DOCTOR OF PHILOSOPHY

in Molecular Biology and Genetics

by
Nurselin ATEŞ

November 2023
İZMİR

We approve the thesis of **Nurselin ATEŞ**

Examining Committee Members

Prof Dr. Volkan SEYRANTEPE
Department of Molecular Biology and Genetics, İzmir Institute of Technology

Prof. Dr. Bünyamin AKGÜL
Department of Molecular Biology and Genetics, İzmir Institute of Technology

Assoc. Dr. Şükrü GÜLEÇ
Department of Food Engineering, İzmir Institute of Technology

Prof. Dr. Kemal Sami KORKMAZ
Department of Bioengineering, Ege University

Prof. Dr. Şerife Esra ERDAL BAĞRIYANIK
Department of Medical Biology and Genetics, Dokuz Eylül University

09 November 2023

Prof Dr. Volkan SEYRANTEPE
Supervisor, Department of Molecular Biology and Genetics, İzmir Institute of Technology

Prof. Dr. Özden YALÇIN ÖZUYSAL
Head of Department of Molecular Biology and Genetics

Prof. Dr. Mehtap EANES
Dean of Graduate School of Engineering and Sciences

ACKNOWLEDGMENTS

I would first like to express my deepest gratitude to my supervisor Prof. Dr. Volkan SEYRANTEPE for his guidance, encouragement, patience, understanding, support and extensive knowledge that helped me throughout my studies and my thesis writing.I would like to express my special thanks to the thesis monitoring and examining committee members Prof. Dr. Bünyamin AKGÜL and Assoc. Prof. Dr. Şükrü GÜLEÇ for their attention, recommendations and contributions during this period. I would also like to thank to Prof.Dr. Kemal Sami KORKMAZ and Prof Dr. Şerife Esra ERDAL BAĞRIYANIK the thesis examining committee members, for attention and recommendations.

I am thankful to The Scientific and Technological Research Council of Turkey for their financial support as I was supported by TÜBİTAK BIDEB 2211A National Scholarship Program for Ph.D. students and I am also thankful for Turkish Higher Education Council (YÖK) for their support within 100/2000 Ph.D. Fellowship Program.

I am also grateful to my co-workers Orhan Kerim İNCİ, Melike CAN, Hatice Hande BASIRLI, Melike CAN ÖZGÜR, Selman YANBUL, Tufan Utku ÇALIŞKAN, Ebru ADA, İlker GÜMÜŞ and Beyza KAYA for their support, assistance, sincere help and kindness during the thesis project. I especially thank to Dr. Secil AKYILDIZ DEMIR who mentored me through my graduate studies. I am also grateful to undergraduate members of Seyrantepe Laboratory for their help through the experiments.

At last but not least, I am deeply grateful to my father Kemal ATEŞ, my mother Hanife ATEŞ and my sisters Gülşah ATEŞ and İrem ATEŞ for their infinite love, motivation, belief, encouragement and support throughout my life and my education. Without their support, I will not be able to be here.

ABSTRACT

INVESTIGATION OF THE EFFECTS OF ANTI-INFLAMMATORY IN THE TISSUES OF GM2 GANGLIOSIDOSIS MOUSE MODEL

Tay- Sachs disease is an autosomal recessively inherited lysosomal storage disorder caused by mutations on the HEXA gene encoding α-subunit of β-Hexosaminidase A enzyme. The enzyme catalyzes GM2 to GM3 conversion but when it is deficient the GM2 degradation is interrupted and GM2 ganglioside is progressively accumulated especially in neurons. Progressive accumulation of GM2 causes increasing death of neurons, disruption in mental and motor functions and eventually death at 2-4 years of age. The Hexa-/- Tay-Sachs model was normal thanks to a bypass mechanism mediated by Neurominidase3. It was determined that *Hexa-/-Neu3-/-* mice mimicked the neuropathologic and clinical phenotype of the Tay-Sachs disease.

Previously we showed GM2 accumulation in *Hexa-/-Neu3-/-* Tay Sachs disease mouse model triggers release of proinflammatory cytokines, microgliosis, astrogliosis consequently activation of inflammatory cascades as well as oxidative stress. These inflammatory events contribute to neurodegeneration observed in the disease pathology. In Sandhoff Disease mouse model it was shown that astrocytes express adenosine A2A receptors which induces ccl2 chemokine overexpression. A2A receptor antagonist istradefylline treatment reduces microglial activation and ccl2 expression in Sandhoff mice.

In this study; A2A receptor antagonist istradefylline treatment was applied to Tay Sachs disease mouse model and whether this treatment would alleviate the neuroinflammation and redox imbalance; and prolong the lifespan was investigated by molecular biological and behavioural analyses. Modulation of ccl2 expression by istradefylline was used as potential therapeutic target to slow down Tay Sachs disease mouse model.

ÖZET

GM2 GANGLİOSİDOZ FARE MODELİNİN DOKULARINDA ANTİ-İNFLAMATUAR TEDAVİSİNİN ETKİSİNİN ARAŞTIRILMASI

Tay-Sachs hastalığı, β-Heksosaminidaz A enziminin α-alt birimini kodlayan HEXA genindeki mutasyonların neden olduğu otozomal resesif geçişli bir lizozomal depo bozukluğudur (LSD). Enzim normalde GM2'den GM3'e dönüşümü katalize eder ancak bu enzim bulunmadığında veya işlevsiz olduğunda GM2 bozunması kesintiye uğrar ve GM2 gangliositi özellikle nöronlarda zamana bağlı olarak giderek birikir. GM2'nin ilerleyici birikimi, nöronların ölümünün artmasına, zihinsel ve motor işlevlerde bozulmaya ve sonunda 2-4 yaşlarında ölüme neden olur. Tay-Sachs modeli olarak oluşturulan Hexa-/- fareler, Neu3 sialidazın aracılık ettiği bir baypass mekanizması sayesinde neredeyse normal bir fenotip göstermiştir. Tay-Sachs hastalığı patolojisinde Neu3 sialidazın gangliosit yıkımında yer aldığı ve *Hexa-/-Neu3-/-* farelerin hastalığın nöropatolojik ve klinik fenotipini taklit ettiği belirlenmiştir.

Daha önce, *Hexa-/-Neu3-/-* Tay Sachs hastalığı fare modelinde GM2 birikiminin, proinflamatuar sitokinlerin salınımını, mikrogliosisi ve astrogliosisi tetiklediğini ve bunun sonucunda oksidatif stresin yanı sıra inflamatuar kaskadların aktivasyonunu tetiklediğini göstermiştik. Bu inflamatuar olaylar, hastalık patolojisinde gözlenen nörodejenerasyona katkıda bulunur. Sandhoff Hastalığı fare modelinde astrositlerin, ccl2 kemokin aşırı ekspresyonunu indükleyen adenozin A2A reseptörlerini eksprese ettiği gösterilmiştir. A2A reseptör antagonisti olan istradefilin tedavisi, SD farelerin geç fazında mikroglial aktivasyonu ve ccl2 ekspresyonunu azalttığı gösterilmiştir.

Bu çalışmada; Tay Sachs hastalığı olan fare modeline A2A reseptör antagonisti olan istradefilin tedavisi uygulanmış ve bu tedavinin nöroinflamasyon ve redoks dengesizliği patolojisini hafifletip hafifletmeyeceği; ve ömrü uzatıp uzatmayacağı moleküler biyolojik ve davranışsal analizlerle araştırılmıştır. Ccl2 ekspresyonunun istradefylline ile modülasyonu, fare modelinde Tay Sachs hastalığını yavaşlatmak için potansiyel terapötik hedef olarak kullanılmıştır.

To My Precious Family

TABLE OF CONTENTS

LIST OF FIGURES..... x

LIST OF TABLES..... xx

CHAPTER 1. INTRODUCTION..... 1

1.1. Lysosomal Storage Diseases..……. 1

1.2. Sphingolipidoses..... ……. 2

1.2.1 Gangliosides…….……... 3

1.2.2 GM2 Gangliosidosis…….……... 4

1.2.2.1 Tay-Sachs Disease…..…….……..…..... 5

1.3. Murine Model of Tay-Sachs Disease…...……... 6

1. 4. Neuroinflammation…..……..……...…. 9

1.4.1 Neuroinflammatory Messengers……..…..…… 12

1.4.2. Neuroinflammation and Oxidative Stress…….……. 14

1.4.3. Neuroinflammation in Lysosomal Storage Disorders..... 15

1.5. Neuroinflammation in GM2 Gangliosidosis Mouse Models..... 17

1.6. Therapeutic Approaches for Neuroinflammation……..... 18

1.7. A2A Receptor…… 19

1.7.1. Istradefylline & Parkinson Disease…….. 20

1.8. The Aim of Study..... 22

CHAPTER 2. MATERIALS AND METHODS……...…… 23

2.1. Mouse Genotyping...……..……...…. 23

2.2. Drug Treatment……. 24

2.3. Tissue Handling……..……...…. 25

2.3.1. Brain Dissection…….....…… 25

2.3.2. Fixation…..…….……... 25

2.4. Real Time PCR..... 26

2.4.1. RNA Isolation…….....……...…..... 26

2.4.2. cDNA Synthesis.……...……... 26

2.4.3. RT-PCR…….....……..…… 27

2.5. Immunohistochemistry…….……. 28

2.6. Thin Layer Chromatography……..……... 29
2.6.1. Ganglioside Isolation…… 29
2.6.1.1. Neutral and Acidic Ganglioside Isolation……..…. 29
2.6.2. Thin Layer Chromatography…… 31
2.6.3. Orcinol Staining of Plates……. 31
2.7. Western Blot..... 32
2.7.1. Protein Isolation..... 32
2.7.2. Bradford Assay..... 32
2.7.3. SDS-PAGE Gel Electrophoresis..... 33
2.8. Behavioural Analysis..... 34
2.8.1. Rotarod Analysis……. 34
2.8.2. Open Field Analysis…… 34

CHAPTER 3. RESULTS……..… 36
3.1. Mouse Genotyping.…….……..… 36
3.2. Behavioural Analysis.....…..……...…….. 36
3.2.1. Body Weight Measurement…….……...……... 37
3.2.2. Rotarod Analysis……..…….…….. 37
3.2.3. Open Field Analysis…....……..……. 38
3.3. Neuroinflammation Analysis..... 39
3.3.1. Real Time PCR..... 39
3.3.2. Western Blot…..... 47
3.3.3. Immunohistochemical Analysis..... 50
3.3.3.1. GFAP Staining……... 50
3.3.3.2. MOMA-2 / LAMP1 Staining……. 54
3.3.3.3. CNPase Staining……... 58
3.3.3.4. IL-6 Staining……...……... 60
3.4. Oxidative Stress Analysis…..... 63
3.4.1. Real Time PCR..... 64
3.4.2. Western Blot…..... 68
3.5. Disease Pathology Analysis..... 69
3.5.1. Real Time PCR..... 69
3.5.2. Thin Layer Chromatography..... 72
3.5.3. Immunohistochemical Analysis..... 74

3.5.3.1. NeuN Staining…….. 74

CHAPTER 4. DISCUSSION…….…...…….. 79

4.1. Conclusion.....……..……..……..... 86

REFERENCES……...….. 87

LIST OF FIGURES

Figure		Page
Figure 1.1.	The connection between the degradation of sphingolipids (SL) within lysosomes and the deficiencies in enzymes leading to storage diseases (Rabbo et al., 2021) ……..	3
Figure 1.2	A diagram representing a segment of the glycosphingolipid breakdown pathway which highlights Neurominidase3 as the predominant enzyme in charge of the metabolic bypass pathway in the Hexa-/- model (Seyrantepe et al. 2018).....	8
Figure 1.3.	GM2 accumulation in the brain of *Hexa-/-Neu3-/-* mice. (A) GA2, and (B) GM3 also appears in the brains of Hexa−/−Neu3−/− mice. (C) GM2 accumulation in the brains of Hexa−/− (mild) and Hexa-/-Neu3-/- (strong) mice (Seyrantepe et al. 2018).....	9
Figure 1.4.	Schematic illustration of positive and negative aspects of neuroinflammation on nervous tissue.(DiSabato et al., 2016b).....	10
Figure 2.1	The schematic illustration of istradefylline administration strategies in *Hexa-/-Neu3-/-* mice as early-stage (10w-13w), late-stage(16w-19w) and two stage treatment (10w-13w & 16w-19w) group with 3mg/kg intraperitoneal istradefylline injections……	24
Figure 3.1.	Gel images of PCR analysis of tail genomic DNA. for Hexa (A) and Neu3(B) genes. 210 bp and 420 bp fragments represent mutant allele and wild type allele of Hexa, respectively(A). 1.6 kb and 2.1 kb fragments represent mutant allele and wild type allele of Neu3, respectively(B)……...	36
Figure 3.2.	Body weight measurements of WT, Hexa-/-, untreated *Hexa-/-Neu3-/-* and istradefylline treated *Hexa-/-Neu3-/-* mice. Body weight measurements of early-stage and two-stage treatment group mice were illustrated together (A) and late stage treatment group measurements were represented separately (B)……..	37
Figure 3.3.	Rotarod analyses of *WT, Hexa-/-* and *Hexa-/-Neu3-/-* mice on an accelerating rod (4 rpm to 40 rpm within 5 minutes). Motor function and motor learning of *Hexa-/- Neu3-/-* mice in early-stage (A), Late-stage (B) and two stage group (B) was compared with its age matched untreated counterparts. Data is representative of mean ± SEM of measurements. Significant levels in the data were presented by using the ONE-way ANOVA…….	38

Figure **Page**

Figure 3.4. Open field analyses of *WT, Hexa-/-* and *Hexa-/-Neu3-/-* were represented. Time spent in center zone of the open field box for 5minutes of controls and early-stage (10w-13w) (A), late-stage(16w-19w) and two stage treatment groups (10w-13w & 16w-19w) (B) were indicated. Total distance traveled in the open field box for 5minutes by mice from control and early-stage (10w-13w) (A), late-stage(16w-19w) and two stage treatment groups (10w-13w & 16w-19w) (B) were demonstrated. Data is representative of mean ± SEM of measurements. Significant levels in the data were presented by using the one-way ANOVA (*p<0.05, **p<0.01,***p<0.001 and ****p<0.0001)..... 39

Figure 3.5. The expression levels of proinflammatory chemokines in **cortex** region of *WT, Hexa-/-* and *Hexa-/-Neu3-/-* were represented. The expression levels of CCL2 (A,B), CCL3 (C,D), CCL5 (E,F) and CXCL10(G,H) in age-matched controls and early-stage (10w-13w), late-stage and two stage treatment groups (10w-13w & 16w-19w) were indicated respectively. Expression ratio calculations were performed by ΔCT method and data was normalized to expression levels of age-matched WT mice. Significant levels in the data were presented by using the one-way ANOVA (*p<0.05, **p<0.01, ***p<0.001, and ****p<0.0001)…… 40

Figure 3.6. The expression levels of astrocyte-related marker and proinflammatory interleukins in cortex region of *WT, Hexa-/-* and Hexa-/-Neu3-/- were represented. The expression levels of GFAP (A,B), IL-1β (C,D) and IL-6 (E,F) in age-matched controls and early-stage (10w-13w), late-stage and two stage treatment groups (10w-13w & 16w-19w) were indicated respectively. Expression ratio calculations were performed by ΔCT method and data was normalized to expression levels of age-matched WT mice. Significant levels in the data were presented by using the one-way ANOVA (*p<0.05, **p<0.01, ***p<0.001, and ****p<0.0001)….. 41

Figure 3.7. Gene expression levels of neuroinflammatory markers in cortex region of untreated and treated *Hexa-/-Neu3-/-* were represented as normalized to age-matched WT and compared to based on untreated, early-stage late-stage and two-stage treatment conditions for CCL2 (A), CCL3(B), CCL5 (C), CXCL10 (D), GFAP (E), IL-1β (F) and IL-6 (G)…….. 42

Figure 3.8. The expression levels of proinflammatory chemokines in **cerebellum** region of *WT, Hexa-/-* and *Hexa-/-Neu3-/-* were represented. The expression levels of CCL2 (A,B), CCL3 (C,D), CCL5 (E,F) and CXCL10(G,H) in age-matched controls and early-stage (10w-13w), late-stage and two stage treatment groups (10w-13w & 16w-19w) were indicated respectively. Expression ratio calculation were performed by ΔCT method and data was normalize

to expression levels of age-matched WT mice. Significant levels in the data were presented by using the one-way ANOVA (*p<0.05, **p<0.01, ***p<0.001, and ****p<0.0001)…..... 43

Figure 3.9. The expression levels of astrocyte-related marker and proinflammatory interleukins in **cerebellum** region of *WT, Hexa-/-* and *Hexa-/-Neu3-/-* were represented. The expression levels of GFAP (A,B), IL-1β (C,D) and IL-6 (E,F) in age-matched controls and early-stage (10w-13w), late-stage and two stage treatment groups (10w-13w & 16w-19w) were indicated respectively. Expression ratio calculations were performed by ΔCT method and data was normalized to expression levels of age-matched WT mice. Significant levels in the data were presented by using the one-way ANOVA (*p<0.05, **p<0.01, ***p<0.001, and ****p<0.0001)….. 44

Figure 3.10. Gene expression levels of neuroinflammatory markers in cerebellum region of untreated and treated *Hexa-/-Neu3-/-* were represented as normalized to age-matched WT and compared to based on untreated, early-stage late-stage and two-stage treatment conditions for CCL2 (A), CCL3(B), CCL5 (C), CXCL10 (D), GFAP (E), IL-1β (F) and IL-6 (G)…….. 46

Figure 3.11. Western-blot analysis for NFκB protein in cortex region of *WT, Hexa-/-* and *Hexa-/-Neu3-/-* were represented. Western blot images and histographic representation were indicated for early-stage(10w-13w) (A,B), Late-stage (16w-19w) (C,D) and two-stage treatment (10w-13w & 16w-19w)(C,D,) groups were indicated respectively… 47

Figure 3.12. Western-blot analysis for IκB protein in cortex region of *WT, Hexa-/-* and *Hexa-/-Neu3-/-* were represented. Western blot images and histographic representation were indicated for early-stage(10w-13w) (A,B), Late-stage (16w-19w) (C,D) and two-stage treatment (10w-13w & 16w-19w)(C,D,) groups were indicated respectively… 48

Figure 3.13. Western-blot analysis for NFκB protein in cerebellum region of *WT, Hexa-/-* and *Hexa-/-Neu3-/-* were represented. Western blot images and histographic representation were indicated for early-stage(10w-13w) (A,B), Late-stage (16w-19w) (C,D) and two-stage treatment (10w-13w & 16w-19w)(C,D,) groups were indicated respectively… 49

Figure 3.14. Western-blot analysis for IκB protein in cerebellum region of *WT, Hexa-/-* and *Hexa-/-Neu3-/-* were represented. Western blot images and histographic representation were indicated for early-stage(10w-13w) (A,B), Late-stage (16w-19w) (C,D) and two-stage treatment (10w-13w & 16w-19w)(C,D,) groups were indicated respectively… 49

Figure **Page**

Figure 3.15. Anti-GFAP staining in cortex region of *WT, Hexa-/-* and *Hexa-/-Neu3-/-* were represented. The 20μm coronal sections were stained in red by anti-GFAP antibody (astrocyte marker) and in blue by DAPI (nucleus). Images for 13W-old controls and early-stage treated *Hexa-/-Neu3-/-* mice (A) and 19W-old controls, late-stage and two-stage treated *Hexa-/-Neu3-/-* mice (B) were represented. GFAP intensity analyses performed by NIH Image J program and histographic representation for 13W-old (C) and 19W-old groups (D) were shown. Scale bar indicates 50μm of cortex. Data is representative of mean ± SEM of measurements. one-way ANOVA was used for statistical analysis (*p<0.05 and **p<0.025)……. 50

Figure 3.16. Anti-GFAP staining in cerebellum region of *WT, Hexa-/-* and *Hexa-/-Neu3-/-* were represented. The 20μm coronal sections were stained in red by anti-GFAP antibody (astrocyte marker) and in blue by DAPI (nucleus). Images for 13W-old controls and early-stage treated *Hexa-/-Neu3-/-* mice (A) and 19W-old controls, late-stage and two-stage treated *Hexa-/-Neu3-/-* mice (B) were represented. GFAP intensity analyses performed by NIH Image J program and histographic representation for 13W-old (C) and 19W-old groups (D) were shown. Scale bar indicates 50μm of cortex. Data is representative of mean ± SEM of measurements. one-way ANOVA was used for statistical analysis (*p<0.05 and **p<0.025)……. 51

Figure 3.17. Anti-GFAP staining in thalamus region of *WT, Hexa-/-* and *Hexa-/-Neu3-/-* were represented. The 20μm coronal sections were stained in red by anti-GFAP antibody (astrocyte marker) and in blue by DAPI (nucleus). Images for 13W-old controls and early-stage treated *Hexa-/-Neu3-/-* mice (A) and 19W-old controls, late-stage and two-stage treated *Hexa-/-Neu3-/-* mice (B) were represented. GFAP intensity analyses performed by NIH Image J program and histographic representation for 13W-old (C) and 19W-old groups (D) were shown. Scale bar indicates 50μm of cortex. Data is representative of mean ± SEM of measurements. one-way ANOVA was used for statistical analysis (*p<0.05 and **p<0.025)……. 52

Figure 3.18. Anti-GFAP staining in hipocampus region of *WT, Hexa-/-* and *Hexa-/-Neu3-/-* were represented. The 20μm coronal sections were stained in red by anti-GFAP antibody (astrocyte marker) and in blue by DAPI (nucleus). Images for 13W-old controls and early-stage treated *Hexa-/-Neu3-/-* mice (A) and 19W-old controls, late-stage and two-stage treated *Hexa-/-Neu3-/-* mice (B) were represented. GFAP intensity analyses performed by NIH Image J program and histographic representation for 13W-old (C) and 19W-old groups (D) were shown. Scale bar indicates 50μm of cortex. Data is representative of mean ± SEM of measurements. one-way ANOVA was used for statistical analysis (*p<0.05 and **p<0.025)……. 53

Figure **Page**

Figure 3.19. MOMA-2 / LAMP1 staining in cortex region of *WT, Hexa-/-* and *Hexa-/-Neu3-/-* were represented. The 20μm coronal sections were stained in red by anti-MOMA-2 antibody (macrophage marker), in green by anti-LAMP1(lysosomal marker) antibody and in blue by DAPI (nucleus). Images for 13W-old controls and early-stage treated *Hexa-/-Neu3-/-* mice (A) and 19W-old controls, late-stage and two-stage treated *Hexa-/-Neu3-/-* mice (B) were represented. MOMA-2/LAMP1 intensity analyses performed by NIH Image J program and histographic representation for 13W-old (C) and 19W-old groups (D) were shown. Scale bar indicates 50μm of cortex. Data is representative of mean ± SEM of measurements. one-way ANOVA was used for statistical analysis (*p<0.05 and **p<0.025)……. 54

Figure 3.20. MOMA-2 / LAMP1 staining in cerebellum region of *WT, Hexa-/-* and *Hexa-/-Neu3-/-* were represented. The 20μm coronal sections were stained in red by anti-MOMA-2 antibody (macrophage marker), in green by anti-LAMP1(lysosomal marker) antibody and in blue by DAPI (nucleus). Images for 13W-old controls and early-stage treated *Hexa-/-Neu3-/-* mice (A) and 19W-old controls, late-stage and two-stage treated *Hexa-/-Neu3-/-* mice (B) were represented. MOMA-2 / LAMP1 intensity analyses performed by NIH Image J program and histographic representation for 13W-old (C) and 19W-old groups (D) were shown. Scale bar indicates 50μm of cortex. Data is representative of mean ± SEM of measurements. one-way ANOVA was used for statistical analysis (*p<0.05 and **p<0.025)……. 55

Figure 3.21. MOMA-2 / LAMP1 staining in thalamus region of *WT, Hexa-/-* and *Hexa-/-Neu3-/-* were represented. The 20μm coronal sections were stained in red by anti-MOMA-2 antibody (macrophage marker), in green by anti-LAMP1(lysosomal marker) antibody and in blue by DAPI (nucleus). Images for 13W-old controls and early-stage treated *Hexa-/-Neu3-/-* mice (A) and 19W-old controls, late-stage and two-stage treated *Hexa-/-Neu3-/-* mice (B) were represented. MOMA-2 / LAMP1 intensity analyses performed by NIH Image J program and histographic representation for 13W-old (C) and 19W-old groups (D) were shown. Scale bar indicates 50μm of cortex. Data is representative of mean ± SEM of measurements. one-way ANOVA was used for statistical analysis (*p<0.05 and **p<0.025)..... 56

Figure 3.22. MOMA-2 / LAMP1 staining in hippocampus region of *WT, Hexa-/-* and *Hexa-/-Neu3-/-* were represented. The 20μm coronal sections were stained in red by anti-MOMA-2 antibody (macrophage marker), in green by anti-LAMP1(lysosomal marker) antibody and in blue by DAPI (nucleus). Images for 13W-old controls and early-

stage treated *Hexa-/-Neu3-/-* mice (A) and 19W-old controls, late-stage and two-stage treated *Hexa-/-Neu3-/-* mice (B) were represented. MOMA-2 / LAMP1 intensity analyses performed by NIH Image J program and histographic representation for 13W-old (C) and 19W-old groups (D) were shown. Scale bar indicates 50μm of cortex. Data is representative of mean ± SEM of measurements. one-way ANOVA was used for statistical analysis (*p<0.05 and **p<0.025)……. 57

Figure 3.23 CNPase staining in cortex region of *WT, Hexa-/-* and *Hexa-/-Neu3-/-* were represented. The 20μm coronal sections were stained in green by anti-CNPase antibody (oligodendriocyte marker) and in blue by DAPI (nucleus). Images for 13W-old controls and early-stage treated *Hexa-/-Neu3-/-* mice (A) and 19W-old controls, late-stage and two-stage treated *Hexa-/-Neu3-/-* mice (B) were represented. GFAP intensity analyses performed by NIH Image J program and histographic representation for 13W-old (C) and 19W-old groups (D) were shown. Scale bar indicates 50μm of cortex. Data is representative of mean ± SEM of measurements. one-way ANOVA was used for statistical analysis (*p<0.05 and **p<0.025).. 58

Figure 3.24 CNPase staining in cerebellum region of *WT*, Hexa-/- and *Hexa-/-Neu3-/-* were represented. The 20μm coronal sections were stained in green by anti-CNPase antibody (oligodendriocyte marker) and in blue by DAPI (nucleus). Images for 13W-old controls and early-stage treated *Hexa-/-Neu3-/-* mice (A) and 19W-old controls, late-stage and two-stage treated *Hexa-/-Neu3-/-* mice (B) were represented. GFAP intensity analyses performed by NIH Image J program and histographic representation for 13W-old (C) and 19W-old groups (D) were shown. Scale bar indicates 50μm of cortex. Data is representative of mean ± SEM of measurements. one-way ANOVA was used for statistical analysis (*p<0.05 and **p<0.025)... 59

Figure 3.25 IL-6 staining in cortex region of *WT, Hexa-/-* and *Hexa-/-Neu3-/-* were represented. The 20μm coronal sections were stained in red by anti-IL-6 antibody (interleukin-6 marker) and in blue by DAPI (nucleus). Images for 13W-old controls and early-stage treated *Hexa-/-Neu3-/-* mice (A) and 19W-old controls, late-stage and two-stage treated *Hexa-/-Neu3-/-* mice (B) were represented. GFAP intensity analyses performed by NIH Image J program and histographic representation for 13W-old (C) and 19W-old groups (D) were shown. Scale bar indicates 50μm of cortex. Data is representative of mean ± SEM of measurements. one-way ANOVA was used for statistical analysis (*p<0.05 and **p<0.025)……. 60

Figure **Page**

Figure 3.26 IL-6 staining in cerebellum region of *WT*, *Hexa-/-* and *Hexa-/-Neu3-/-* were represented. The 20μm coronal sections were stained in red by anti-IL-6 antibody (interleukin-6 marker) and in blue by DAPI (nucleus). Images for 13W-old controls and early-stage treated *Hexa-/-Neu3-/-* mice (A) and 19W-old controls, late-stage and two-stage treated *Hexa-/-Neu3-/-* mice (B) were represented. GFAP intensity analyses performed by NIH Image J program and histographic representation for 13W-old (C) and 19W-old groups (D) were shown. The scale bar indicates 50μm of cortex. Data is representative of mean ± SEM of measurements. one-way ANOVA was used for statistical analysis (*p<0.05 and **p<0.025)…… 61

Figure 3.27 IL-6 staining in thalamus region of *WT*, *Hexa-/-* and *Hexa-/-Neu3-/-* were represented. The 20μm coronal sections were stained in red by anti-IL-6 antibody (interleukin-6 marker) and in blue by DAPI (nucleus). Images for 13W-old controls and early-stage treated *Hexa-/-Neu3-/-* mice (A) and 19W-old controls, late-stage and two-stage treated *Hexa-/-Neu3-/-* mice (B) were represented. GFAP intensity analyses performed by NIH Image J program and histographic representation for 13W-old (C) and 19W-old groups (D) were shown. Scale bar indicates 50μm of cortex. Data is representative of mean ± SEM of measurements. one-way ANOVA was used for statistical analysis (*p<0.05 and **p<0.025)……. 62

Figure 3.28 IL-6 staining in hipocampus region of *WT*, *Hexa-/-* and *Hexa-/-Neu3-/-* were represented. The 20μm coronal sections were stained in red by anti-IL-6 antibody (interleukin-6 marker) and in blue by DAPI (nucleus). Images for 13W-old controls and early-stage treated *Hexa-/-Neu3-/-* mice (A) and 19W-old controls, late-stage and two-stage treated *Hexa-/-Neu3-/-* mice (B) were represented. GFAP intensity analyses performed by NIH Image J program and histographic representation for 13W-old (C) and 19W-old groups (D) were shown. Scale bar indicates 50μm of cortex. Data is representative of mean ± SEM of measurements. one-way ANOVA was used for statistical analysis (*p<0.05 and **p<0.025)……. 63

Figure 3.29 The expression levels of SOD2, Catalase and TTase-1 in cortex region of WT, Hexa-/- and Hexa-/-Neu3-/- were represented. The expression levels of SOD2 (A,B), Catalase (C,D) and TTase-1(E,F) in age-matched controls and early-stage (10w-13w), late-stage and two stage treatment groups (10w-13w & 16w-19w) were indicated respectively. SOD2 (G), Catalse (H) and TTase-1 (I) gene expression levels in cortex region of untreated and treated Hexa-/-Neu3-/- were represented as normalized to age-matched WT that are compared based on untreated, early-stage late-stage and two-stage treatment conditions Expression ratio calculations were performed by ΔCT method and data was normalized to expression levels of age-matched WT mice. Significant levels in the data were presented by

using the one-way ANOVA (*p<0.05, **p<0.01, ***p<0.001, and ****p<0.0001)…..... 65

Figure 3.30 The expression levels of SOD2, Catalase and TTase-1 in cerebellum region of *WT, Hexa-/-* and Hexa-/-Neu3-/- were represented. The expression levels of SOD2 (A,B), Catalase (C,D) and TTase-1(E,F) in age-matched controls and early-stage (10w-13w), late-stage and two stage treatment groups (10w-13w & 16w-19w) were indicated respectively. SOD2 (G), Catalse (H) and TTase-1 (I) gene expression levels in cerebellum region of untreated and treated *Hexa-/-Neu3-/-* were represented as normalized to age-matched *WT* that are compared based on untreated, early-stage late-stage and two-stage treatment conditions Expression ratio calculations were performed by ΔCT method and data was normalized to expression levels of age-matched *WT* mice. Significant levels in the data were presented by using the one-way ANOVA (*p<0.05, **p<0.01, ***p<0.001, and ****p<0.0001)…… 67

Figure 3.31 Western-blot analysis for APE1 protein in cortex region of *WT*, *Hexa-/-* and *Hexa-/-Neu3-/-* were represented. Western blot images and histographic representation were indicated for early-stage(10w-13w) (A,B), Late-stage (16w-19w) (C,D) and two-stage treatment (10w-13w & 16w-19w)(C,D,) groups were indicated respectively… 68

Figure 3.32 Western-blot analysis for APE1 protein in cerebellum region of *WT*, *Hexa-/-* and *Hexa-/-Neu3-/-* were represented. Western blot images and histographic representation were indicated for early-stage(10w-13w) (A,B), Late-stage (16w-19w) (C,D) and two-stage treatment (10w-13w & 16w-19w)(C,D,) groups were indicated respectively.... 69

Figure 3.33 The expression levels of HexB and GM2AP in cortex region of *WT*, *Hexa-/-* and *Hexa-/-Neu3-/-* were represented. The expression levels of HexB (A,B) and GM2AP (D,E) in age-matched controls and early-stage (10w-13w), late-stage and two stage treatment groups (10w-13w & 16w-19w) were indicated respectively. HExB (C) and GM2AP (F) gene expression levels in cortex region of untreated and treated *Hexa-/-Neu3-/-* were represented as normalized to age-matched *WT* that are compared based on untreated, early-stage late-stage and two-stage treatment conditions Expression ratio calculations were performed by ΔCT method and data was normalized to expression levels of age-matched *WT* mice. Significant levels in the data were presented by using the one-way ANOVA (*p<0.05, **p<0.01, ***p<0.001, and ****p<0.0001)….. 70

Figure **Page**

Figure 3.34 The expression levels of HexB and GM2AP in cerebellum region of *WT*, *Hexa-/-* and *Hexa-/-Neu3-/-* were represented. The expression levels of HexB (A,B) and GM2AP (D,E) in age-matched controls and early-stage (10w-13w), late-stage(16w-19w) and two stage treatment groups (10w-13w & 16w-19w) were indicated respectively. HExB (C) and GM2AP (F) gene expression levels in cerebellum region of untreated and treated *Hexa-/-Neu3-/-* were represented as normalized to age-matched *WT* that are compared based on untreated, early-stage late-stage and two-stage treatment conditions Expression ratio calculations were performed by ΔCT method and data was normalized to expression levels of age-matched *WT* mice. Significant levels in the data were presented by using the one-way ANOVA (*p<0.05, **p<0.01, ***p<0.001, and ****p<0.0001)…….. 71

Figure 3.35 TLC plate images and histograps of GM2 intensity in cortex of early-stage (A), late-stage and two-stage treatment (B) groups were represented for acidic GSLs. The levels of GM2 ganglioside normalized to GD1a level in the cerebellum region were indicated in histographs. Data is representative of mean ± SEM of measurements. Significant levels in the data were presented by using the one-way ANOVA (*p<0.05, ***p<0.001 and ****p<0.0001)…. 72

Figure 3.36 TLC plate images and histograps of GM2 intensity in cerebellum of early-stage (A), late-stage and two-stage treatment (B) groups were represented for acidic GSLs. The levels of GM2 ganglioside normalized to GD1a level in the cerebellum region were indicated in histographs. Data is representative of mean ± SEM of measurements. Significant levels in the data were presented by using the one-way ANOVA (*p<0.05, ***p<0.001 and ****p<0.0001)…. 73

Figure 3.37 Anti-NeuN staining in cortex region of *WT*, *Hexa-/-* and *Hexa-/-Neu3-/-* were represented. The 20μm coronal sections were stained in red by anti-NeuN antibody (neuron marker). Images for 13W-old controls and early-stage treated *Hexa-/-Neu3-/-* mice (A) and 19W-old controls, late-stage and two-stage treated *Hexa-/-Neu3-/-* mice (B) were represented. NeuN intensity analyses performed by NIH Image J program and histographic representation for 13W-old (C) and 19W-old groups (D) were shown. Scale bar indicates 50μm of cortex. Data is representative of mean ± SEM of measurements. one-way ANOVA was used for statistical analysis (*p<0.05 and **p<0.025)……. 75

Figure 3.38 Anti-NeuN staining in cerebellum region of WT, Hexa-/- and Hexa-/-Neu3-/- were represented. The 20μm coronal sections were stained in red by anti-NeuN antibody (neuron marker). Images for 13W-old controls and early-stage treated Hexa-/-Neu3-/- mice (A) and 19W-old controls, late-stage and two-stage treated Hexa-/-Neu3-/- mice

(B) were represented. NeuN intensity analyses performed by NIH Image J program and histographic representation for 13W-old (C) and 19W-old groups (D) were shown. Scale bar indicates 50μm of cortex. Data is representative of mean ± SEM of measurements. one-way ANOVA was used for statistical analysis (*p<0.05 and **p<0.025)…… 76

Figure 3.39 Anti-NeuN staining in thalamus region of *WT*, *Hexa-/-* and *Hexa-/-Neu3-/-* were represented. The 20μm coronal sections were stained in red by anti-NeuN antibody (neuron marker). Images for 13W-old controls and early-stage treated *Hexa-/-Neu3-/-* mice (A) and 19W-old controls, late-stage and two-stage treated *Hexa-/-Neu3-/-* mice (B) were represented. NeuN intensity analyses performed by NIH Image J program and histographic representation for 13W-old (C) and 19W-old groups (D) were shown. Scale bar indicates 50μm of cortex. Data is representative of mean ± SEM of measurements. one-way ANOVA was used for statistical analysis (*p<0.05 and **p<0.025)……. 77

Figure 3.40 Anti-NeuN staining in hipocampus region of *WT*, *Hexa-/-* and *Hexa-/-Neu3-/-* were represented. The 20μm coronal sections were stained in red by anti-NeuN antibody (neuron marker). Images for 13W-old controls and early-stage treated *Hexa-/-Neu3-/-* mice (A) and 19W-old controls, late-stage and two-stage treated *Hexa-/-Neu3-/-* mice (B) were represented. NeuN intensity analyses performed by NIH Image J program and histographic representation for 13W-old (C) and 19W-old groups (D) were shown. Scale bar indicates 50μm of cortex. Data is representative of mean ± SEM of measurements. one-way ANOVA was used for statistical analysis (*p<0.05 and **p<0.025)……. 78

LIST OF TABLES

Table		Page
Table 2.1.	Primer sequences used for genotyping of Hexa and Neu3 alleles..	23
Table 2.2.	Primer sequences and RT-PCR product length of the genes to be analysed……	28
Table 2.3.	Ingredients for resolving and stacking gel preparation of SDS-PAGE gel electrophoresis……..	33

CHAPTER 1

INTRODUCTION

1.1. Lysosomal Storage Disorders

Lysosomal storage disorders (LSDs) are a group of inborn errors of metabolism characterized by lysosomal dysfunction leading to disturbance in lysosomal homeostasis (Platt et al., 2012). LSDs are rare genetic disorders mostly inherited in an autosomal recessively except for 3 that are X-linked. Mutations in genes encoding not only lysosomal enzymes or other proteins like acid hydrolases, activator of the hydrolases or transporters but also non-lysosomal proteins involving in lysosome activity lead to LSD pathology (Parenti et al., 2015). Loss of function of specific proteins or molecules causes dysregulation in degradation process in lysosomes which leads to accumulation of specific storage molecules within lysosomes.

The incidence of LSDs is proven to be roughly 1:5000 live births however the incidence level is probably greater when undiagnosed cases are taken into account as well (Fuller et al., 2014). The build-up of monomers or macromolecules carried by secretory vesicles and in the organelles associated with the endosomal-autophagic pathway is a feature shared by all LSDs. The biochemical analysis of these accumulating compounds allows for identifying defective proteins or molecules causing the disease (Platt et al., 2012).

The LSDs are classified based on either the structure of accumulating substance like sphingolipids or glycosaminoglycans; or the nature of the molecular defect like hydrolytic enzyme deficiency, cofactor/activator deficiency, etc. (Marques & Saftig, 2019; Sun, 2018). Lysosomal accumulation leads to a wide range of clinical symptoms depending on the residual activity of the mutant protein, the storage molecule, or its location. These conditions are typically progressive; however, the pace of advancement varies depending on the disease of interest and the age of onset of the disease (Sun, 2018). While certain signs are detected from birth, other indications may arise in early toddler years or childhood. Although the majority of LSDs emerge in infancy and are known as

pediatric neurodegenerative diseases, some can be diagnosed in maturity (late-infantile, juvenile, and adult types) (Parenti et al., 2015).

Failure to develop, muscle weakness, vision problems, morphologic defects, organomegaly, seizures, and neuromotor regression are all common signs of LSDs. In most cases, these neuropathological and motor problems increase morbidity and reduce the patient's life quality, ultimately leading to death(Pará et al., 2020).

Neuronal dysfunction and neurodegeneration can arise when lysosomal function is disrupted. Accordingly, genetic and biochemical analyses for many LSDs revealed that CNS is involved in over two-thirds of LSDs (Schultz et al., 2011).

1.2. Sphingolipidosis

Sphingolipids (SLs) are one of the key components of plasma membrane structure and also play important roles in cellular homeostasis, adhesion, signaling cascades, senescence, development, and apoptosis (Abou-Ghali & Stiban, 2015; Lahiri & Futerman, 2007). Previously it was reported that SLs are also linked to the pathophysiology of a number of immunological and neurological disorders (Albeituni & Stiban, 2019). SLs can be synthesized from the fusion of serine and palmitoyl-CoA in the endoplasmic reticulum (ER) via a chain of reactions that produce Ceramide, which serves as the parent SL in the formation of other SLs (Abou-Ghali & Stiban, 2015). Sphingolipids are categorized as phosphosphingolipids and glycosphingolipids (GSLs) based on the head groups attached to ceramide. GSLs have one or more sugar on the ceramide chain creating diverse structures classified into 4 subgroups: cerebrosides, sulfatides, globosides, and gangliosides (Abed Rabbo et al., 2021). Lysosomal hydrolysis of GSLs is necessary as the end products are reutilized in recycling cascades (Sandhoff & Harzer, 2013). Abnormalities in this systematic lysosomal hydrolysis of SLs causes a collection of diseases called sphingolipidoses (Puri et al., 1999). Deficiency and dysfunctionality of the enzymes involving in synthesis and degradation pathways of SLs leads to several sphingolipidoses (Figure1.1). Sphingolipidoses are reported to induce severe membrane damage, affecting the longevity and proliferation of most cells, particularly affecting CNS. Thus, neurodegeneration and other visceral problems are common features of many sphingolipidoses (Staretz-Chacham et al., 2009; G. Wang & Bieberich, 2018).

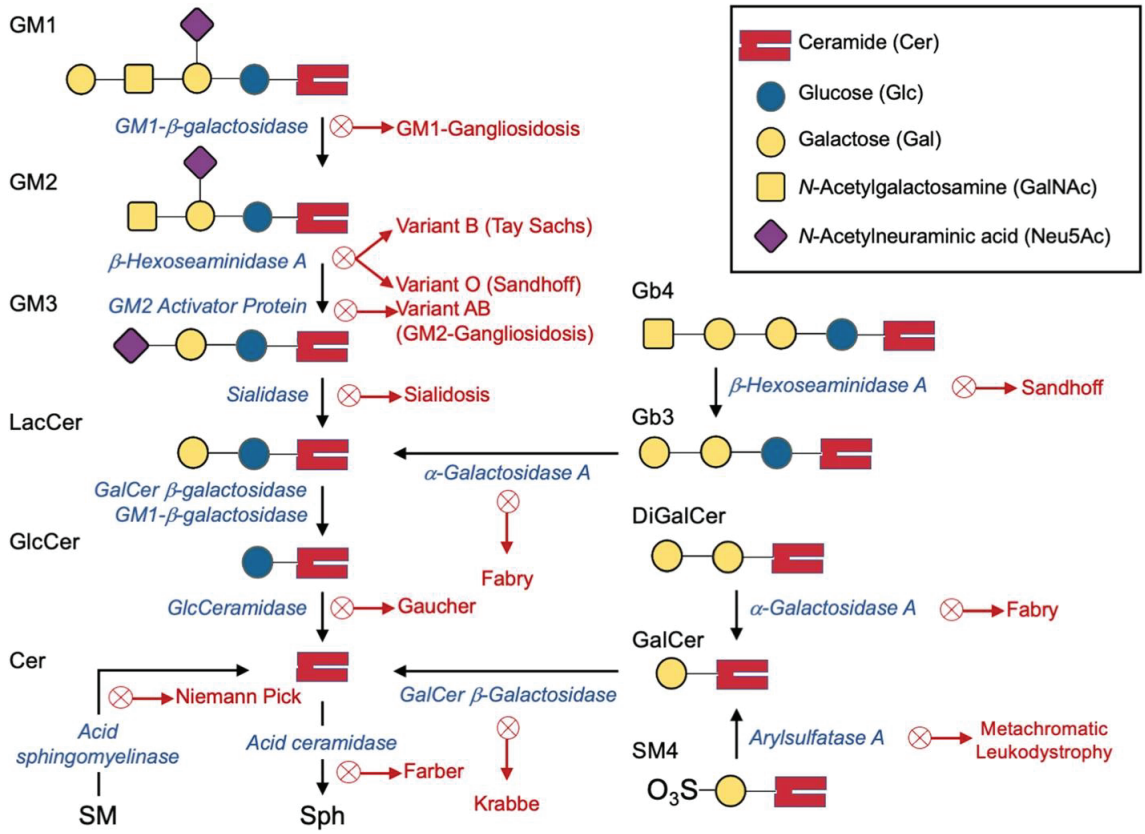

Figure 1.1. The connection between the degradation of sphingolipids (SL) within lysosomes and the deficiencies in enzymes leading to storage diseases (Rabbo et al., 2021)

1.2.1. Gangliosides

Along with a diverse number of cell surface glycans, gangliosides are also produced within Golgi Apparatus, and their heterogenous ceramide backbones are generated in the ER (Varki, 2011). Salvage of sialic acids, sugars, fatty acids, and sphingoid bases through recycling mechanism enables de novo synthesis of gangliosides (Tettamanti, 2003).

Gangliosides are acidic glyco-sphingolipids containing sialic acid groups and they are structural components of cell membranes widely distributed throughout the body (Sonnino et al., 2007). Gangliosides are known to be mostly present in nerve cells, particularly in the plasma membrane comprising up 10-12% of neuronal membranes, therefore they are approximately 5-fold higher in the grey matter than in the white matter of the brain (Palmano et al., 2015). Gangliosides infiltrate the extracellular space via the glycosyl group and become connected to the plasma membrane through the ceramide backbone. They are thought to segregate into membrane domains called lipid rafts with

high concentrations of cholesterol and sphingolipids rather than being distributed uniformly on the cell surface. These lipid raft structures mediate signaling cascades depending on the specific GPI-anchored protein and lipid composition in the raft (Kolter, 2012).

In the brain, gangliosides make up the majority (around 75%) of the sialic acid linked to other molecules. They are essential for creating the carbohydrate structures on the surface of neural cells (Schnaar et al. 2014). Ganglioside production in the brain is linked to neurogenesis, synapse formation, synaptic transmission, and cell propagation(Palmano et al., 2015; Sipione et al., 2020). Besides developing and maintaining the nervous system; gangliosides are important for many cellular functions, including cell-to-cell communication, cell recognition, signal transduction, regulating immune responses, transporting molecules, and formation of myelin sheaths around nerve cells (Lopez & Schnaar, 2009; Sipione et al., 2020). Gangliosides in the brain are expressed at different levels and with varying patterns during the process of development (Yu et al., 2011). The quantity of gangliosides and their degree of sialylation tend to increase as brain development proceeds. These complex molecules are mainly found in the neural cell membrane and are crucial for functions such as axon-myelin interaction, maintaining calcium levels, and facilitating signaling pathways (Y. Ohmi et al., 2012; Schnaar, 2010).

1.2.2. GM2 Gangliosidosis

GM2 gangliosidosis is a rare and debilitating autosomal recessive lysosomal storage disease caused by the deficiency of beta-hexosaminidaseA enzyme. GM2 gangliosidosis is categorized into three types depending on the severity of the disease and the time when symptoms first appear: Tay-Sachs disease, Sandhoff disease, and AB variant which results from the mutations in different genes (HEXA, HEXB, and GM2AP, respectively) (Leal et al., 2020). HEXA and HEXB genes produce two (α and β) subunits of an enzyme called β-N-acetylhexosaminidase and GM2A gene encodes for the GM2 activator protein that enhances the degradation of GM2 ganglioside by β-N-acetylhexosaminidase A. The enzyme typically converts GM2 into GM3 by elimination of N-acetylgalactosamine, but if one or more of these components is missing or not working properly, the breakdown process is interrupted and the undegraded GM2

ganglioside starts to accumulate in lysosomes (Gravel et al., 2014). GM2 is an important molecule in the formation of complex brain gangliosides, which are mainly found in neurons. Consequently, GM2 gangliosidosis primarily impacts the central nervous system of affected individuals and can lead to progressive neurodegeneration. The three types are clinically similar and characterized by a progressive dissipation of motor and cognitive function, seizures, and blindness, leading to premature death in early childhood for TSD and SD, and in late adolescence or adulthood for AB variant.

The diagnosis of GM2 gangliosidosis is based on clinical presentation, genetic testing, and the measurement of enzymatic activity in leukocytes or fibroblasts. Prenatal diagnosis through chorionic villus sampling or amniocentesis is also possible. There is currently no cure for GM2 gangliosidosis, and treatment options are limited to symptomatic and supportive care. (Toro et al., 2021)

1.2.2.1. Tay-Sachs Disease

As mentioned above; TSD is caused by the deficiency in the beta-hexosaminidaseA enzyme leading to abnormal GM2 accumulation primarily in the nervous system (Americo et al., 2010). The disease is classified into three forms based on the age of onset: infantile, juvenile, and chronic. The most common form is the infantile type, which is characterized by a rapid and devastating decline in neurological function. It is particularly predominant among the Ashkenazi Jewish population, with an occurrence rate of 1 in 3,500 births. In other populations, the incidence rate is much lower, at around 1 in 360,000 births (M. Kaback et al., 1994). The seriousness and timing of onset in Tay-Sachs disease are influenced by the extent of remaining HEXA enzyme activity (Mahuran, 1998). The adverse impacts of the disease commence during early pregnancy, but the affected baby remains in good health until approximately 6 months of age. Subsequently, the baby's developmental progress halts, and by the age of 2, the child begins to experience recurring seizures, cognitive impairment, and a decline in motor skills. With the progression of the disease, the child eventually loses their vision, experiences severe cognitive dysfunction, and becomes paralyzed. The disease usually leads to the child's passing by the age of 4 due to the severely affected nervous system (M. M. Kaback, 2001).

Research shows that Tay-Sachs disease is the most frequently occurring sphingolipidosis type(M. M. Kaback & O'Brien, 1973). Advances in genetic testing have made it possible to identify carriers of the disease, which can lead to informed reproductive decision-making for at-risk individuals and families (Mahuran, 1998). Additionally, various therapeutic approaches, such as enzyme replacement therapy, gene therapy, and substrate reduction therapy, are currently being investigated as potential treatments for Tay-Sachs disease (Maegawa et al., 2009; Picache et al., 2022).

Tay-Sachs disease currently has no cure, and patients can only receive palliative care. Enzyme replacement therapy and bone marrow transplantation have not fully prevented the neuropathology in infants with Tay-Sachs disease (Jacobs et al., 2005). Animal models, such as mice, are being utilized to develop new therapies, including stem cell transplantation. Nevertheless, overcoming the challenge of breaching the blood-brain barrier remains a barrier for treatment of the disease.

Substrate deprivation therapy, which has been reported to be efficient in treating Gaucher disease, is have been trialed for late onset Tay-Sachs disease (Aerts et al., 2006; Lachmann, 2009). Pharmacological chaperones that can help refold and correct the transport of mutated proteins could potentially offer advantages in managing long-term Tay-Sachs disease. (Clarke et al., 2011; Osher et al., 2011).

It is most probably that combining different treatment strategies would provide most effective therapy for Tay-Sachs disease.

1.3. Murine Model of Tay-Sachs Disease

To create mouse models for GM2 gangliosidoses, researchers targeted the Hexa and Hexb genes(Phaneuf et al., 1996; Yamanaka et al., 1994). HEXB knockout mice exhibited a neuropathological phenotype similar to Sandhoff Disease pathology, but deficiency of HEXA did not lead to the severe phenotype of the early-onset pathology of Tay-Sachs disease due to a metabolic bypass pathway suggested in ganglioside biosynthesis and degradation pathway in mice. It was suggested that in this bypass pathway sialidases in mice can catalyze removal of sialic acid residue from GM2 ganglioside and transform it into GA2 ganglioside which in turn is transformed into ceramide by HexB enzyme (Sango et al., 1995; Yuziuk et al., 1998). As GM2 is degraded via GA2 instead of GM3 routed degradation through this bypass mechanism in the

deficiency of Hexa; Hexa-/- mouse model didn't exhibit abnormal GM2 accumulation or other neuropathology as in patients. Rather than that, the *Hexa*$^{-/-}$ mice display symptoms observed in late-onset TSD with inclusion bodies in lysosomes and mild GA2 accumulation which is asialyted form of GM2. Mice with a Hexa gene deficiency exhibited the buildup of GM2 in their neurons. Examination of brain and liver tissues revealed that this accumulation remained below a critical threshold and did not result in lethality (Igdoura et al., 1999; Phaneuf et al., 1996; Yamanaka et al., 1994).

Sialidases are a group of enzymes that are involved in the removal of sialic acid from glycoconjugates such as glycoproteins, glycolipids, and gangliosides. There are four types of mammalian sialidases: NEU1, NEU2, NEU3, and NEU4 (Monti et al., 2010). NEU1 is found in lysosomes and is responsible for the catabolism of sialylated glycoconjugates (D'Azzo & Bonten, 2010). NEU2 is found in the cytosol and is involved in the regulation of cell growth and differentiation. NEU3 is found on the cell surface and is involved in the regulation of cell adhesion, migration, and signaling (Miyagi & Yamaguchi, 2012; Smutova et al., 2014). NEU4 is also found in lysosomes and is involved in the degradation of sialylated glycoconjugates (Okun et al., 2023). Dysregulation of sialidase activity has been linked to various diseases including cancer, neurodegenerative disorders, and lysosomal storage disorders (Miyagi & Yamaguchi, 2012).

In order to determine the main sialidase responsible for the metabolic bypass pathway, *Hexa-/-Neu4-/-* mice were created. However, the resulting phenotype was relatively mild, and it was determined that NEU4 acted as a modifier gene rather than the main sialidase (Seyrantepe et al., 2010).

When we generated *Hexa-/-Neu3-/-* mice to further investigate the role of Neu3 sialidase in this pathway we observed that Neu3 sialidase is the primary enzyme involved in the bypass mechanism in mouse pathology of Tay-Sachs disease (Seyrantepe, Demir, Timur, Gerichten, et al., 2018). As a result, *Hexa-/-Neu3-/-* mice have been identified as a suitable mouse model for early-onset Tay-Sachs disease. Figure 1.2 illustrates the role of Neu3 sialidase in the metabolic bypass pathway of Tay-Sachs disease in mice.

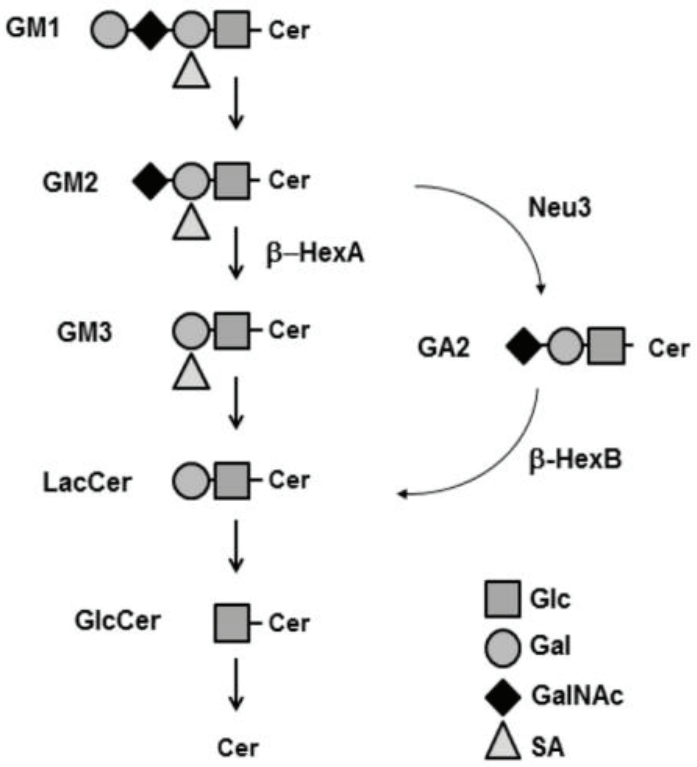

Figure 1.2. A diagram representing a segment of the glycosphingolipid breakdown pathway which highlights Neurominidase3 as the predominant enzyme in charge of the metabolic bypass pathway in the Hexa-/- model. (Seyrantepe, Demir, Timur, Von Gerichten, et al., 2018).

The inactivation of both Hexa and Neu3 genes led to the termination of the GM2 ganglioside degradation and previously reported thin layer chromatography data demonstrated a severe buildup of GM2 ganglioside in the CNS tissue of *Hexa-/-Neu3-/-* mice (Figure 1.3). The examination of neuronal lysosomes in *Hexa-/-Neu3-/-* mice through electron microscopy indicated that there was an unusual escalation in the amount of lysosomes and the presence of ring-like structures, which resembled the phenotype observed in humans with Tay-Sachs disease. Pathological indications observed in *Hexa-/-Neu3-/-* mice closely resembled those seen in humans suffering from TSD, including tremors, ataxia, and weakened hind limbs. Additionally, these mice displayed growth impairment when compared to their littermates, which is another characteristic commonly observed in Tay-Sachs patients (Seyrantepe, Demir, Timur, Gerichten, et al., 2018).

The *Hexa-/-Neu3-/-* mice exhibited a significant incidence of sudden death attributed to advancing neuropathology and neurodegeneration, which was similar to the phenotype observed in Sandhoff (*Hexb-/-*) mice(Seyrantepe, Demir, Timur, Gerichten, et al., 2018).

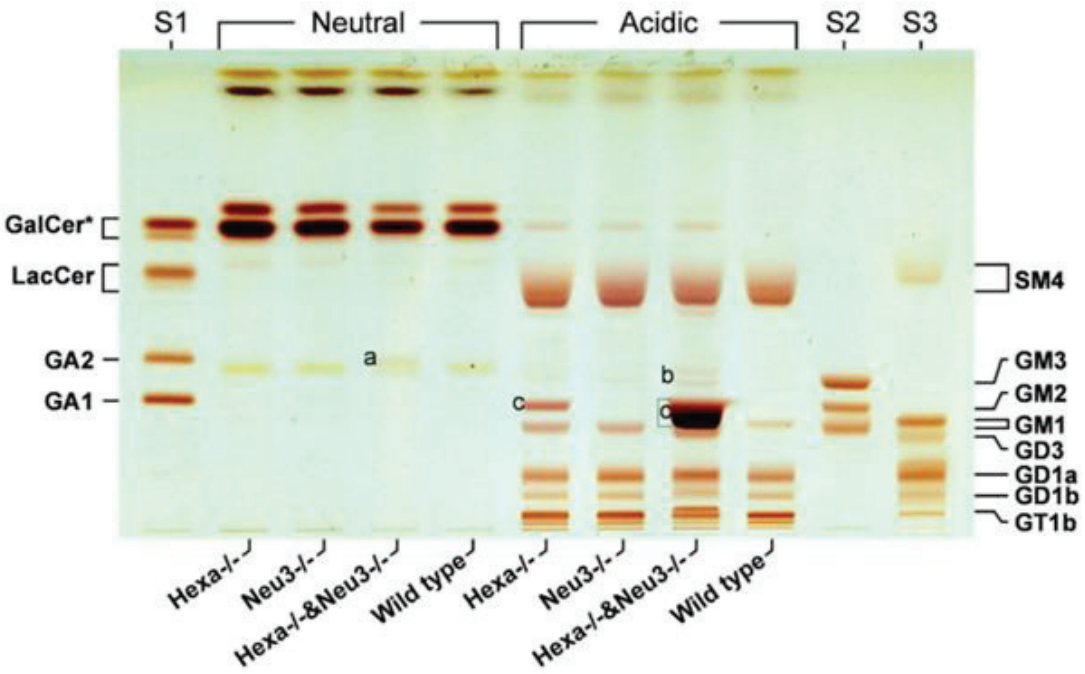

Figure 1.3. GM2 accumulation in the brain of Hexa-/-Neu3-/- mice. (a) GA2, and (b) GM3 appears in the brains of Hexa-/-Neu3-/- mice. (c) GM2 accumulation in the brains of Hexa−/− (mild) and Hexa-/-Neu3-/- (strong) mice (Seyrantepe, Demir, Timur, Von Gerichten, et al., 2018).

1.4. Neuroinflammation

Neuroinflammation is a multifaceted process that arises in the nervous system in response to various injuries, infections, and diseases. It involves the stimulation of immune cells and the release of various pro-inflammatory molecules, such as cytokines, chemokines, and reactive oxygen species (ROS), which can cause damage to the surrounding tissues. These mediators and secondary messengers are generated by glial cells in the CNS (microglia and astrocytes), endothelia, and peripherally derived immune cells (DiSabato et al., 2016a). While neuroinflammation is initially a protective response to prevent further damage, it can also contribute to the pathogenesis of several neurodegenerative and lysosomal storage disorders (Figure 1.4.).

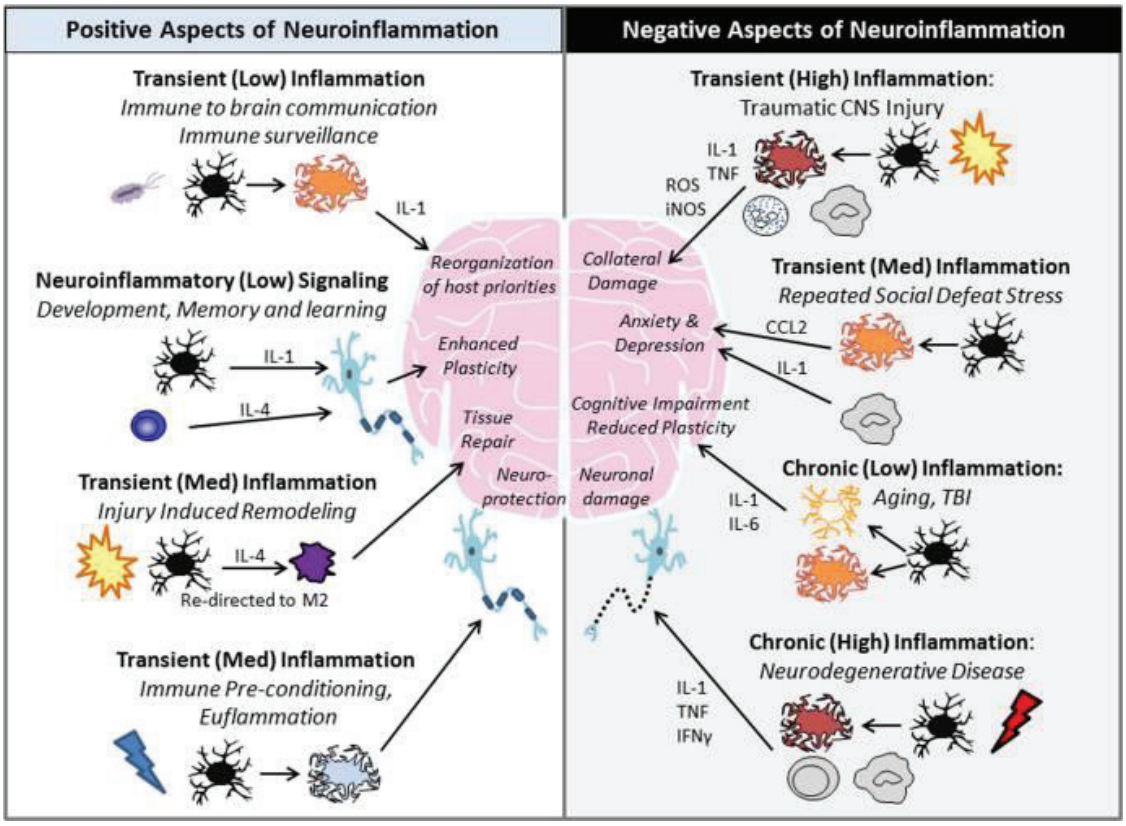

Figure 1.4. Schematic illustration of positive and negative aspects of neuroinflammation on nervous tissue.(DiSabato et al., 2016b)

Neuroinflammation involves various cells, including microglia, astrocytes, and infiltrating immune cells, such as T cells and macrophages (Carson et al., 2006). Microglia have a close connection with neurons and play significant functions in the maintenance of normal CNS function and development by providing essential growth factors to support brain health (Raivich, 2005). Microglia as the primary immune cells involved in neuroinflammation within the central nervous system tissue and they have a constant role in the detection of stress signals (like DAMPs) and cleaning up cellular waste by phagocytosis (Rock et al., 2004). The activation of microglia is triggered by damage-associated molecular patterns (DAMPs) released from dying or damaged neurons (Thundyil & Lim, 2015). This process is mediated through various receptors, including Toll-like receptors and other pattern-recognition receptors(Lyman et al., 2014). Microglia activation is marked by changes in their shape, increased cell division, elevated expression of surface receptors, and the release of cytokines and chemokines (Wendimu & Hooks, 2022). Microglia, upon activation, change their morphology and produce inflammatory mediators like chemokines and cytokines that help in recruiting and activating immune cells from peripheral tissues to the affected site, thus contributing to

the inflammatory response (Amor et al., 2014; Arroyo et al., 2014). Resting microglia can be activated into M1 or M2 phenotypes creating heterogeneous microglia with different functions. The M1 phenotype is characterized by its proinflammatory properties, whereas the M2 phenotype is associated with neuroprotection, immunosuppression, anti-inflammatory actions, and tissue healing processes (Orihuela et al., 2016). In the vicinity of the damage, M1 are more prevalent than M2 microglia. Researchers have explored the M1/M2 pattern in the context of neurodegenerative diseases to gain insights into the functions of microglia in both protection and degeneration of neurons. M1 microglia releases proinflammatory mediators while M2 microglia produces anti-inflammatory cytokines. The balance between activation of M1 and M2 microglia is shown to be disrupted in neurodegenerative diseases, and consequently, shifting between M1 and M2 states could enhance therapeutic outcomes in these conditions (Tang & Le, 2016).

The function of microglia is not limited to inflammatory or immune responses in the brain, but they can sense and quickly react to changes in the environment (Carson et al., 2007). The idea that all activated microglia are harmful and lead to degeneration is not always accurate since microglia can change their morphology and behaviour based on their specific function. Thus, they may have a positive role in the recovery process of CNS injuries by monitoring and regulating the extracellular environment and eliminating cells that are dead, damaged, or not functioning properly(Harry & Kraft, 2008). Microglia overexpress a variety of surface receptors and produce multiple secreted factors, which can be either pro- or anti-inflammatory, and also have a role in the apoptosis and phagocytosis of infiltrating T cells resulting in the downregulation of microglial immune response(Magnus et al., 2002). Therefore, microglia reactivity is dichotomous and can either promote neuronal survival or degeneration.

Astrocytes are another type of glial cells that can be activated by various stimuli, including inflammation. and constitute approximately 35% of the total CNS cell population. Similar to microglia; astrocytes are localized throughout the CNS, involved in neuroinflammation and their reaction can either aid or harm tissue repair, based on the nature of the stimuli they receive from the inflamed environment.

Astrocytes are involved in various important functions, including regulation of blood flow, preservation of the blood-brain barrier, supplying of energy metabolites to neurons, modulation of synaptic activity, mediating neurotrophin secretion, removal of dead cells, regulation of extracellular ion and fluid homeostasis, neurotransmitter recycling and formation of scar tissue (Colombo & Farina, 2016). The seriousness of astrogliosis, a

characteristic feature of central nervous system (CNS) disorders can be determined by determining differences in the gene expression patterns and morphology of astrocytes using astrocyte-specific glial fibrillary acidic protein (GFAP) (Sofroniew, 2009).

Overall, neuroinflammation is a strictly regulated complex process that can have both beneficial and detrimental effects on the nervous system. Although it is initially a neuroprotective response, chronic and excessive neuroinflammation has been shown to contribute to the pathogenesis of several lysosomal storage and neurological disorders (Bosch & Kielian, 2015a; Wyss-Coray & Mucke, 2002). Therefore, understanding the underlying mechanisms of neuroinflammation is crucial for the development of effective therapeutic interventions for these disorders.

1.4.1. Neuroinflammatory Messengers

Neuroinflammatory responses are caused by the action of numerous vital pro-inflammatory cytokines, such as IL-1β, IL-6, and TNFα, as well as chemokines like CCL2, CCL5, and CXCL10. In addition to these, secondary messengers like nitric oxide and prostaglandins, and reactive oxygen species (ROS) are also involved in mediating the response. Stimulated inhabitant CNS cells, particularly microglia, and astrocytes, are responsible for producing many of these mediators. The release of pro- and/or anti-inflammatory mediators by active microglia and astrocytes regulate downstream pathways leading to either exacerbated inflammation and neurodegeneration or neuroprotection (Singh, 2022). IL-1β (Interleukin 1 beta) is a major proinflammatory cytokine that is released by both microglia and astrocytes in pro-form (pro-IL-1β) which is then activated through cleavage by inflammasome-activated caspase-1 (Lamkanfi & Dixit, 2012; W. Y. Wang et al., 2015). Under neuronal injury conditions; microgliosis causes the transcription of pro-IL-1β, which accumulates in the cell until apoptosis occurs, and then released into the extracellular space. Once extracellular, pro-IL-1β can be cleaved into its active form, IL-1β, by the protease caspase-1, and released after neurodegeneration by apoptosis, necrosis, or shedding from secretory lysosomes or microvesicles(P. Wang et al., 2008). When IL-1β binds to its receptor on a cell, it triggers a series of signals inside the cell that lead to the production of both NF-κB and IL-6 (Allan et al., 2005; Tsakiri et al., 2008). It was suggested that the IL-1β/IL-6 pathway and NF-κB are participating in neuroinflammation and have a significant role in the response to

neuronal injury (Bouma et al., 2009). In addition, IL-1β is known to be released by activated microglia and can bind to the IL1 receptor on astrocytes, leading to the activation of downstream signaling pathways.

When activated by a lipopolysaccharide like IFN-γ or TNF-α, microglia are described as in 'classically activated' M1 form (Boche et al., 2013). These microglia produce proinflammatory cytokines like IL-1β, TNF-α, STAT3, IL-6, IL-12, IL-23 and ROS to fight against pathogens and cancer. However, this form of activation is also linked to neurodegeneration (W. Y. Wang et al., 2015).

Astrogliosis involves several signaling pathways such as NF-κB, JAK/STAT, MAPK, and PI3K pathways, which can result in the production of various substances like inflammatory mediators, growth factors, and ROS. These substances can further influence the duration and extent of astrogliosis in the brain (Giovannoni & Quintana, 2020). One important signaling pathway involved in astrogliosis is the nuclear factor-kappa B (NFκB) pathway. NFκB is a protein that controls the activity of many genes involved in immune responses, inflammation, and cell survival. It gets activated in response to different stimuli, such as proinflammatory cytokines, reactive oxygen species (ROS), and pathogen-associated molecular patterns (PAMPs), and transfers to the nucleus to regulate the expression of specific target genes (T. Liu et al., 2017). In astrocytes, the activation of NFκB leads to the production of molecules such as proinflammatory cytokines, chemokines, and adhesion molecules, as well as the upregulation of iNOS, COX-2, and MMPs (Shih et al., 2015). These molecules are known to contribute to inflammation and tissue damage in the CNS. Consequently, the NFκB pathway is a key player in astrogliosis and the development of various neurological disorders.

Basal level of cytokines and chemokines for example TNF-α and chemokine (C-C motif) ligand 2 (CCL2) release is required for standard physiology of the body (O'Connor et al., 2015). When microglia become active, they release certain chemokines, including CCL2 and CXCL1. In addition to these chemokines, they also release proinflammatory cytokines like IL-12 and TNF-α, as well as anti-inflammatory cytokines like IL-10 and TGF-β.

Pro-inflammatory cytokines released by astrocytes include tumor necrosis factor-α (TNF-α), and interleukin-6 (IL-6). These cytokines can induce inflammation and tissue damage in the CNS by increasing the expression of adhesion molecules, chemokines, and other inflammatory players. Conversely, astrocytes can also release anti-inflammatory cytokines like interleukin-10 (IL-10) and TGF-β. These cytokines can repress microglial

activation and restrict the production of pro-inflammatory cytokines, thus stimulating the resolution of inflammation and tissue repair in the CNS. (Linnerbauer et al., 2020; Norden et al., 2014)

Astrocytes can be triggered by cytokines like TNF-α and IL-1β, which are released by microglia. This astroglial activation cause the initiation of reactive oxygen and nitrogen species production. In a co-culture model, it has been demonstrated that astrocytes boost inflammatory reactions of microglia via an NF-κB-related process (Singh, 2022; Tjalkens et al., 2017).

1.4.2. Neuroinflammation and Oxidative Stress

Reactive oxygen species at basal levels are necessary for maintaining cellular homeostasis, and excessive amounts are eliminated through antioxidant defense mechanisms. Oxidative stress occurs when the balance between the production of ROS within cells and antioxidant defense mechanisms is disrupted (Bardaweel et al., 2018; Ghosh et al., 2017). It has been shown that ROS causing imbalance in redox equilibrium lead to alterations in intercellular signaling pathways, resulting in a loss of signal transduction (Rhee et al., 2003). These changes in signaling pathways eventually activate damage-related molecular pathways, leading to the synthesis of proinflammatory molecules. Microglia serve a vital function in the central nervous system by acting as the primary producers of reactive oxygen species (ROS). This occurs through intracellular peroxidases, oxidative processes within mitochondria, and NADPH oxidase activities located on the cell surface (Block & Hong, 2007).

Oxidative stress is a critical factor in the regulation of the body's inflammatory response. In a state of stability within the redox system, inflammation serves as a protective mechanism, responding to threats, promoting tissue repair, and ultimately self-regulating to prevent excessive damage. This well-controlled, self-regulating inflammatory response is vital for the body's defense against infections, injuries, and various stressors. However, in cases of continuing redox imbalance, as often observed in CNS-related diseases like Alzheimer's or Parkinson's disease, the intricate pathways that normally modulate the immune system become disrupted (Goldsteins et al., 2022). This disruption can lead to a dysregulation of the immune response. The immune system, which typically maintains a balanced equilibrium between pro-inflammatory and anti-

inflammatory processes, begins to shift towards a pro-inflammatory predominance. This pro-inflammatory dominance can contribute to the chronic, progressive, and destructive nature of neurodegenerative diseases. In these conditions, the body's immune response may become excessive and sustained, which can result in the chronic activation of inflammatory pathways and the production of harmful substances, ultimately causing damage to nervous tissue and exacerbating the disease process(Cappellano et al., 2013). As mentioned in cases of persistent redox imbalance, these reactive species like ROS and RNS can turn harmful by oxidizing proteins and lipids and potentially causing DNA damage (Pizzino et al., 2017).Therefore, understanding and addressing the role of oxidative stress in this context is crucial for developing effective therapies to manage neurodegenerative diseases and restore the delicate balance of the immune response (De la Fuente, 2019; Morris et al., 2022).

Reactive species can also initiate signaling processes that enable microgliosis and astrogliosis (Forrester et al., 2018). Furthermore, when they exist at elevated levels within various cell types, ROS can stimulate signaling pathways that perpetuate the excessive release of proinflammatory modulators. The pro-inflammatory modulators like IL-6, IL-1β, TNF, and IFNs, have been shown to have the ability to induce ROS generation in specific cell types (Yang et al., 2007).

1.4.3. Neuroinflammation in Lysosomal storage disorders

Chronic neuroinflammation is associated with the pathogenesis of several neurological disorders, including Alzheimer's disease and Parkinson's disease (Kempuraj et al., 2016). In Alzheimer's disease, amyloid beta plaques activate microglia, which release pro-inflammatory cytokines and chemokines that exacerbate inflammation and contribute to the degeneration of neurons (W. Y. Wang et al., 2015). Similarly, in Parkinson's disease, alpha-synuclein aggregates can activate microglia and astrocytes, leading to the production of pro-inflammatory cytokines and chemokines that exacerbate inflammation and contribute to the degeneration of dopaminergic neurons (Isik et al., 2023; Q. Wang et al., 2015).

The buildup and incorrect positioning of substrates in lysosomal storage disorders (LSDs) can affect signaling pathways (Scerra et al., 2022). For example, fragments of glycosaminoglycans attached to proteoglycans can interfere with signaling pathways in

Mucopolysaccharidoses (Couchman & Pataki, 2012). Similarly, gangliosides, sphingolipids, and cholesterol accumulating in Lipidoses can form specialized cell surface domains that participate in signaling pathways (Quinville et al., 2021). When these pathways are altered, it can lead to changes in autophagy and mitophagy, causing neuroinflammation and storage of lysosomal substrates, contributing to the phenotypes observed in individuals with LSDs.

As mentioned above; LSDs are a group of inherited metabolic disorders with the accumulation of undigested materials in the lysosomes of various tissues including the brain. Among the various pathological mechanisms contributing to the neurodegeneration observed in LSDs, neuroinflammation has been proposed to play a critical role (Bosch & Kielian, 2015b). In LSDs, the accumulation of undigested materials in the lysosomes of glial cells triggers the activation of these cells and the release of pro-inflammatory cytokines and chemokines. This leads to the recruitment of more immune cells to the CNS and the activation of microglia and astrocytes, resulting in chronic neuroinflammation (Kreher et al., 2021).

Neuroinflammation in LSDs has been implicated in the pathogenesis of various neurological symptoms including seizures, cognitive impairment, and motor dysfunction (Bosch & Kielian, 2015b; Gorji, 2022). In addition, neuroinflammation is thought to contribute to the progression of the disease and exacerbate the neurodegeneration observed in LSDs. The mechanisms underlying the interaction between neuroinflammation and LSDs are complex and multifaceted, involving various signaling pathways and cellular mechanisms (Batista et al., 2019; Kinney et al., 2018; Kwon & Koh, 2020)

Recent studies have identified potential therapeutic strategies for targeting neuroinflammation in LSDs, including the use of anti-inflammatory agents and immunomodulatory drugs. However, the effectiveness of these therapies remains to be fully evaluated in clinical trials. In conclusion, neuroinflammation plays a critical role in the pathogenesis of neurodegeneration in LSDs and represents a promising target for the development of novel therapeutic strategies for these devastating disorders.(P. Liu et al., 2022; Moore & O'Banion, 2002)

1.5. Neuroinflammation in GM2 Gangliosidosis mouse models

Mouse models of GM2 gangliosidoses have been extensively studied to understand the mechanisms underlying the neuroinflammatory response in these disorders. Hexa-/- mice, which lack the Hexa gene encoding hexosaminidase A, show evidence of neuroinflammation, including activation of microglia and astrocytes, and increased expression of cytokines and chemokines in the brain. Neuropathological changes, such as neuronal loss and astrogliosis, are also observed in these mice.(Lawson & Martin, 2016; Leal et al., 2020)

Similar to Hexa-/- mice, Hexb-/- mice, which lack the Hexb gene encoding hexosaminidase B, also show evidence of neuroinflammation. Microglial activation and increased levels of cytokines and chemokines have been reported in the brain of Hexb-/- mice. Furthermore, infiltration of T cells into the CNS has been observed in these mice, suggesting a role for adaptive immunity in the neuroinflammatory response (Kyrkanides et al., 2008, 2012).

Recent studies have focused on investigating the contribution of different cell types to the neuroinflammatory response in GM2 gangliosidoses. For example, it has been shown that microglia are the primary cell type responsible for cytokine production and astrocytes in *Hexa-/-Neu3-/-* mice show a reactive phenotype, characterized by increased expression of GFAP and other markers of astrogliosis (Demir et al., 2020). Additionally, In *Hexa-/-Neu3-/-* TSD mouse model, decreased oligodendrocyte level, elevated proinflammatory cytokine release were observed in cortex cerebellum thalamus and hippocampus region and microgliosis was also demonstrated in this model (Demir et al., 2020). In summary, neuroinflammation is a prominent feature of GM2 gangliosidoses in mouse models. Microglial and astrocyte activation, cytokine production, and infiltration of immune cells into the CNS are some of the hallmarks of the neuroinflammatory response in these disorders. Understanding the mechanisms underlying neuroinflammation in GM2 gangliosidoses may provide new insights into the pathogenesis of these disorders and identify potential targets for therapeutic intervention.

1.6. Therapeutic Approaches for Neuroinflammation

Neuroinflammation is an intricate procedure characterized by the stimulation of immune cells within the central nervous system (CNS) and the discharge of molecules that promote inflammation. This process holds significant importance in the context of neurodegenerative conditions like Alzheimer's, Parkinson's disease, multiple sclerosis and lysosomal storage disorders. Therapeutic approaches for neuroinflammation in these disorders aim to reduce inflammation and prevent further damage to neurons.(Zhang et al., 2023)

One approach to treating neuroinflammation involves the usage of non-steroidal anti-inflammatory drugs (NSAIDs) such as ibuprofen, aspirin, and naproxen. These drugs can reduce inflammation by inhibiting the activity of enzymes that produce pro-inflammatory molecules such as cytokines and prostaglandins (Krause & Müller, 2010). Nevertheless, the extended utilization of NSAIDs has been linked to adverse effects, including the potential for gastrointestinal bleeding and an elevated risk of heart disease (Meek et al., 2010).

Another approach is to target specific components of the inflammatory pathway. For example, monoclonal antibodies that target pro-inflammatory cytokines such as tumor necrosis factor-alpha (TNF-α) have been developed for the treatment of multiple sclerosis and rheumatoid arthritis(Jang et al., 2021; Sedger & McDermott, 2014). Other strategies include the use of small molecule inhibitors of inflammatory enzymes and the modulation of signaling pathways involved in inflammation (Dinarello, 2010).

Recently, there has been interest in using immunomodulatory therapies to treat neuroinflammation in neurodegenerative disorders. This involves the use of drugs that target immune cells in the CNS, such as microglia and astrocytes (Kopp et al., 2023; Mortada et al., 2021). These cells play a crucial role in neuroinflammation by releasing pro-inflammatory molecules and engulfing damaged neurons. Immunomodulatory therapies aim to either suppress the activity of these cells or promote their anti-inflammatory properties (Strzelec et al., 2023).

Another promising therapeutic approach for neuroinflammation is the use of stem cells. Stem cells can undergo differentiation into a range of cell types, including neurons and immune cells (Cecerska-Heryć et al., 2023; Joshi et al., 2021). Transplantation of stem cells has been shown to reduce inflammation and promote neural regeneration in

animal models of neurodegenerative disorders (De Gioia et al., 2020; Sivandzade & Cucullo, 2021).

In conclusion, neuroinflammation is a complex process that plays a crucial role in neurodegenerative disorders. Therapeutic approaches for neuroinflammation aim to reduce inflammation and prevent further damage to neurons. While current treatments are limited, ongoing research into immunomodulatory therapies and stem cell transplantation holds promise for the development of more effective treatments for neuroinflammation in the future**.**

1.7. A2A Receptor

The purine nucleoside adenosine serves as a modulating compound with a wide range of functions in various organs and tissues. One of its most notable roles is in regulating the functions of the central nervous system (CNS) under both normal and abnormal conditions. Adenosine interacts with four distinct receptors known as A1, A2A, A2B, and A3 receptors. Despite its typically low concentrations in the extracellular environment, situations involving metabolic stress substantially elevate the levels of adenosine in the extracellular space (Haskó et al., 2005).

The adenosine A2A receptor is a G protein-coupled receptor that is widely distributed in the brain, particularly in the striatum, where it is highly expressed in medium spiny neurons. It plays an important role in modulating dopaminergic transmission and has been associated with a variety of neurological and psychiatric disorders, including Parkinson's disease, Huntington's disease, schizophrenia, and addiction (Pinna et al., 2020).

When the A2A receptor is activated, it triggers adenylate cyclase, resulting in the generation of cyclic AMP (cAMP). This, in turn, activates protein kinase A (PKA) and various other signaling pathways downstream. Additionally, A2A receptor activation can influence ion channels and the release of neurotransmitters like dopamine, glutamate, and GABA (Ibrisimovic et al., 2012).

The A2A receptor has become an attractive target for drug development due to its involvement in various neurological and psychiatric disorders. In Parkinson's disease, A2A receptor antagonists have been shown to improve motor function and reduce dyskinesias when used in combination with L-DOPA (Jenner, 2014; Mori et al., 2022).

In Huntington's disease, A2A receptor antagonists have been shown to improve motor and cognitive function in animal models, although clinical trials have been less successful (Franco & Navarro, 2018).

Overall, the adenosine A2A receptor is a complex signaling molecule that plays an important role in the modulation of dopaminergic transmission and neurotransmitter release in the brain. Targeting the A2A receptor has the potential to provide therapeutic benefits for a wide range of neurological and psychiatric disorders.(Haynes et al., 2019; Wydra et al., 2020)

In a study conducted on the Hexb-/- mouse model, another GM2 gangliosidosis model similar to Sandhoff disease, a strong increase in astrocytic A2A receptor expression was observed in Hexb-/- mice. Furthermore, this study demonstrated that this increase in A2A receptors triggered ccl2 expression in the Sandhoff mouse model, leading to increased microglial activation. To reverse these effects observed in the Sandhoff mouse model, a drug called istradefylline, an A2A receptor antagonist, was used. This resulted in a reduction in ccl2 chemokine expression, decreased microglial activation, and improvement in motor functions (Ogawa et al., 2018). Moreover, adenosine receptors have been reported to exhibit cytoprotective effects against hypoxia and ischemia (Kobayashi & Millhorn, 1999; von Lubitz, 1999). This protective effect is believed to be achieved through the regulation of oxidative stress by modulating antioxidant defense mechanisms (Huang, 2003). Many studies have explained the involvement of oxidative stress triggered by reactive oxygen species (ROS) and mitochondrial dysfunction in the etiology of neurodegenerative disorders and lysosomal storage diseases (X. Chen et al., 2012; Stepien et al., 2020).

1.7.1. Istradefylline & Parkinson Disease

Glial cells of the central nervous system like monocytes, macrophage, oligodendrocytes microglia and astrocytes are types of immune cells that express wide range of chemokine receptors, one of which is CCR2 (CC-chemokine receptor 2)(Baaklini et al., 2019; Charo & Ransohoff, 2006). It has been found that CCR2 have a role in the infiltration of peripheral blood mononuclear cells into the brain (Cui et al., 2020; Izikson et al., 2000). Additionally, research demonstrated that mice with deficiency of CCR2 was resistant to experimental autoimmune encephalitis (Fife et al., 2000; Gaupp

et al., 2003). Furthermore, in Alzheimer's disease brains, the CCL2, which is the primary ligand for CCR2, is found to be upregulated. This provides more evidence that CCR2 have a crucial role in facilitating the trafficking of microglial precursor cells into the brain affected by Alzheimer's disease (Azizi et al., 2014). These findings have implications for our understanding of neurological conditions and may offer insights into potential therapeutic strategies targeting CCR2-CCL2 axis to modulate the immune response in the brain. In this thesis study, we aimed to target CCR2 receptor to reduce neuroinflammation in *Hexa-/-Neu3-/-* mouse model. Previously, researchers have shown that astrocytes of Hexb-/- mice model overexpresses adenosine A2A receptor which in turn increases ccl2 expression in astrocytes (Ogawa et al., 2018). A2A receptors are key modulators in adenosine signaling in brain and increased activity of them led to neurodegenerative effects (Stockwell et al., 2017). It has been implicated in several neurodegenerative disorders and antagonism against this receptor have been studied in clinical research (Kondo & Mizuno, 2015; Yuzlenko & Kiec-Kononowicz, 2006). Istradefylline is an FDA approved nondopaminergic drug which works as an antagonist of A2A receptor and widely used for Parkinson disease along with L-DOPA to reduce “off” episodes observed in patients (Cummins & Cates, 2022).

Parkinson's disease is a neurodegenerative condition marked by the depletion of neurons that produce dopamine in the substantia nigra area of the brain. Adenosine A2A receptor antagonists like istradefylline have been shown to have a beneficial effect on the symptoms of Parkinson's disease by increasing the release of dopamine in the striatum, a region of the brain involved in the control of movement.

Istradefylline works by blocking the adenosine A2A receptor, which is a G protein-coupled receptor that is widely distributed in the brain. Adenosine is a neuromodulator that can have both inhibitory and excitatory effects on neuronal activity, depending on the receptor subtype and the region of the brain involved. In Parkinson's disease, the A2A receptor is overexpressed in the striatum, where it can inhibit the release of dopamine and exacerbate the symptoms of the disease.

Several clinical trials have shown that istradefylline can improve motor function and reduce "off" time (periods of decreased mobility and increased symptoms) in patients with Parkinson's disease who are already receiving standard therapy with levodopa and other medications. The drug is generally well-tolerated, with the most common side effects being dyskinesias (abnormal involuntary movements), hallucinations, and dizziness.

Overall, istradefylline represents a promising new approach to the treatment of Parkinson's disease that targets the adenosine A2A receptor, a novel mechanism of action that has the potential to improve the quality of life for millions of patients suffering from this debilitating condition.

1.8. Aim of the Study

Neuroinflammation and neurobehavioral pathology have been previously observed in *Hexa-/-Neu3-/-* TSD model. In this thesis study, it was aimed to reduce neuroinflammation and accordingly neuropathology by istradefylline administration in TSD mouse model with three different administration strategies. The purpose was to determine whether anti-inflammatory therapy is effective to reduce neuroinflammation and which strategy of istradefylline administration is the most effective to reverse the pathology in brain tissue of *Hexa-/-Neu3-/-* mice.

CHAPTER 2

MATERIALS AND METHODS

2.1. Mouse Genotyping

DNA was extracted from fresh tail tissue using 250 µL of lysis buffer (10% Tris-HCl pH:7.6, 2.5% 0.2M EDTA, 20% SDS, 4% 5M NaCl) and 6 ul proteinase K (25 µg/µl, Sigma) and incubated overnight in shaking incubator at 55^{o}C / 70rpm. Homogenized samples were centrifuged at 14000 rpm for 10 minutes. and same volume of isopropanol (100%) were added on supernatant. After precipitating the DNA by isopropanol; DNA was collected and put into 70% ethanol. 1 min centrifugation at 14000 rpm was performed in order to precipitate DNA and remove ethanol. Remaining ethanol was air dried and DNA samples were dissolved in ultrapure water.

PCRs for Hexa and Neu3 gene amplification were performed by using 100ng genomic DNA in 25ul reaction mixture: (25µl reaction mix containing 50pmol of each primer (Table2.1), 10mM of dNTP mix, 1.5 units Taq polymerase (GeneAid), 1.5mM MgCl2, 10mM Tris-HCl and 50mM KCl buffer containing 10% DMSO. Conditions for PCR are; 1 cycle 30 seconds at 95˚C; 30 cycles 30 seconds at 95˚C, 45 seconds at 60˚C, 45 seconds at 72˚C; and 1 cycle 5 minutes at 72˚C).

Table 2.1. Primer sequences used for genotyping of Hexa and Neu3 alleles

Gene	Primer	Primer Sequence
Neu3	Neu3 Forward	5’-CTCTTCTTCATTGCCGTGCT-3’
	Neo Forward	5’-GCCGAATATCATGGTGGAAA-3’
	Neu3 Reverse	5’-GACAAGGAGAGCCTCTGGTG-3’
HexA	HexA Forward	5’-GGCCAGATACAATCATACAG-3’
	PKG Forward	5’-CACCAAAGAAGGGAGCCGGT-3’
	HexA Reverse	5’-CTGTCCACATACTCTCCCCACAT-3’

2.2. Drug Treatment

In order to reduce neuroinflammation and reverse neuropathology istradefylline was selected as neuroinflammatory drug for the study and 3 different strategies were used for its administration (Figure 2.1). In the 1st strategy, which is also called early-stage treatment, *Hexa-/-Neu3-/-* mice were intraperitoneally injected by 3mg/kg istradefylline daily for 21 days starting from 10week to 13week and sacrificed at the end of injection time. To determine the effects of late-stage treatment 2nd strategy in which the *Hexa-/-Neu3-/-* mice were intraperitoneally injected by 3mg/kg istradefylline daily for 21 days starting from 16week to 19week was employed and sacrificed at the end of injection time. For the last strategy, continued treatment strategy with a wash out phase was applied. In the 3rd strategy intraperitoneal istradefylline was administered from 10th to the 13th week; after 3 weeks of no drug treatment the injection was continued from the 16th to the 19th week and mice were sacrificed at the end of second injection.

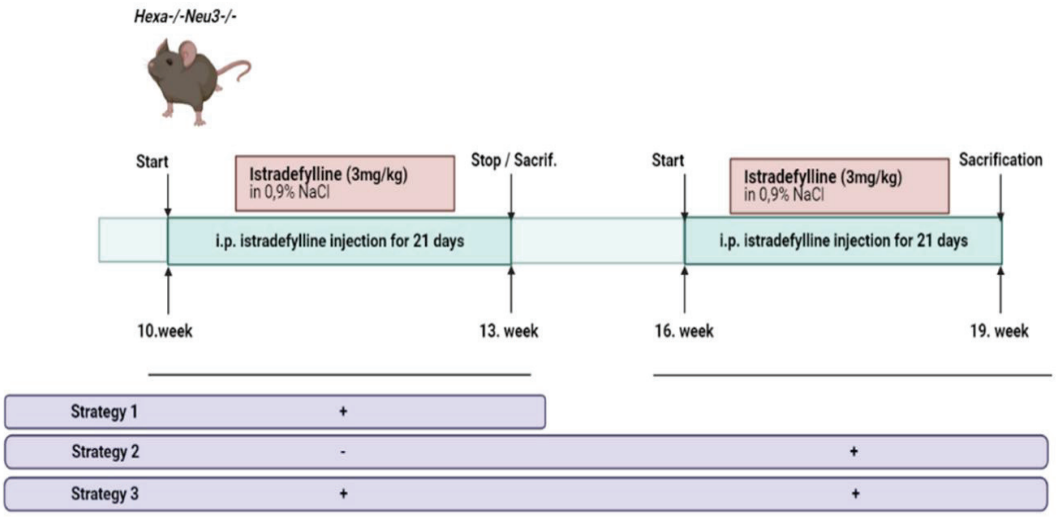

Figure 2.1. The schematic illustration of istradefylline administration strategies in Hexa-/-Neu3-/- mice as early-stage (10w-13w), late-stage(16w-19w) and two stage treatment (10w-13w & 16w-19w) group with 3mg/kg intraperitoneal istradefylline injections.

2.3. Tissue Handling

Untreated *WT, Hexa-/-* and *Hexa-/-Neu3-/-* were used as control samples. For early stage 13W-old; for late and two-stage treatments 19W-old age-matched mice were used as controls. Brain samples of control and treatment groups were collected by either dissection or fixation.

2.3.1. Brain Dissection

Age matched control and treatment groups of *WT, Hexa-/-* and *Hexa-/-Neu3-/-* were sacrificed by using CO_2 cabinet. The brains were dissected into two halves of cortex and cerebellum by using dissector blade. All tissue samples were quick frozen in liquid nitrogen and stored in -80^{o}C until required.

2.3.2. Fixation

In order to be able to perform immunohistochemical analysis, the brains required to be fixated by applying trans cardiac perfusion. Ksilazin and ketamine were used to anesthetize the mice by intraperitoneal injection. An incision was made through abdomen and thoracic cavity was opened by cutting through rib cage. When the heart is exposed the needle was inserted to the left ventricle in a secure position and right atrium was cut by a sharp scissors and ~10ml 0.9% NaCl solution (pH 7.4) was flowed through circulation system. After the mice drained from blood, circulation of NaCl was switched to freshly prepared 4% paraformaldehayde in 1XPBS and circulated until all of the organs were fixed (~10ml). Excised brains were incubated in 4%paraformaldehyde solution at +4^{o}C overnight. Then the samples were put through sucrose gradient in which they were incubated 2 hours in each of 10%, 20% and 30% sucrose in 1X PBS solution (pH 7.6) at +4^{o}C. In 30% sucrose, samples were incubated overnight. After that incubation, the brains were embedded in OCT (optimal cutting temperature) containing cryomolds and they were slowly frozen in dry ice containing buckets. Tissues were stored at -80^{o}C. By using Leica Cryostat, 10μm coronal sections of each brain were sectioned and collected on

adhesive-coated slides. These slides were also stored at -80ºC for further immunohistochemical analysis (Risher et al., 2014; Schneider Gasser et al., 2006).

2.4. Real Time PCR

Real time PCR protocol is comprised of mainly three steps as: RNA isolation, cDNA synthesis, and RT-PCR procedures.

2.4.1. RNA Isolation

50 mg of each brain region (cortex and cerebellum) of both control and treatment groups were measured and homogenized in 500µl GeneZol (GeneAid) with sterilized RNase free teflon beads by using tissue homogenizator (Retsch MM100). After that, samples were incubated at room temperature for 5 minutes and transferred into 1.5 ml tubes. 100µL chloroform was added on each sample and the tubes were shaken vigorously for 10 seconds. In order to provide phase separation, the samples were centrifuged at 15000g for 15 minutes at +4ºC. After the successful phase separation occurred colorless aqueous upper level containing RNA were transferred into new 1.5 ml Eppendorf tube and one volume of isopropanol (~200-300µl) was added on each sample. The tube was inverted several times, incubated for 10 minutes at room temperature and then centrifuged for 10 minutes at 15000g at +4ºC to provide tight RNA pellet formation. Supernatants were carefully discarded and 1ml 70% ethanol was added on each sample to wash the RNA and they were centrifuged again for 5 minutes at 15000xg at +4ºC. Supernatants were carefully removed and the RNA pellets were air-dried at 55ºC for 5 minutes. RNA pellets were resuspended in 20-50µl RNase free water and they were incubated in water bath at 50ºC for 10 minutes to provide dissolving of RNA pellet in water. Finally, concentrations of RNAs were measured by using NanoDrop Spectrophotometer (ND-1000).

2.4.2. cDNA Synthesis

Isolated RNA's were converted into cDNAs by using EvoScript Universal cDNA Master (Roche). 50ng/ul cDNA producing reaction mix was prepared according to

manufacturer's instruction. Initially, the concentration of RNAs were measured by NanoDrop. The reaction mix was composed of 1 X RT buffer, 4 mM dNTP mix, 1X RT Random primers, 50 units MultiScribe Reverse Transcriptase were mixed with calculated volume of water and RNA depending on the RNA concentration level of each sample. Total volume of the mixture was arranged to be 20 ul. The reaction was conducted with the conditions: 1 cycle 10 minutes at 25˚C; 1 cycles 120 minutes at 37˚C, 1 cycle 5 minutes at 85˚C.

2.4.3. RT-PCR

The relative gene expression levels of the genes listed in Table-x were analyzed by RT-PCR for cortex and cerebellum region of control and treatment groups. Primer sequences of genes of interest are presented on the Table 2.1 and expression levels were measured by using Roche LightCycler® 96 System with Roche LightCycler 480 SYBR Green I Master Mix. The reaction mixture was optimized as 20µl reaction mix containing 0.4 uM each primer (Table 2.2) and 1X Roche LightCycler 480 SYBR Green I Master Mix and 75ng cDNA. The reaction was performed under conditions: 1 cycle 10 minutes at 95˚C; 45 cycles 20 seconds at 95˚C, 15 seconds at 60˚C, 22 seconds at 72˚C. For each sample triplicate technique replicas were prepared and average of the three results were used as gene expression level of sample of interest. The gene expression levels were normalized to GAPDH as internal control and gene expression ratio was calculated by ΔCt method. One-way ANOVA was used for statistical analysis through Graphpad Prism Software.

Table 2.2. Primer sequences and RT-PCR product length of the genes to be analyzed

Gene	Primer Sequences	PCR Product
CCL2	F: 5'-ATGCAGTTAATGCCCCACTC-3' R: 5'-TTCCTTATTGGGGTCAGCAC-3'	167 bp
CCL3	F: 5'-TCTGTACCATGACACTCTGC- 3' R: 5'- AATTGGCGTGGAATCTTCCG-3'	103 bp
CXCL10	F: 5'- GACGGTCCGCTGCAACTG-3' R: 5'-CTTCCCTATGGCCCTCATTCT -3'	64 bp
CCL5	F:5'-AGTGCTCCAATCTTGCAGTC-3' R:5'-AGCTCATCTCCAAATAGTTG-3'	108 bp
GFAP	F: 5'-AGTAACATGCAAGAGACAGAG-3' R: 5'- TAGTCGTTAGCTTCGTGCTTG-3'	113 bp
IL-1β	F:5'-TGAGTCACAGAGGATGGGCTC-3' R:5'-CCTTCCAGGATGAGGACATGA-3'	71 bp
IL-6	F:5'-AAGTGCATCATCGTTGTTCATACA-3' R:5'-GAGGATACCACTCCCAACAGACC-3'	141 bp
SOD2	F:5'- GTGTCTGTGGGAGTCCAAGG -3' R:5'- CCCCAGTCATAGTGCTGCAA -3'	339 bp
Catalase	F:5'- TTCGTCCCGAGTCTCTCCAT -3' R:5'- GAGGCCAAACCTTGGTCAGA -3'	351 bp
Ttase1	F:5'- CTGCAAGATCCAGTCTGGGAA -3' R:5'- CTCTGCCTGCCACCCCTTTTAT -3'	322 bp
HexB	F: 5'- AGTGCGAGTCCTTCCCTAGT -3' R: 5'- ATCCGGACATCGTTTGGTGT -3'	412 bp
GM2AP	F: 5'- CCTCACGATCCAACCTGACC -3' R: 5'- CTTCCCACCACTGCTCAAGA -3'	388 bp
GAPDH	F:5'- CCCCTTCATTGACCTCAACTAC-3' R:5'- ATGCATTGCTGACAATCTTGAG-3'	347 bp

2.5. Immunohistochemistry

The fixated brain samples for both control and treatment groups were sectioned into 10um cryosections on HistoBond slide by using Leica Cryostat (CM1850-UV).

Firstly, the slides were incubated on ice for 30 minutes and then they were washed with 1X PBS for 10 minutes. To enable permeabilization of plasma membranes; incubation in 100% acetone for 10 minutes was applied and then they were washed twice with 1X PBS for 5 minutes. To avoid nonspecific binding; the slides were incubated in blocking solution (10% goat-serum, 4%BSA, 0.3M Glycine in 1X PBS) for 1 hour at room temperature. After that, primary antibodies (GFAP, MOMA-2, LAMP1, CNPase,) dissolved in blocking solution were added on each brain sample on the slides and incubated overnight (16 hours) at +4^{o}C. Following day; the slides were washed three times with 1XPBS and incubated in humidity chamber for 1 hour at room temperature with secondary antibody solution which includes 1/500 of antibody of interest (ab175476, Alexa Fluor®-568 and ab150077 Alexa Fluor®-488) in blocking solution. After that the slides were washed three times with 1XPBS- and they were mounted on slides with Fluoroshield mounting medium DAPI (abcam). Images were obtained by using fluorescent microscope (Olympus BX53). Co-localization analysis of red and green fluorescence was applied by using ImageJ.

2.6. Thin Layer Chromatography

In order to measure GM2 ganglioside accumulation level, thin layer chromatography protocol comprising of Ganglioside isolation, TLC and orcinol staining of plates by using cortex and cerebellum regions of control and treatment groups.

2.6.1. Ganglioside Isolation

The isolation of acidic gangliosides and their visualization were generated by using brains of both control and treatment groups according to the previously optimized protocol in our laboratory.

2.6.1.1. Neutral and Acidic Ganglioside Isolation

In order to isolate ganglioside molecules, ~50mg of brain tissues -cortex and cerebellum- from both control and treatment groups (9 samples totally) were homogenized in the borosilicate tubes with 2ml of dH_2O via the ultra turax homogenizer

(IKA T10, Sigma, Darmstadt, Germany) at 6000rpm for 30 seconds. Then, sonication was performed to homogenized samples by using sonicator (Bandelin-sonopuls, Berlin, Germany) for 4 cycles of 1.5minutes after. Next, the H_2O in the samples were evaporated by using a nitrogen flow in the Reacti-Therm Heating module (Thermo, Massachusetts, USA). After evaporation of entire water, 3ml of 100% acetone were added the pellet and the tubes were vortexed and centrifuged at 2000rpm for 5 minutes. This process was repeated on two occasions to ensure the thorough removal of phospholipids and other lipid components from the membrane. Then the pellets were washed twice by 1.5ml of chloroform: methanol: water (10:10:1) solution and centrifuged each time at 2000 rpm for 5 minutes. During this washing steps; each supernatant was collected into new neutral glass tubes by using Pasteur pipettes and first step of ganglioside isolation was started by this way. After that, 2ml of a chloroform: methanol: water (30:60:8) solution was added to pellets twice and the samples were centrifuged each time again at 2000rpm for 5 minutes. Supernatant from each step were put over the previously collected supernatants and the collected solution at the end contained both acidic and neutral gangliosides which were separated by using the DEAE Sephadex A-25 ion exchange columns. For this purpose, we freshly prepared the DEAE Sephadex columns. 1 gr of DEAE Sephadex A-25 resin (GE Health Care, Little Chalfont, United Kingdom) were incubated in 10 ml of chloroform: methanol: 0.8M sodium acetate (30:60:8) solution for 5 minutes. After the incubation, the solution including resin particles were centrifuged at 2000rpm for 1 minute and the supernatant was removed. Resins were washed with the same solution twice and left for overnight incubation in 10 ml of chloroform: methanol: sodium acetate (0.8M) (30:60:8). Following day, the resins were washed twice again with the same solution as described above and the DEAE Sephadex A-25 resin were ready to use at the end. In order to prepare the glass separation colons; tips of glass Pasteur pipettes closed with glass woolen and freshly prepared resin was loaded on top of glass woolen up to 2cm height. The columns were washed twice with 1ml of chloroform: methanol: water (10:10:1) solution, and 1ml of chloroform: methanol: water (30:60:8) solution respectively, and new neutral glass tubes were placed under the columns. Then the total ganglioside samples were loaded onto the column. After the total ganglioside solution was passed through the column, 4ml of 100% methanol were used to wash the column. The resulting solution in the neutral tubes under the columns were collected as neutral gangliosides and these were subjected to evaporation by a nitrogen flow in the Reacti-Therm Heating module (Thermo, Massachusetts, USA) and stored at +4°C until the TLC

analyses. In order to elute acidic gangliosides from columns, 5ml of 500mM potassium acetate in methanol were passed through the columns and collected in new neutral tubes. Then desalting procedure with the Supelclean LC-18 column (Supelco, Sigma, Darmstadt, Germany) were performed by locating specific columns called LC-18 columns in the Chromabond Vacuum manifold (Macherey-Nagel, Düren, Germany) fixed to 5Hg. Firstly, the columns were equilibrated by washing with 2ml of methanol, and with 2ml of 500mM potassium acetate in methanol solution. Then, collected acidic ganglioside samples were added onto the columns and the column bound samples were washed with 10ml of dH_2O. Desalted acidic gangliosides were eluted by 4ml of methanol and 4ml of chloroform: methanol (1:1) under low vacuum into new tubes. Lastly, the water in the eluted samples were evaporated by nitrogen flow in the Reacti-Therm Heating module (Thermo, Massachusetts, USA) and the pellets were stored at +4°C.

2.6.2. Thin Layer Chromatography

The Thin Layer Chromatography (TLC) is process to separate and determine gangliosides according to their specific weights and structures. Firstly, to remove the humidity, 20cm x 20cm silica TLC plates (Merck, New Jersey, USA) were incubated at 100°C for 30minutes. Then, TLC running solution containing Chloroform: methanol: 0.2% $CaCl_2$ (30:65:8) were prepared and poured into the TLC tank (Camag, Muttenz, Switzerland). The tank with solution were incubated for 2hours at RT. Acidic and neutral ganglioside samples stored at +4°C in N_2-dried forms were resuspended in 100µl of chloroform: methanol: water (10:10:1) solution and were loaded onto the previously heated silica plates with the Linomat 5 (Camag, Muttenz, Switzerland) machine automatically. After loading was completed, the plates were placed onto the solution in pre-incubated tanks to run until the endpoint of approximately 10 cm at room temperature.

2.6.3. Orcinol Staining of Plates

After running of the gangliosides on TLC plates were completed, the visualization of gangliosides was obtained by using freshly prepared Orcinol (Sigma, Darmstadt, Germany) stain. The orcinol is prepared with 0.06g of orcinol, 3.75ml of sulphuric acid and 11.25ml of dH_2O in sprayer and used at room temperature. The solution were sprayed

on TLC plates and the plates were incubated on TLC plate heater (Camag, Muttenz, Switzerland) at 120°C until the ganglioside bands becomes visible. Lastly, the plates with visible ganglioside bands were scanned and the band intensities were measured by NIH ImageJ program.

2.7. Western Blot

Western blot protocol comprised of 3 sub steps as protein isolation, Bradford assay and SDS-PAGE gel electrophoresis.

2.7.1. Protein Isolation

In order to obtain protein lysates of cortex and cerebellum regions of both control and treatment groups were homogenized with mini manual homogenizator in 500ul protein lysis buffer (1% TritonX100, 50mMHepes, 150mM NaCl, 10%Glycerol, 50mM Tris-Base, 1%PMSF, 1% protease inhibitor). Once the tissues were homogenized thoroughly, the samples were incubated on ice for 1 hour and during that they vortexed every 10 minutes. Then the samples were centrifuged for 15 minutes at 0^{o}C 14000rpm. Supernatants with isolated proteins were collected into fresh tubes.

2.7.2. Bradford Assay

In order to create a standard curve to be able to calculate protein concentrations of the samples, BSA solutions with different concentrations (100,80,40,20...ug/ml) were prepared by serial dilution. Isolated proteins were diluted 1:20 ratio (2ul protein+38ul dh2o) and 5ul diluted protein samples and each of the BSA solutions for curve were added to the 96well plate and 200ul Bradford Reagent (Sigma) was added onto each sample on 96 well plate. After 10 minutes incubation in dark at RT, the absorbance levels of the samples were measured at 595nm by using microplate reader (BioRad). By using the absorbance level of serially diluted BSA solutions; standard curve graph was plotted and curve equation was calculated. By using this equation, concentrations of each sample were calculated and 20ug of each protein were prepared with 4:1 loading buffer (40%

Glycerol, 240mM Tris-HCl pH 6.8, 8%SDS, 0.04%Bromophenol Blue, 5% β-mercaptoethanol. Boiling the protein samples in loading dye including β-mercaptoethanol enables disruption of 3D structures of proteins by breaking the disulphide bonds.

2.7.3. SDS-PAGE Gel Electrophoresis

Resolving gel and stacking gel were prepared with the ingredients listed in the Table 2.3 and two gels were poured up over each other after the first one dried with a comb inserted in stacking gel.

Table 2.3. Ingredients for resolving and stacking gel preparation of SDS-PAGE gel

Resolving Gel(10%)	**Stacking Gel (5%)**
3 ml Lower buffer (1.5 M Tris-HCl)	1.5 ml Upper Buffer (1M Tris-HCl)
4 ml Acrylamide (30%)	1 ml Acrylamide (30%)
5 ml Water	3.5 ml Water
60µl SDS (10%)	60µl SDS (10%)
60µl APS (10%)	60µl APS (10%)
6 µl TEMED	6 µl TEMED

After the gels were polymerized and the comb was removed; the glass was taken out from casting frames and set into the cell buffer dam. Running buffer (0.25M Tris-Base, 1.92M Glycine, 1%SDS) was poured into the inner chamber and overflowed to outer chamber. After Bradford assay prepared protein samples were loaded into the wells upon boiling. The proteins were separated by SDS-PAGE gel electrophoresis at 80V until the proteins passed the stacking gel then the volt is increased to 120V. Then the proteins were transferred onto the nitrocellulose membrane (BioRad) by transfer buffer (48mM Tris-Base, 39mM Glycine, 20%Methanol, pH 9.2) and running at 250mA for 1hour. After that, to avoid nonspecific bindings blocking was performed by incubation in 5%milk in PBS-T for 1hour with shaking at room temperature. After rinsing and washing the milk, the blots were incubated overnight at +4^{o}C in primary antibodies of NFκB(1:1000, abcam, ab137708), IκB(1:1000, abcam, ab137708), APE1/Ref-1 (1:1000, abcam, ab137708), β-actin (1:1000, cell signalling, 4970) in red solution (5%BSA, 0.02% NaAzide, Phenol Red, in PBS-T pH 7.5). The blots were washed three times with PBS-T solution for 10

minutes followed by incubation with HRP-conjugated secondary antibody (Jackson ImmunoResearch Lab) for 1 hour at room temperature. Then the blots were washed three times again and the proteins were visualized by using LuminataTM Forte Western HRP Substrate (Millipore) on a digital imaging system (Fusion SL, Vilber).

2.8. Behavioral Analysis

In order to determine whether three different strategies of istradefylline treatment affects locomotory functions or anxiety of the mice control and treatment groups were analyzed by Rotarod and Open Field test.

2.8.1. Rotarod Analysis

Rotarod Test have been used to examine the loss of motor coordination by measuring the ability of mice to maintain itself on a rod that turns at accelerating speeds. Mice from control and treatment groups (n= 5-8) were initially trained at 4rpm spped on a 5-line Rotarod unit (Pan-Lab Harvard Apparatus, Barcelona, Spain). After the mice learns to maintain itself on the rod; they were examined in the increasing acceleration mode from 4 to 40rpm within the 5minute period of time. Each mouse were put on the rod three times with 15 minutes of rest time in between the trials. The time each mouse spent on the rod was recorded and analyzed using the One-Way ANOVA method with GraphPad.

2.8.2. Open Field Analysis

The open field test is an experimental evaluation employed to measure overall locomotor activity, anxiety levels, and the inclination to explore in animals, typically rodents (Walsh & Cummins, 1976). The equipment used for this assessment comprised a 40×40 cm surface area enclosed on all sides by a 40 cm transparent barrier with a digital camera installed directly above the setup. Mice were positioned in one of the corners of the open field and permitted to explore without interruption for a duration of 5 minutes. Variations in locomotory functions and anxiety levels were assessed using the Panlab SMART Video Tracking System v0.3 (Harvard Apparatus, USA). The testing area is

separated into two zones as center and periphery, and this tracking devices enables measurement of times spent in each zone and the total distance of locomotion. The data were analyzed by One-way ANOVA with GraphPad Prism (Thompson and Kim 1996).

CHAPTER 3

RESULTS

3.1. Mouse Genotyping

The mice were genotyped based on the *WT* and mutant alleles of *Hexa* and *Neu3* genes by individual PCRs for each gene. Illustrated band sizes for wt and mutant alleles for the genes *Hexa* (Figure 3.1.A) and *Neu3* (Figure 3.1.B) were detected and based on the amplified bands the mice were labelled as +/+, +/- or -/- .

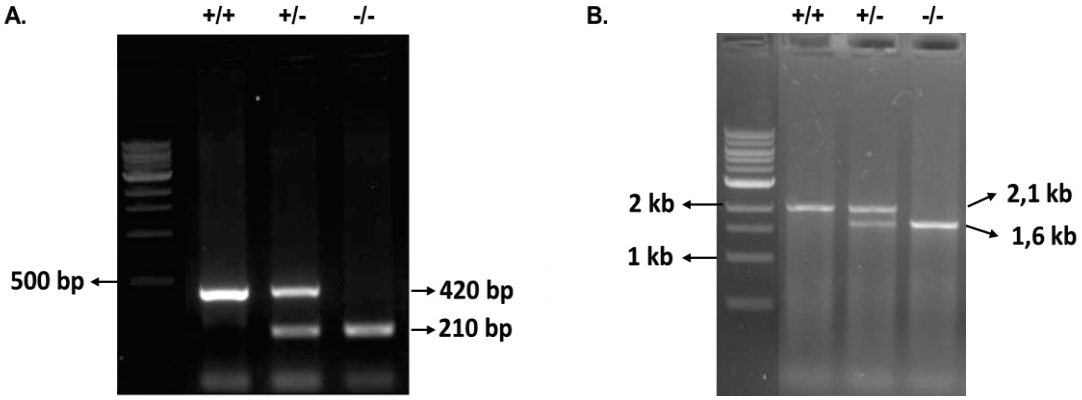

Figure 3.1. Gel images of PCR analysis of tail genomic DNA. for Hexa (A) and Neu3(B) genes. 210 bp and 420 bp fragments represent mutant allele and wild type allele of Hexa, respectively(A). 1.6 kb and 2.1 kb fragments represent mutant allele and wild type allele of Neu3, respectively(B).

3.2. Behavioral Analysis

Control and treatment groups of *WT, Hexa-/-,* and *Hexa-/-Neu3-/-* mice were subjected to rotarod test to measure motor coordination and open field test to measure anxiety and locomotor activity. Also, the body weight of the mice were measured twice for a week.

3.2.1. Body Weight Measurement

Gross body weights of untreated *WT*, *Hexa-/-, Hexa-/-Neu3-/-* and treated *Hexa-/-Neu3-/-* mice with 3 different strategies were measured weekly from 10 weeks to ~20 weeks of male mice of each group. Untreated *Hexa-/-Neu3-/-* mice significantly increased weight loss when compared to age matched *WT* and Hexa-/- (Figure 3.2). Early-stage and two-stage treatment groups showed decreased weight loss pattern when compared to untreated *Hexa-/-Neu3-/-* (Figure 3.2 A). However, in the late stage treated mice group, there was no significant change in weight loss rate (Figure 3.2 B).

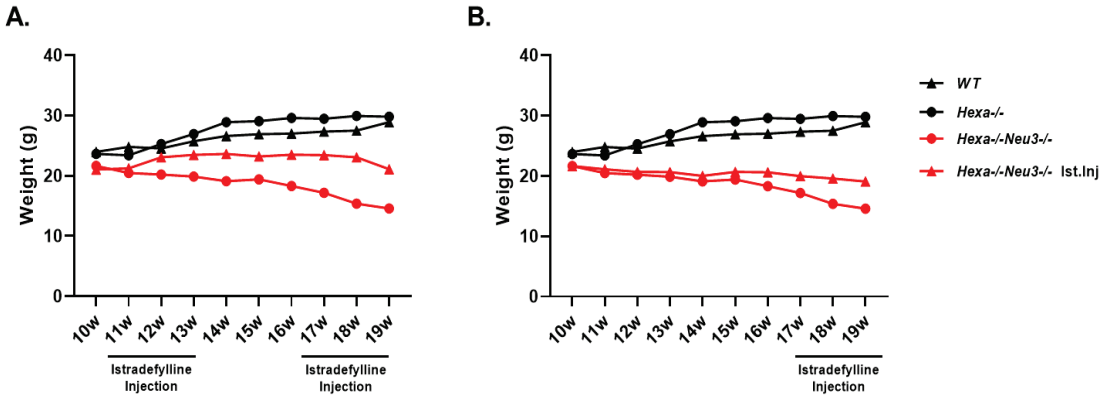

Figure 3.2. Body weight measurements of WT, Hexa-/-, untreated Hexa-/-Neu3-/- and istradefylline treated Hexa-/-Neu3-/- mice. Body weight measurements of early-stage and two-stage treatment group mice were illustrated together (A) and late stage treatment group measurements were represented separately (B).

3.2.2. Rotarod Analysis

The Rotarod Test was employed to assess motor coordination deterioration by gauging the mice's capacity to stay on a rotating rod with gradually increasing speed. It was observed that treated or untreated *Hexa-/-Neu3-/-* mice for all strategies showed significantly decreased durability on the rod when compared to *WT* and *Hexa-/-* controls (Figure 3.3). Early-stage treatment in *Hexa-/-Neu3-/-* mice led to a slight increase in time on rod period compared to untreated *Hexa-/-Neu3-/-* (Figure 3.3A). In addition, significantly increased durability on the rod was shown in two-stage treatment group mice

when compared to untreated *Hexa-/-Neu3-/-*and there was no change for late stage treatment group (Figure 3.3 B).

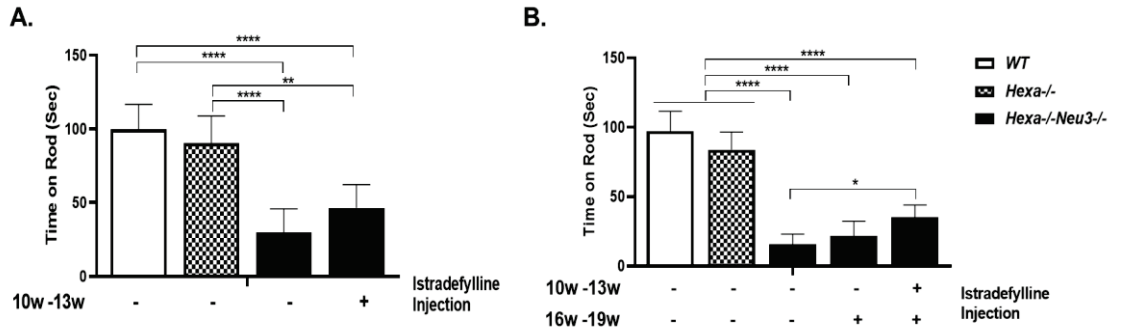

Figure 3.3. Rotarod analyses of WT, Hexa-/- and Hexa-/-Neu3-/- mice on an accelerating rod (4 rpm to 40 rpm within 5 minutes). Motor function and motor learning of Hexa−/− Neu3−/− mice in early-stage (A), Late-stage (B) and two stage group (B) was compared with its age matched untreated counterparts. Data is representative of mean ± SEM of measurements. Significant levels in the data were presented by using the ONE-way ANOVA.

3.2.3. Open Field Test

The anxiety levels and locomotor activity of control and treatment groups were measured by 5-min open field test. Time spend in the center zone and total traveled distance were evaluated for untreated *WT, Hexa-/-* and *Hexa-/-Neu3-/-* and early, late, and two-stage istradefylline treated *Hexa-/-Neu3-/-* mice. While early-stage treated *Hexa-/-Neu3-/-* mice spent significantly decreased time in the center (Figure 3.4A); late and two-stage treatment groups showed no difference when compared to age-matched untreated counterparts (Figure 3.4C). When we look at the total distance traveled by mice in each group, it was shown that treated or untreated *Hexa-/-Neu3-/-* mice traveled significantly less distance in the 5-minute period of time when compared to untreated *WT* and *Hexa-/-* counterparts. However, the treatments did not change the total distance traveled by *Hexa-/-Neu3-/-* mice applied with early (Figure 3.4B), late-stage, and two-stage (Figure 3.4D) treatment strategies compared to untreated *Hexa-/-Neu3-/-* mice.

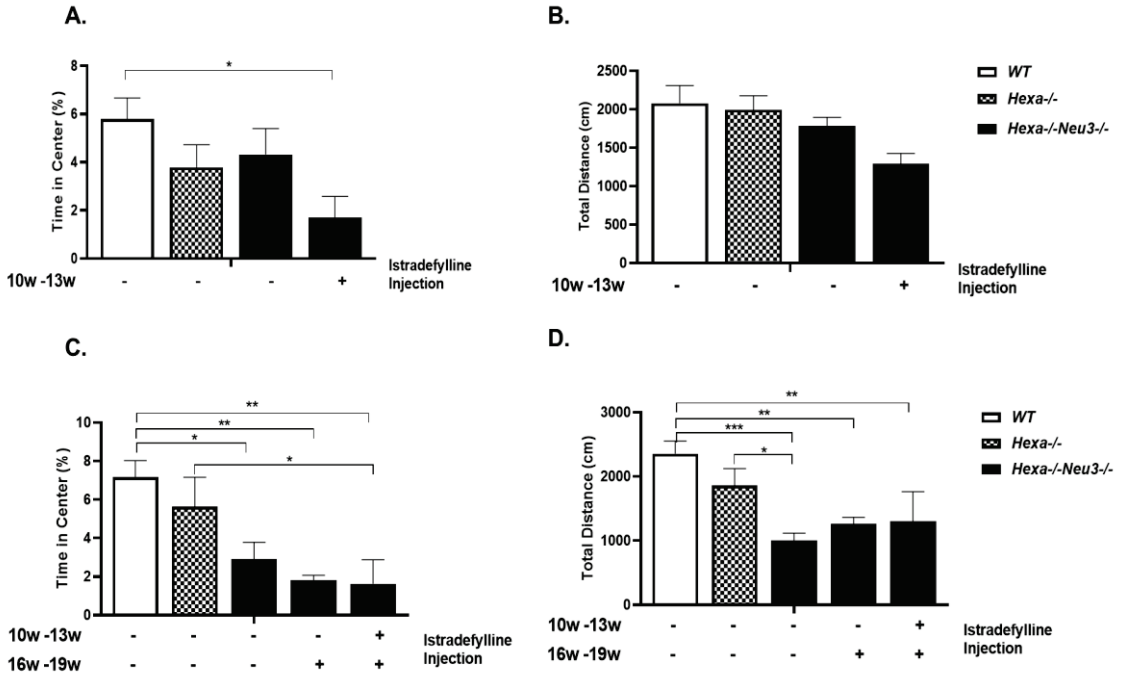

Figure 3.4. Open field analyses of WT, Hexa-/- and Hexa-/-Neu3-/- were represented. Time spent in center zone of the open field box for 5minutes of controls and early-stage (10w-13w) (A), late-stage(16w-19w) and two stage treatment groups (10w-13w & 16w-19w) (B) were indicated. Total distance traveled in the open field box for 5minutes by mice from control and early-stage (10w-13w) (A), late-stage(16w-19w) and two stage treatment groups (10w-13w & 16w-19w) (B) were demonstrated. Data is representative of mean ± SEM of measurements. Significant levels in the data were presented by using the one-way ANOVA (*p<0.05, **p<0.01,***p<0.001 and ****p<0.0001).

3.3. Neuroinflammation Analysis

Neuroinflammatory markers were analyzed in cortex and cerebellum of control and treatment groups by RT-PCR, immunohistochemistry and western blot analyses.

3.3.1. Real Time PCR

RT-PCR analysis was performed to observe the possible changes in gene expression levels of neuroinflammation-related markers after anti-inflammatory therapy. Gene expression levels of proinflammatory chemokines in cortex and cerebellum regions of untreated *WT*, *Hexa*$^{-/-}$, *Hexa*$^{-/-}$*Neu3*$^{-/-}$ control groups and early-stage (10w-13w), late-stage (16w-19w) and two stage treatment groups (10w-13w & 16w-19w) were measured.

CCL2, CCL3, CCL5 and CXCL10 gene expression levels were significantly increased in cortex region of untreated *Hexa-/-Neu3-/-* mice compared to untreated age-matched *WT* and Hexa-/- counterparts (Figure 3.5). The levels of CCL2 expression *Hexa-/-Neu3-/-* mice were significantly reduced with early-stage (Figure 3.5A), late-stage and two-stage treatment (Figure 3.5B) of istradefylline in cortex region of *Hexa-/-Neu3-/-* mice compared to untreated ones. In addition, gene expression levels of CCL3 (Figure 3.5C, D), CCL5(Figure 3.5 E,F), and CXCL10 (Figure 3.5 G,H) in cortex showed a significant increase with early-stage treatment, while they significantly decreased with late-stage and two-stage treatment strategies.

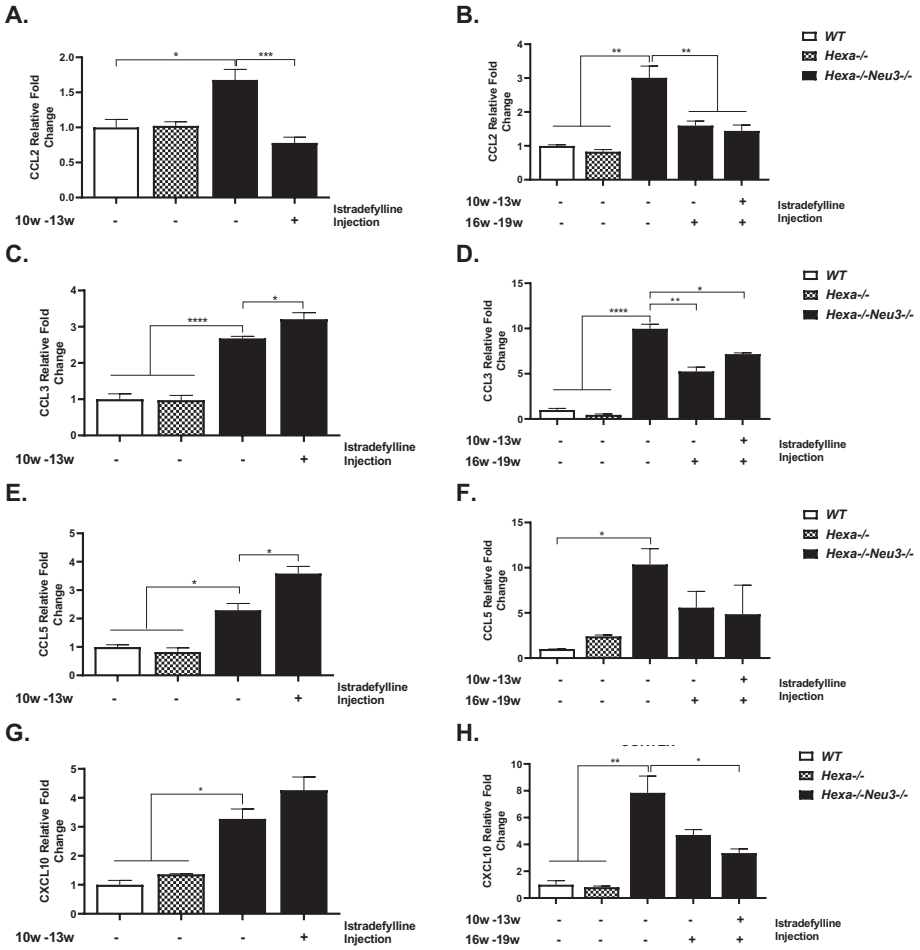

Figure 3.5. The expression levels of proinflammatory chemokines in cortex region of WT, Hexa-/- and Hexa-/-Neu3-/- were represented. The expression levels of CCL2 (A,B), CCL3 (C,D), CCL5 (E,F) and CXCL10(G,H) in age-matched controls and early-stage (10w-13w), late-stage and two stage treatment groups (10w-13w & 16w-19w) were indicated respectively. Expression ratio calculations were performed by ΔCT method and data was normalized to expression levels of age-matched WT mice. Significant levels in the data were presented by using the one-way ANOVA (*p<0.05, **p<0.01, ***p<0.001, and ****p<0.0001).

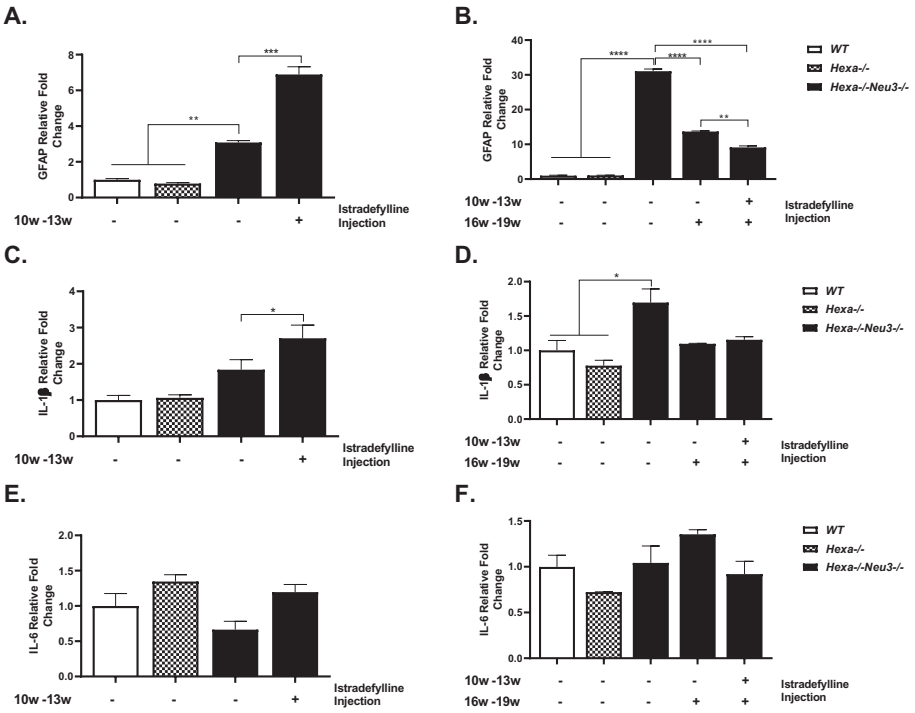

Figure 3.6. The expression levels of astrocyte-related marker and proinflammatory interleukins in cortex region of WT, Hexa-/- and Hexa-/-Neu3-/- were represented. The expression levels of GFAP (A,B), IL-1β (C,D) and IL-6 (E,F) in age-matched controls and early-stage (10w-13w), late-stage and two stage treatment groups (10w-13w & 16w-19w) were indicated respectively. Expression ratio calculations were performed by ΔCT method and data was normalized to expression levels of age-matched WT mice. Significant levels in the data were presented by using the one-way ANOVA (*p<0.05, **p<0.01, ***p<0.001, and ****p<0.0001).

When we look at the GFAP gene expression levels in the cortex region, significantly increased expression levels of GFAP were observed in untreated *Hexa-/-Neu3-/-* mice compared to untreated age-matched *WT* and *Hexa-/-* mice (Figure 3.6 A, B). Early-stage treatment led to a significant increase in GFAP expression (Figure 3.6 A), however with late and two-stage treatment GFAP expression was significantly reduced in the cortex of *Hexa-/-Neu3-/-* mice compared to age-matched untreated *Hexa-/-Neu3-/-* (Figure 3.6 B). At the early stage (13W-old) IL-1β expression in the cortex of untreated *Hexa-/-Neu3-/-* did not show significant change when compared to age-matched *WT* and *Hexa-/-* counterparts however early-stage treatment significantly increased IL-1β expression in treated *Hexa-/-Neu3-/-* compared to untreated one (Figure 3.6 C). On the other hand, IL-1β expression was significantly increased in the cortex of untreated *Hexa-*

/-Neu3-/- compared to age-matched *WT* and *Hexa-/-* counterparts, and late-stage and two-stage treatments slightly reduced IL-1β expression in the same region compared to untreated condition (Figure 3.6 D). When we look at the expression levels of IL-6 interleukin, it was observed that there was not a significant change in cortex region of untreated *WT, Hexa-/-* and *Hexa-/-Neu3-/-* or treated *Hexa-/-Neu3-/-* mice (Figure 3.6 E,F).

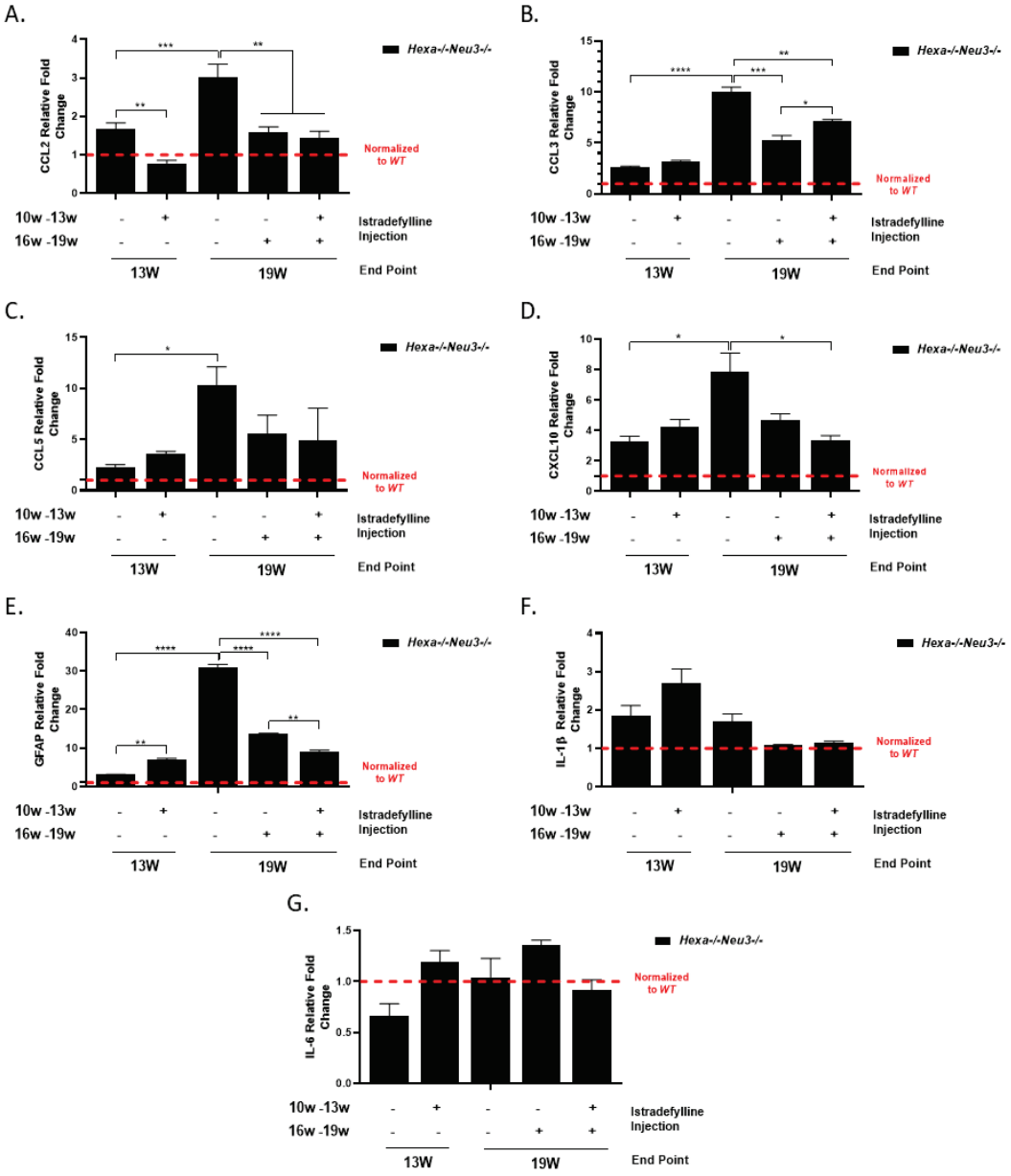

Figure 3.7. Gene expression levels of neuroinflammatory markers in cortex region of untreated and treated Hexa-/-Neu3-/- were represented as normalized to age-matched WT and compared to based on untreated, early-stage late-stage and two-stage treatment conditions for CCL2 (A), CCL3(B), CCL5 (C), CXCL10 (D), GFAP (E), IL-1β (F) and IL-6 (G).

The effect of three different strategies on gene expression levels of neuroinflammatory markers were normalized to age-matched *WT* and compared with each other and untreated conditions for CCL2 (Figure 3.7 A), CCL3(Figure 3.7 B), CCL5 (Figure 3.7 C), CXCL10 (Figure 3.7 D), GFAP (Figure 3.7 E), IL-1β (Figure 3.7 F) and IL-6 (Figure 3.7 G). Except for IL-1β and IL-6, all markers were significantly increased in cortex of 19W-old untreated *Hexa-/-Neu3-/-* mice compared to 13W-olds. In addition, except for increasing expression of GFAP and IL-6 in early stage treatment, all markers showed a decreasing pattern in expression levels of other markers in the anti-inflammatory treatment condition (Figure 3.7).

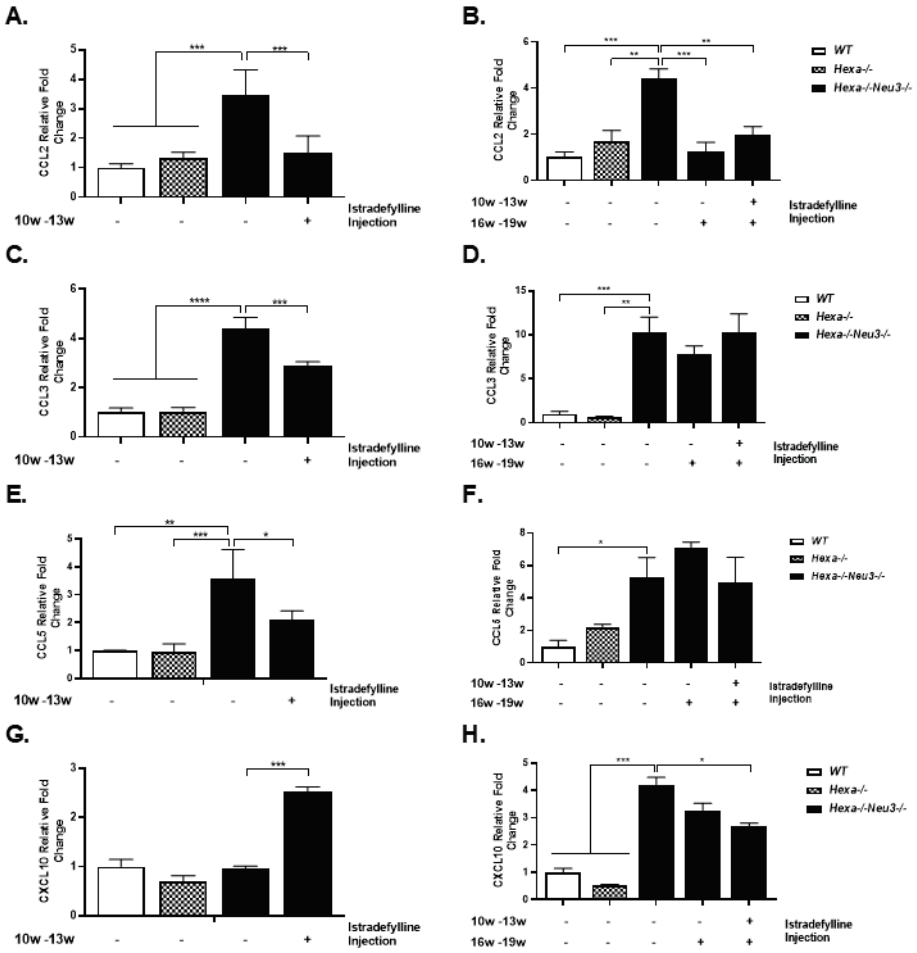

Figure 3.8. The expression levels of proinflammatory chemokines in cerebellum region of WT, Hexa-/- and Hexa-/-Neu3-/- were represented. The expression levels of CCL2 (A,B), CCL3 (C,D), CCL5 (E,F) and CXCL10(G,H) in age-matched controls and early-stage (10w-13w), late-stage and two stage treatment groups (10w-13w & 16w-19w) were indicated respectively. Expression ratio calculations were performed by ΔCT method and data was normalized to expression levels of age-matched WT mice. Significant levels in the data were presented by using the one-way ANOVA (*p<0.05, **p<0.01, ***p<0.001, and ****p<0.0001).

The gene expression levels of proinflammatory chemokines in cerebellum regions of untreated *WT*, *Hexa-/-*, *Hexa-/-Neu3-/-* control groups and early-stage (10w-13w), late-stage (16w-19w) and two-stage treatment groups (10w-13w & 16w-19w) were measured as well. Except for CXCL10 at 13W-old stage; CCL2, CCL3, CCL5 and CXCL10 gene expression levels were significantly increased in cerebellum region of untreated *Hexa-/-Neu3-/-* mice compared to untreated age-matched *WT* and *Hexa-/-* counterparts (Figure 3.8). The levels of CCL2 expression *Hexa-/-Neu3-/-* mice were significantly reduced with early-stage (Figure 3.8A), late-stage and two-stage istradefylline treatment (Figure 3.8B) in the cerebellum region of *Hexa-/-Neu3-/-* mice compared to untreated ones. In early stage treatment strategy, the expression levels of CCL3 and CCL5 were significantly decreased compared to age-matched untreated *Hexa-/-Neu3-/-* (Figure 3.8C, E) however late-stage and two-stage strategies did not significantly affect CCL3 and CCL5 expression in cerebellum region (Figure 3.8 D, F). On the other hand, expression levels of CXCL10 were increased by early-stage treatment (Figure 3.8 G) but late and two-stage treatments did not affect CXCL10 expression level in cerebellum region of 19W-old *Hexa-/-Neu3-/-* mice compared to age-matched untreated *Hexa-/-Neu3-/-* mice (Figure 3.8H).

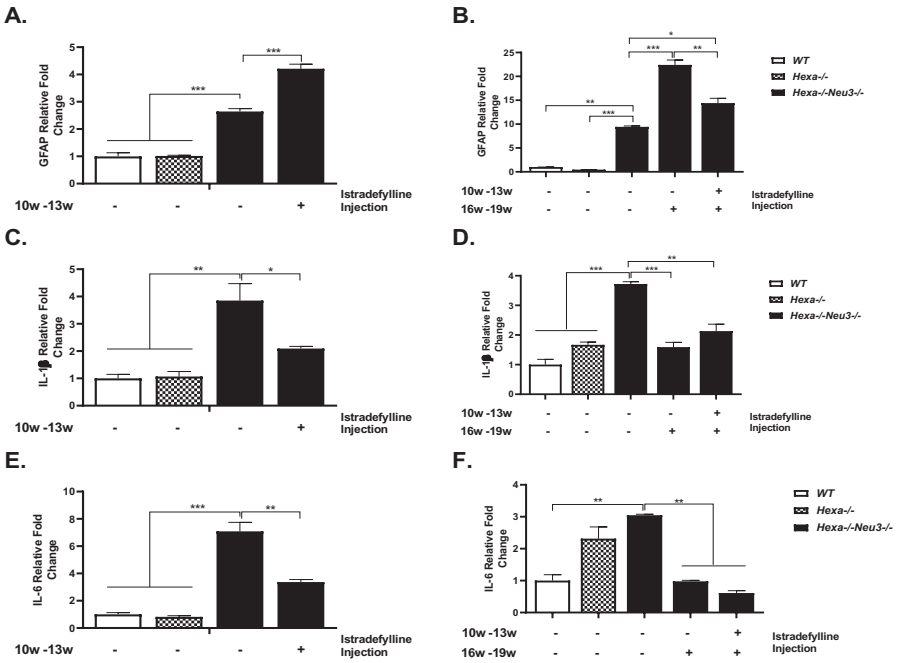

Figure 3.9. The expression levels of astrocyte-related marker and proinflammatory interleukins in cerebellum region of WT, Hexa-/- and Hexa-/-Neu3-/- were represented. The expression levels of GFAP (A,B), IL-1β (C,D) and IL-6 (E,F) in age-matched controls and early-stage (10w-13w), late-stage and two stage treatment groups (10w-13w & 16w-19w) were indicated respectively. Expression ratio calculations

were performed by ΔCT method and data was normalized to expression levels of age-matched WT mice. Significant levels in the data were presented by using the one-way ANOVA (*p<0.05, **p<0.01, ***p<0.001, and ****p<0.0001).

Besides proinflammatory chemokines; GFAP, IL-1β and IL-6 gene expression levels in the cerebellum region were also analyzed, and significantly increased expression levels of GFAP were observed in untreated *Hexa-/-Neu3-/-* mice compared to untreated age-matched *WT* and *Hexa-/-* mice (Figure 3.9). Early-stage and late-stage treatment led to a significant increase in GFAP expression (Figure 3.9 A, B), however, with two-stage treatment GFAP expression was significantly reduced in the cerebellum of *Hexa-/-Neu3-/-* mice compared to age-matched untreated *Hexa-/-Neu3-/-* (Figure 3.9 B). IL-1β and IL-6 gene expression levels were significantly increased in the cerebellum region of untreated *Hexa-/-Neu3-/-* mice compared to untreated age-matched *WT* and *Hexa-/-* counterparts (Figure 3.9 C, D,E and F). On the other hand, their expression levels were significantly reduced with early-stage (Figure 3.9 C and E), late-stage and two-stage istradefylline treatment (Figure 3.9 D and F) in the cerebellum region of *Hexa-/-Neu3-/-* mice compared to untreated ones.

The effect of three different strategies on gene expression levels of neuroinflammatory markers in cerebellum region was also normalized to age-matched *WT* and compared with each other and untreated conditions for CCL2 (Figure 3.10. A), CCL3(Figure 3.10. B), CCL5 (Figure 3.10. C), CXCL10 (Figure 3.10. D), GFAP (Figure 3.10. E), IL-1β (Figure 3.10. F) and IL-6 (Figure 3.10. G). The gene expression levels of CCL3 (Figure 3.10. B), CXCL10 (Figure 3.10. D), and GFAP (Figure 3.10.E) were significantly increased in the cerebellum region of 19W-old untreated *Hexa-/-Neu3-/-* mice compared to 13W-old untreated *Hexa-/-Neu3-/-* mice. All three strategies for istradefylline administration reduced the expression levels of CCL2 (Figure 3.10 A), IL-1β (Figure 3.10 F), and IL-6 (Figure 3.10 G) in the cerebellum of *Hexa-/-Neu3-/-* mice compared to age-matched untreated *Hexa-/-Neu3-/-*.

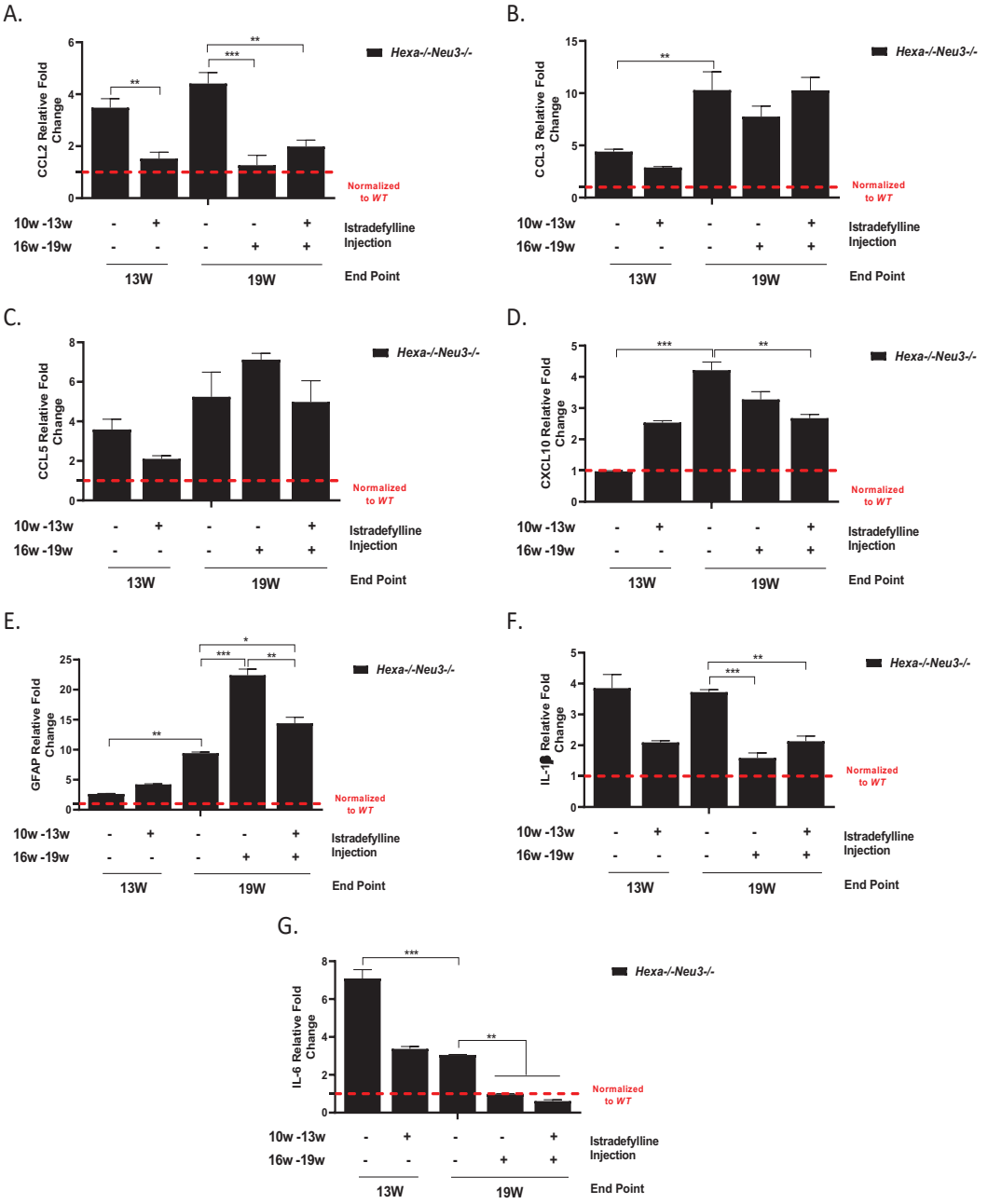

Figure 3.10. Gene expression levels of neuroinflammatory markers in cerebellum region of untreated and treated Hexa-/-Neu3-/- were represented as normalized to age-matched WT and compared to untreated, early-stage late-stage and two-stage treatment conditions for CCL2 (A), CCL3(B), CCL5 (C), CXCL10 (D), GFAP (E), IL-1β (F) and IL-6 (G).

3.3.2. Western Blot

NFκB and IκB protein expression were analyzed by Western Blot in cortex and cerebellum region of untreated *WT*, *Hexa*$^{-/-}$, *Hexa-/-Neu3-/-* control groups and early-stage (10w-13w), late-stage (16w-19w) and two-stage (10w-13w & 16w-19w) treated *Hexa-/-Neu3-/-*. In the cortex region, NFκB protein level did not change in 13W-old untreated *WT*, Hexa-/-, *Hexa-/-Neu3-/-* and early-stage treated *Hexa-/-Neu3-/-* mice (Figure 3.11 A,B) however when we look at the 19W-old group, late-stage treatment slightly, two-stage treatment significantly reduced NFκB expression in cortex region of *Hexa-/-Neu3-/-* compared to untreated condition (Figure 3.11 C,D). In addition, IκB expression did not displayed any difference in cortex region untreated control groups and treatment groups (Figure 3.12).

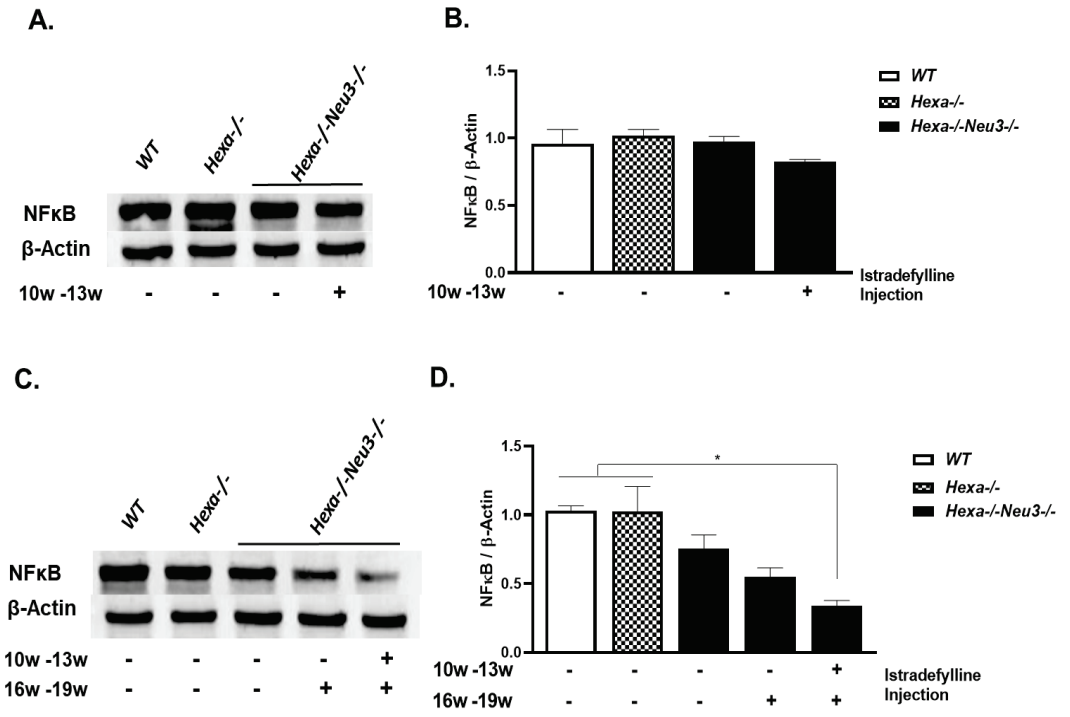

Figure 3.11. Western-blot analysis for NFκB protein in cortex region of WT, Hexa-/- and Hexa-/-Neu3-/- were represented. Western blot images and histographic representation were indicated for early-stage(10w-13w) (A,B), Late-stage (16w-19w) (C,D) and two-stage treatment (10w-13w & 16w-19w)(C,D,) groups were indicated respectively.

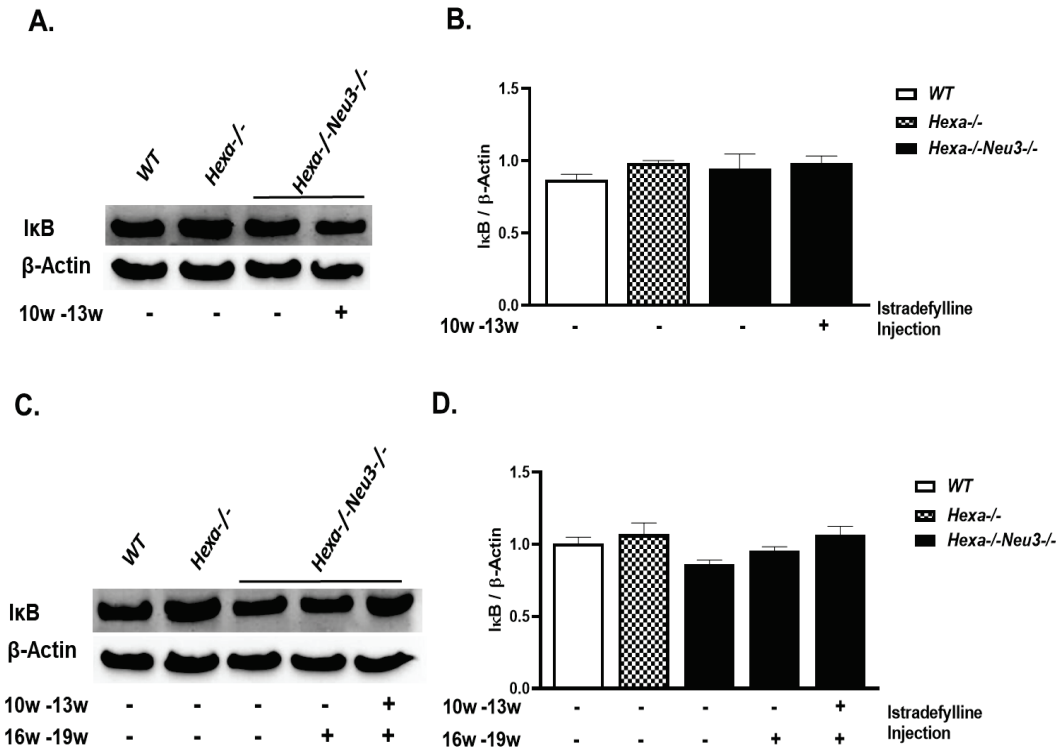

Figure 3.12. Western-blot analysis for IκB protein in cortex region of WT, Hexa-/- and Hexa-/-Neu3-/- were represented. Western blot images and histographic representation were indicated for early-stage(10w-13w) (A,B), Late-stage (16w-19w) (C,D) and two-stage treatment (10w-13w & 16w-19w)(C,D,) groups were indicated respectively.

When we look at the cerebellum region NFκB expression did not significantly change between untreated *WT*, *Hexa-/-*, *Hexa-/-Neu3-/-* control groups and early-stage (10w-13w) treated *Hexa-/-Neu3-/-* in the 13W-old group (Figure 3.13 A,B). On the other hand, in the 19W-old group, it is shown that late-stage and two-stage treatment in *Hexa-/-Neu3-/-* significantly reduce NFκB protein expression in the cerebellum region compared to untreated *WT, Hexa-/-* and *Hexa*-/-Neu3-/- (Figure 3.13 C,D). Similar to cortex region there was no change in IκB expression between the cerebellum region of untreated control groups and treatment groups, as well (Figure 3.14).

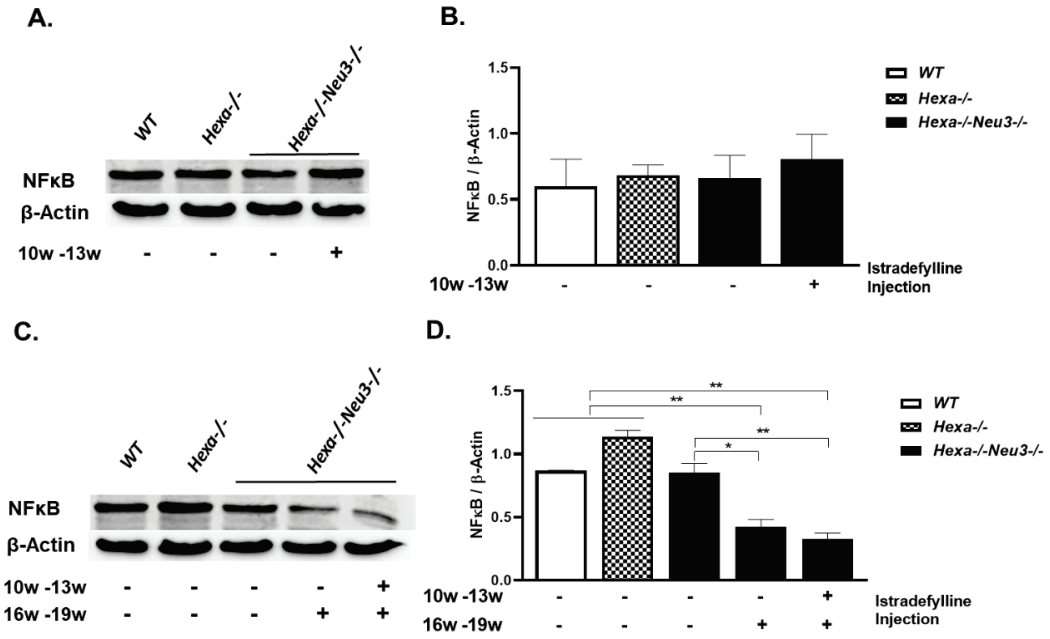

Figure 3.13. Western-blot analysis for NFκB protein in cerebellum region of WT, Hexa-/- and Hexa-/-Neu3-/- were represented. Western blot images and histographic representation were indicated for early-stage(10w-13w) (A,B), Late-stage (16w-19w) (C,D) and two-stage treatment (10w-13w & 16w-19w)(C,D,) groups were indicated respectively.

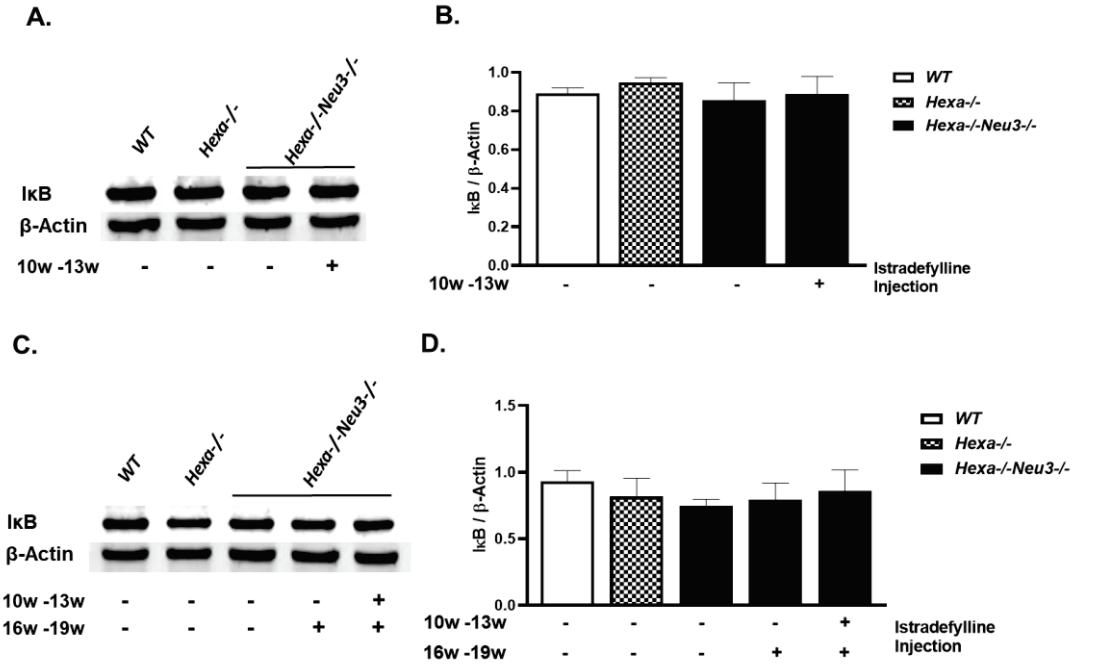

Figure 3.14. Western-blot analysis for IκB protein in cerebellum region of WT, Hexa-/- and Hexa-/-Neu3-/- were represented. Western blot images and histographic representation were indicated for early-stage(10w-13w) (A,B), Late-stage (16w-19w) (C,D) and two-stage treatment (10w-13w & 16w-19w)(C,D,) groups were indicated respectively.

3.3.3. Immunohistochemical Analysis

The expression and localization of GFAP, MOMA-2/LAMP1, CNPase and IL-6 immunohistochemistry analyses were performed by using fixated brain slides of control and treatment groups.

3.3.3.1. GFAP Staining

Cortex, cerebellum, hippocampus and thalamus regions of untreated *WT*, *Hexa-/-*, *Hexa-/-Neu3-/-* control groups and early-stage (10w-13w), late-stage (16w-19w) and two-stage (10w-13w & 16w-19w) treated *Hexa-/-Neu3-/-* were stained with GFAP to analyze astrocyte localization.

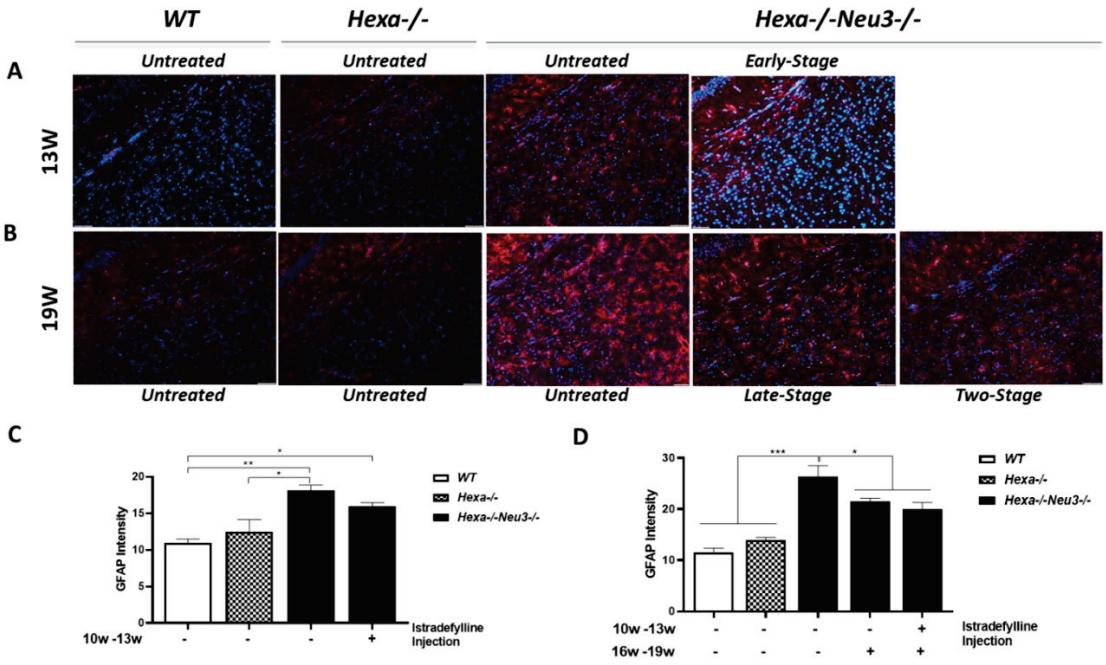

Figure 3.15. Anti-GFAP staining in cortex region of WT, Hexa-/- and Hexa-/-Neu3-/- were represented. The 20μm coronal sections were stained in red by anti-GFAP antibody (astrocyte marker) and in blue by DAPI (nucleus). Images for 13W-old controls and early-stage treated Hexa-/-Neu3-/- mice (A) and 19W-old controls, late-stage and two-stage treated Hexa-/-Neu3-/- mice (B) were represented. GFAP intensity analyses performed by NIH Image J program and histographic representation for 13W-old (C) and 19W-old groups (D) were shown. Scale bar indicates 50μm of cortex. Data is representative of mean ± SEM of measurements. one-way ANOVA was used for statistical analysis (*p<0.05 and **p<0.025)

In the cortex region, significantly increased GFAP level was observed in untreated *Hexa-/-Neu3-/-* mice compared to untreated age-matched *WT* and *Hexa-/-* mice (Figure 3.15 C, D). Early-stage treatment did not affect GFAP level (Figure 3.15 C) however in late and two stage treatment led to a significant decrease in GFAP level (Figure 3.15 D).

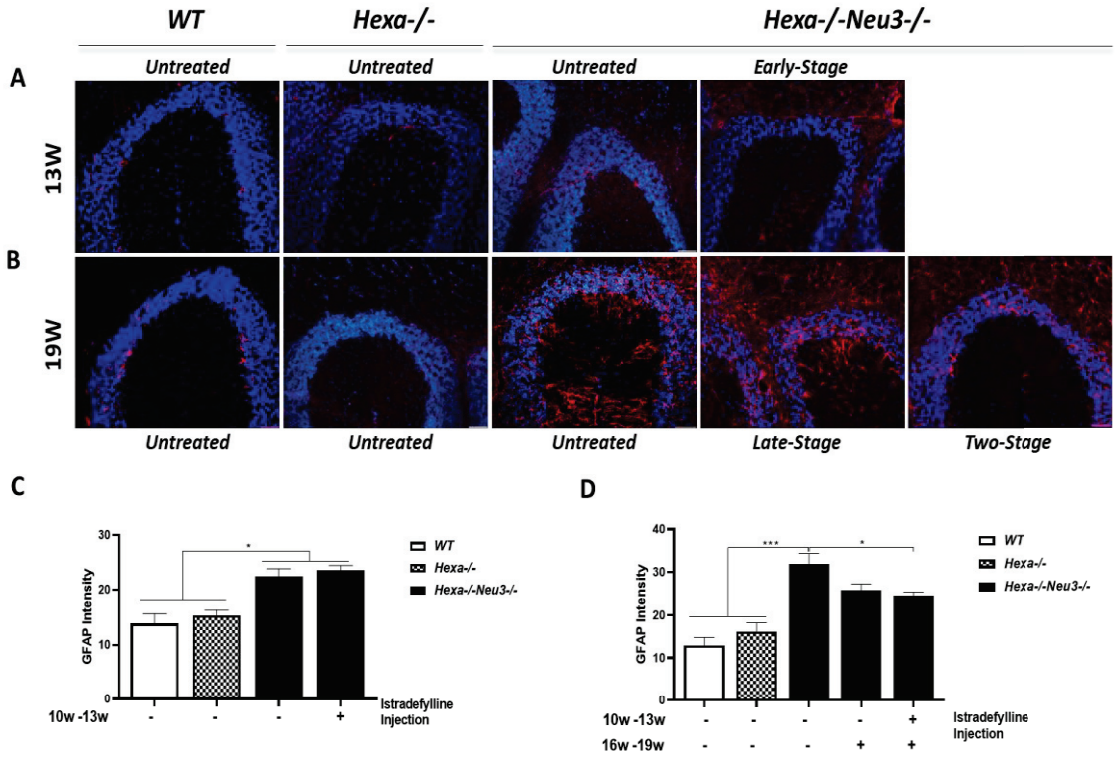

Figure 3.16. Anti-GFAP staining in cerebellum region of WT, Hexa-/- and Hexa-/-Neu3-/- were represented. The 20μm coronal sections were stained in red by anti-GFAP antibody (astrocyte marker) and in blue by DAPI (nucleus). Images for 13W-old controls and early-stage treated Hexa-/-Neu3-/- mice (A) and 19W-old controls, late-stage and two-stage treated Hexa-/-Neu3-/- mice (B) were represented. GFAP intensity analyses performed by NIH Image J program and histographic representation for 13W-old (C) and 19W-old groups (D) were shown. Scale bar indicates 50μm of cortex. Data is representative of mean ± SEM of measurements. one-way ANOVA was used for statistical analysis (*p<0.05 and **p<0.025)

In cerebellum region, GFAP level was significantly increased in both 13W-old and 19W-old untreated *Hexa-/-Neu3-/-* when compared to age matched *WT* and *Hexa-/-* controls (Figure 3.16 C,D). When we look at the istradefylline treatment group; it was observed that early-stage (Figure 3.16C) and late stage treatment (Figure 3.16D) did not significantly change GFAP level but two stage treatment (Figure 3.16D) significantly

reduced GFAP level in cerebellum of *Hexa-/-Neu3-/-* when compared to untreated condition.

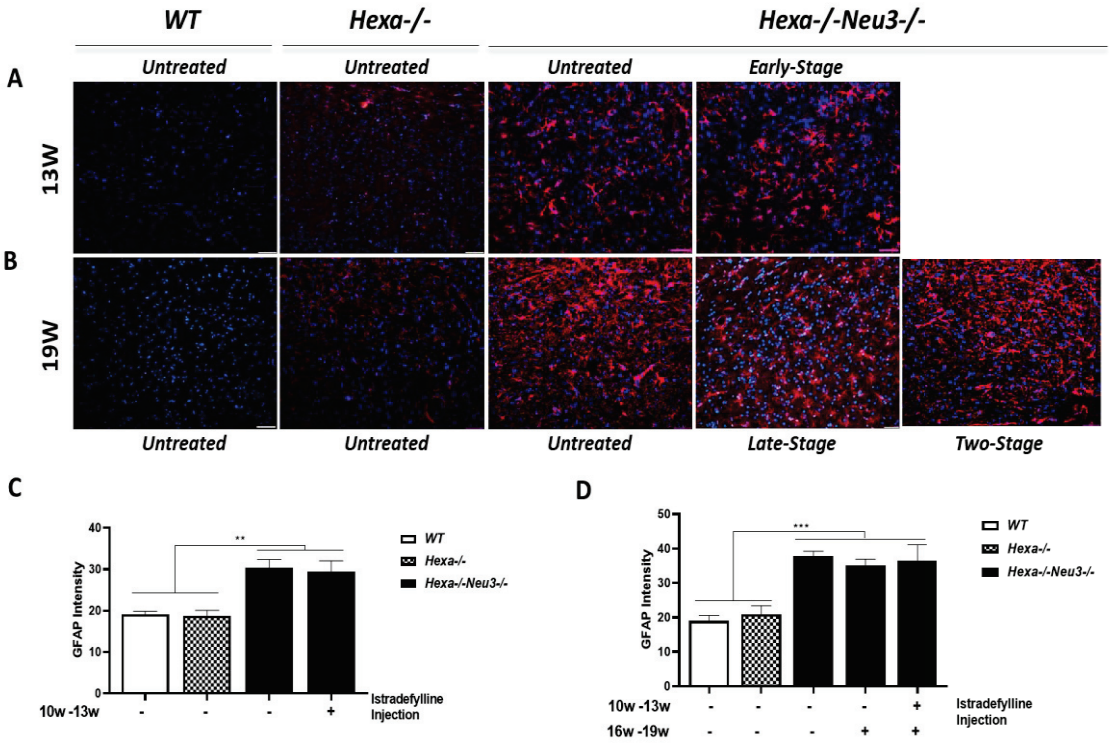

Figure 3.17. Anti-GFAP staining in thalamus region of WT, Hexa-/- and Hexa-/-Neu3-/- were represented. The 20μm coronal sections were stained in red by anti-GFAP antibody (astrocyte marker) and in blue by DAPI (nucleus). Images for 13W-old controls and early-stage treated Hexa-/-Neu3-/- mice (A) and 19W-old controls, late-stage and two-stage treated Hexa-/-Neu3-/- mice (B) were represented. GFAP intensity analyses performed by NIH Image J program and histographic representation for 13W-old (C) and 19W-old groups (D) were shown. Scale bar indicates 50μm of cortex. Data is representative of mean ± SEM of measurements. one-way ANOVA was used for statistical analysis (*p<0.05 and **p<0.025)

As in cortex and cerebellum, GFAP level was also significantly increased in thalamus region of untreated *Hexa-/-Neu3-/-* when compared to age matched *WT* and Hexa-/- mice. All three different istradefylline treatment strategies did not affect GFAP level in thalamus region of *Hexa-/-Neu3-/-* mice (Figure 3.17 C,D).

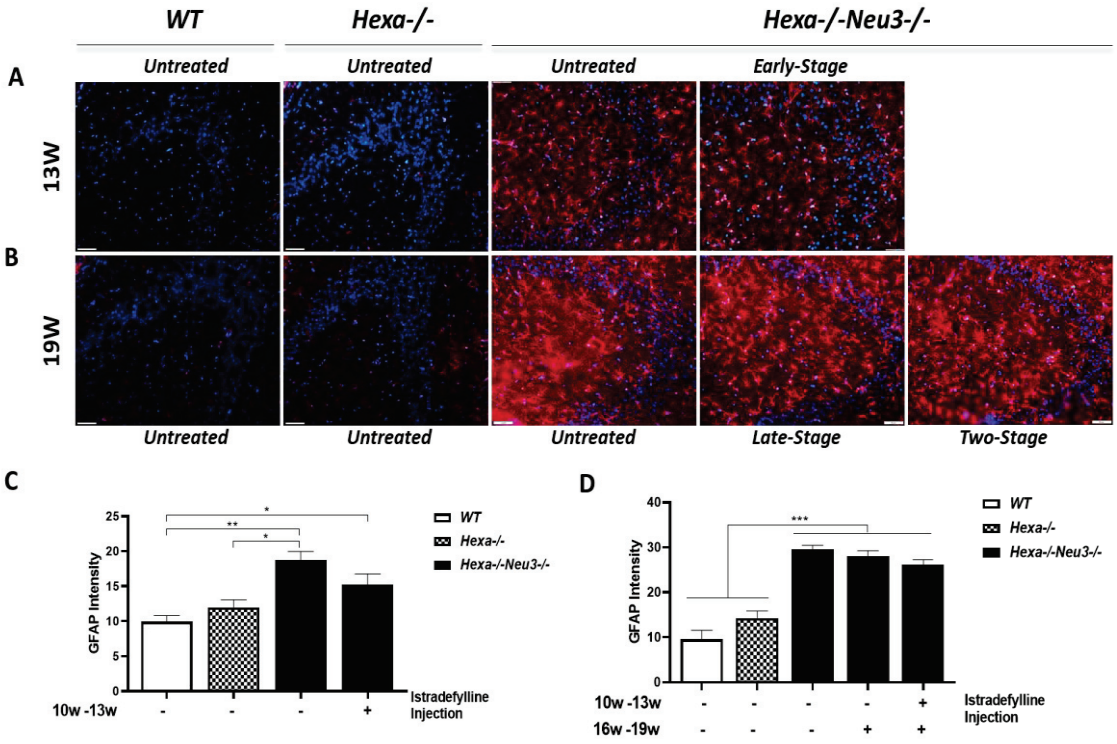

Figure 3.18. Anti-GFAP staining in hippocampus region of WT, Hexa-/- and Hexa-/-Neu3-/- were represented. The 20μm coronal sections were stained in red by anti-GFAP antibody (astrocyte marker) and in blue by DAPI (nucleus). Images for 13W-old controls and early-stage treated Hexa-/-Neu3-/- mice (A) and 19W-old controls, late-stage and two-stage treated Hexa-/-Neu3-/- mice (B) were represented. GFAP intensity analyses performed by NIH Image J program and histographic representation for 13W-old (C) and 19W-old groups (D) were shown. Scale bar indicates 50μm of cortex. Data is representative of mean ± SEM of measurements. one-way ANOVA was used for statistical analysis (*p<0.05 and **p<0.025)

Similar to cortex, cerebellum and thalamus region; GFAP level was significantly increased in hippocampus region of both 13W-old and 19W-old untreated *Hexa-/-Neu3-/-* when compared to age matched *WT* and *Hexa-/-* mice, as well (Figure 3.18 C, D). While early stage treatment significantly reduced GFAP level (Figure 3.18C); late- and two-stage treatment did not affect GFAP level in thalamus region of *Hexa-/-Neu3-/-* mice when compared to untreated condition (Figure 3.18 C, D).

3.3.3.2. MOMA-2 / LAMP1 Staining

In order to detect microglial activation; cortex, cerebellum, hippocampus and thalamus regions of untreated *WT*, *Hexa-/-*, *Hexa-/-Neu3-/-* control groups and early-stage (10w-13w), late-stage (16w-19w) and two-stage (10w-13w & 16w-19w) treatment groups of *Hexa-/-Neu3-/-* were stained with macrophage marker MOMA-2 and lysosomal marker LAMP1 by colocalization analysis.

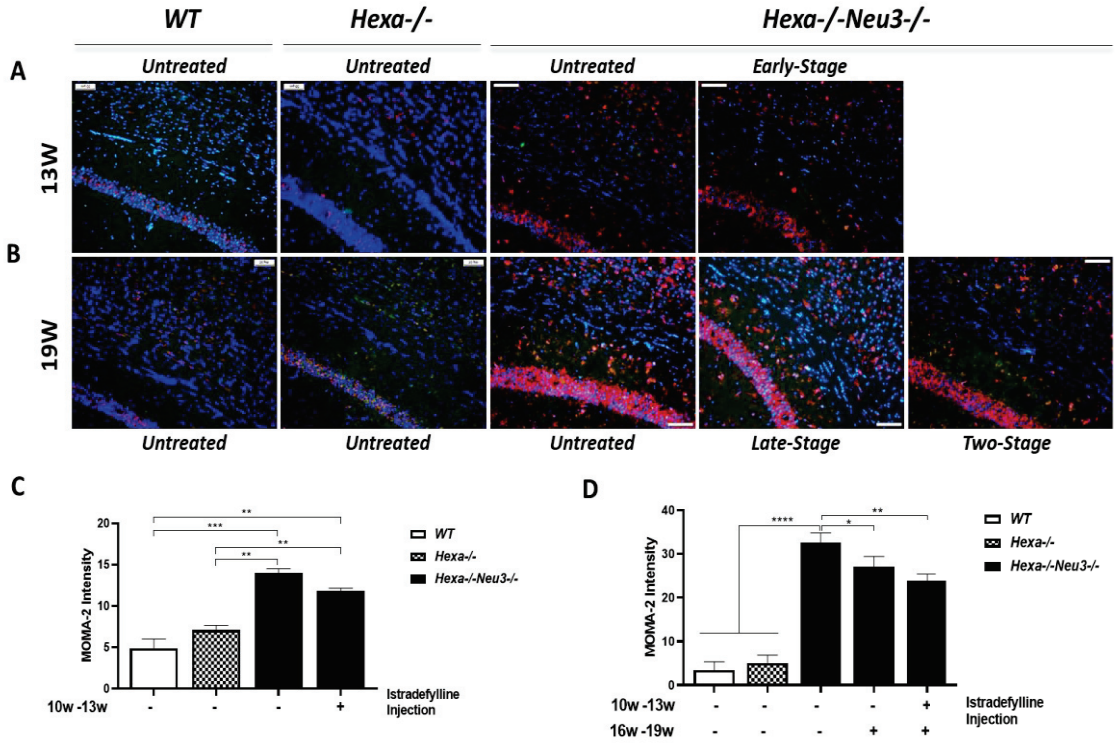

Figure 3.19. MOMA-2 / LAMP1 staining in cortex region of WT, Hexa-/- and Hexa-/-Neu3-/- were represented. The 20μm coronal sections were stained in red by anti-MOMA-2 antibody (macrophage marker), in green by anti-LAMP1(lysosomal marker) antibody and in blue by DAPI (nucleus). Images for 13W-old controls and early-stage treated Hexa-/-Neu3-/- mice (A) and 19W-old controls, late-stage and two-stage treated Hexa-/-Neu3-/- mice (B) were represented. MOMA-2 / LAMP1 intensity analyses performed by NIH Image J program and histographic representation for 13W-old (C) and 19W-old groups (D) were shown. Scale bar indicates 50μm of cortex. Data is representative of mean ± SEM of measurements. one-way ANOVA was used for statistical analysis (*p<0.05 and **p<0.025)

MOMA-2 level-was significantly increased in all of the regions of both 13W-old and 19W-old untreated *Hexa-/-Neu3-/-* mice when compared to age matched *WT* and *Hexa-/-* mice (Figure 3.19, 20, 21 and 22). Istradefylline administration at early stage did not change MOMA-2 level in cortex of early-stage treated *Hexa-/-Neu3-/-* when compared to age matched untreated *Hexa-/-Neu3-/-* (Figure 3.19C). On the other hand, late- and two-stage treatment of istradefylline significantly reduced MOMA-2 level in the cortex of *Hexa-/-Neu3-/-* mice when compared to untreated *Hexa-/-Neu3-/-* (Figure 3.19D). In addition, two-stage treatment was more effective in reduction of MOMA-2 in cortex.

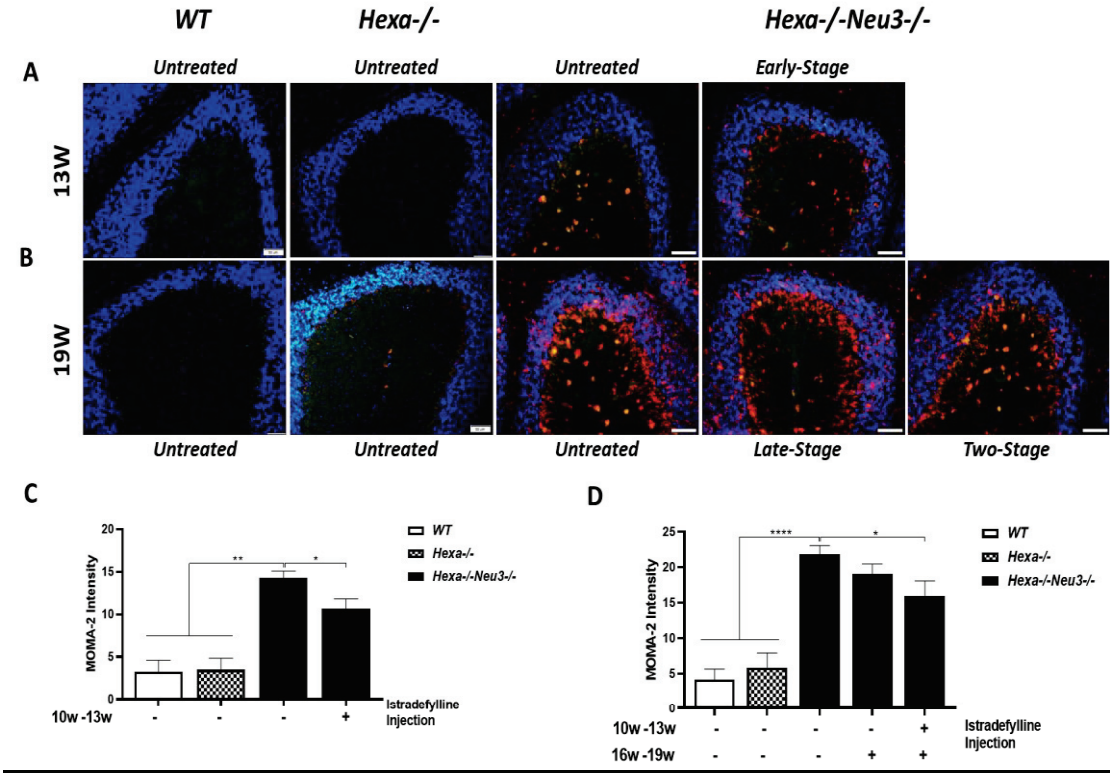

Figure 3.20. MOMA-2 / LAMP1 staining in cerebellum region of WT, Hexa-/- and Hexa-/-Neu3-/- were represented. The 20μm coronal sections were stained in red by anti-MOMA-2 antibody (macrophage marker), in green by anti-LAMP1(lysosomal marker) antibody and in blue by DAPI (nucleus). Images for 13W-old controls and early-stage treated Hexa-/-Neu3-/- mice (A) and 19W-old controls, late-stage and two-stage treated Hexa-/-Neu3-/- mice (B) were represented. MOMA-2 / LAMP1 intensity analyses performed by NIH Image J program and histographic representation for 13W-old (C) and 19W-old groups (D) were shown. Scale bar indicates 50μm of cortex. Data is representative of mean ± SEM of measurements. one-way ANOVA was used for statistical analysis (*p<0.05 and **p<0.025)

When we look at the MOMA-2 level in cerebellum region, it can be observed that early-stage and two-stage treatment was able to significantly reduce increased MOMA-2 in untreated *Hexa-/-Neu3-/-* (Figure 3.20 C, D). Late-stage treatment of istradefylline also slightly reduced the MOMA-2 level in cerebellum of *Hexa-/-Neu3-/-* however it was not statistically significant (Figure 3.20D).

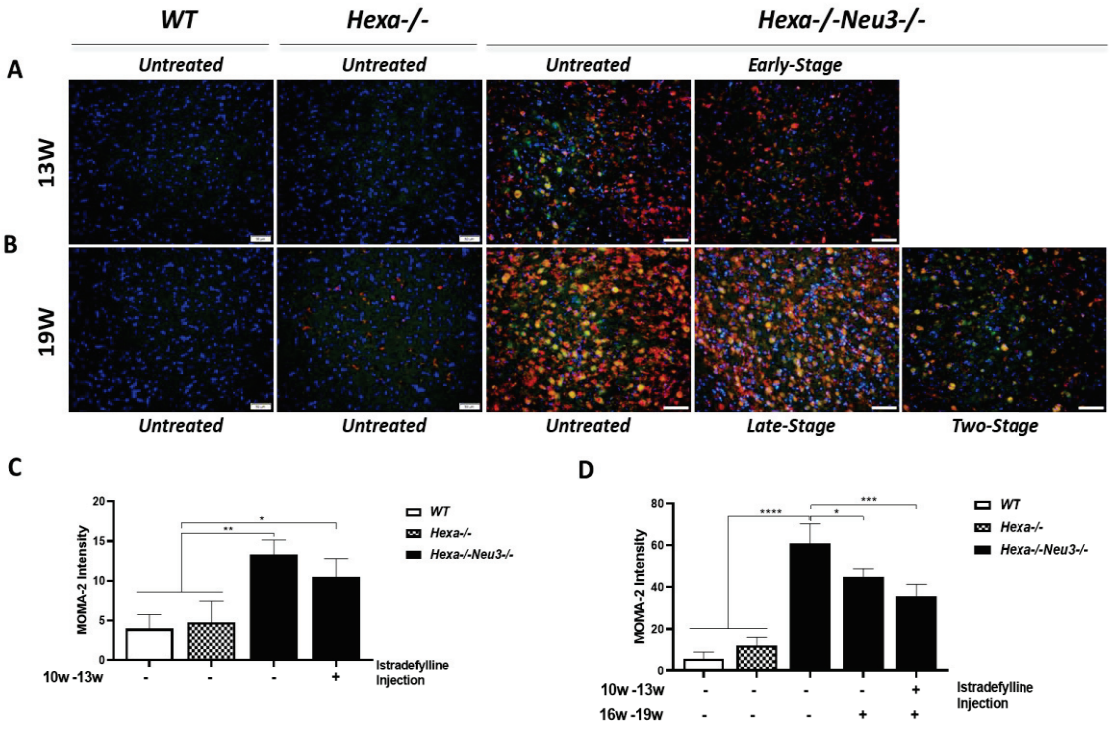

Figure 3.21. MOMA-2 / LAMP1 staining in thalamus region of WT, Hexa-/- and Hexa-/-Neu3-/- were represented. The 20μm coronal sections were stained in red by anti-MOMA-2 antibody (macrophage marker), in green by anti-LAMP1(lysosomal marker) antibody and in blue by DAPI (nucleus). Images for 13W-old controls and early-stage treated Hexa-/-Neu3-/- mice (A) and 19W-old controls, late-stage and two-stage treated Hexa-/-Neu3-/- mice (B) were represented. MOMA-2 / LAMP1 intensity analyses performed by NIH Image J program and histographic representation for 13W-old (C) and 19W-old groups (D) were shown. Scale bar indicates 50μm of cortex. Data is representative of mean ± SEM of measurements. one-way ANOVA was used for statistical analysis (*p<0.05 and **p<0.025)

In thalamus region, MOMA-2 level was significantly reduced by all three different strategies of istradefylline administration in treated *Hexa-/-Neu3-/-* mice when compared to age matched untreated *Hexa-/-Neu3-/-* mice (Figure 3.21). When we compare all three strategies with each other, it can be observed that two-stage treatment

was the most effective in reducing MOMA-2 in thalamus among other administration strategies.

Similar to the thalamus region, MOMA-2 level was also significantly reduced in the hippocampus region by all three different strategies in treated *Hexa-/-Neu3-/-* mice compared to untreated conditions with two stage treatment being the most effective strategy (Figure 3.22).

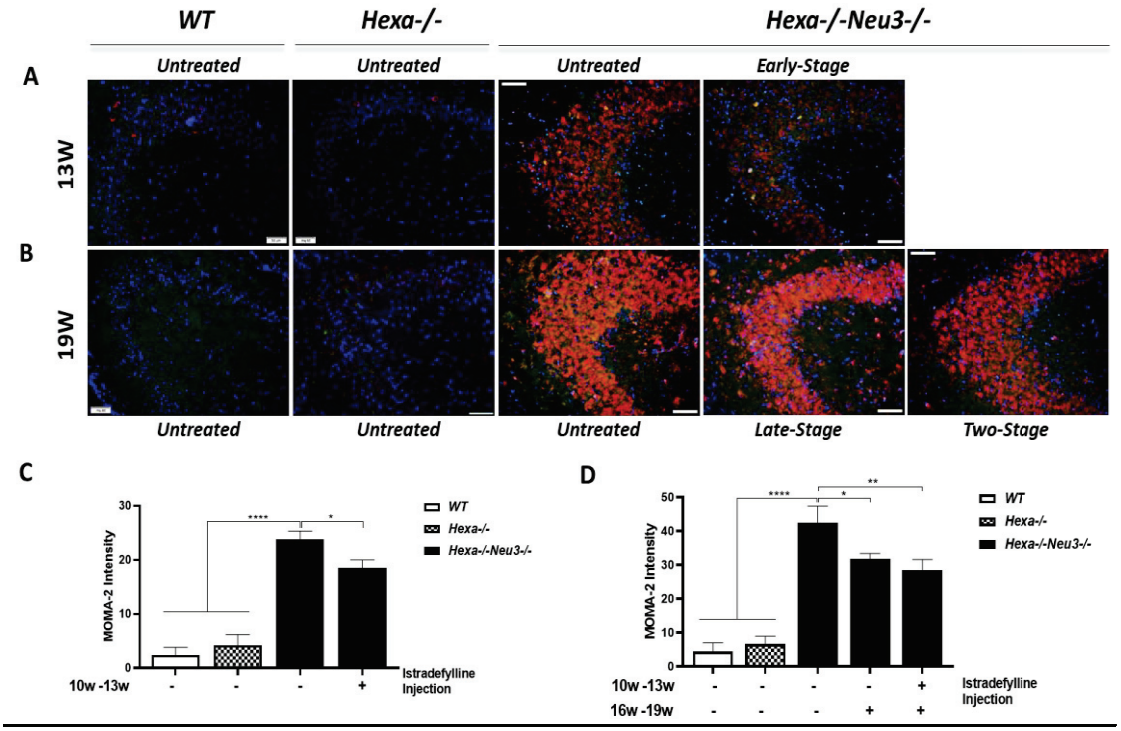

Figure 3.22. MOMA-2 / LAMP1 staining in hippocampus region of WT, Hexa-/- and Hexa-/-Neu3-/- were represented. The 20μm coronal sections were stained in red by anti-MOMA-2 antibody (macrophage marker), in green by anti-LAMP1(lysosomal marker) antibody and in blue by DAPI (nucleus). Images for 13W-old controls and early-stage treated Hexa-/-Neu3-/- mice (A) and 19W-old controls, late-stage and two-stage treated Hexa-/-Neu3-/- mice (B) were represented. GFAP intensity analyses performed by NIH Image J program and histographic representation for 13W-old (C) and 19W-old groups (D) were shown. Scale bar indicates 50μm of cortex. Data is representative of mean ± SEM of measurements. one-way ANOVA was used for statistical analysis (*p<0.05 and **p<0.025)

3.3.3.3. CNPase Staining

In order to detect oligodendrocyte level; cortex and cerebellum regions of untreated *WT*, *Hexa-/-*, *Hexa-/-Neu3-/-* control groups and early-stage (10w-13w), late-stage (16w-19w) and two-stage (10w-13w & 16w-19w) treatment groups of *Hexa-/-Neu3-/-* were stained with anti-CNPase antibody which is an oligodendrocyte marker.

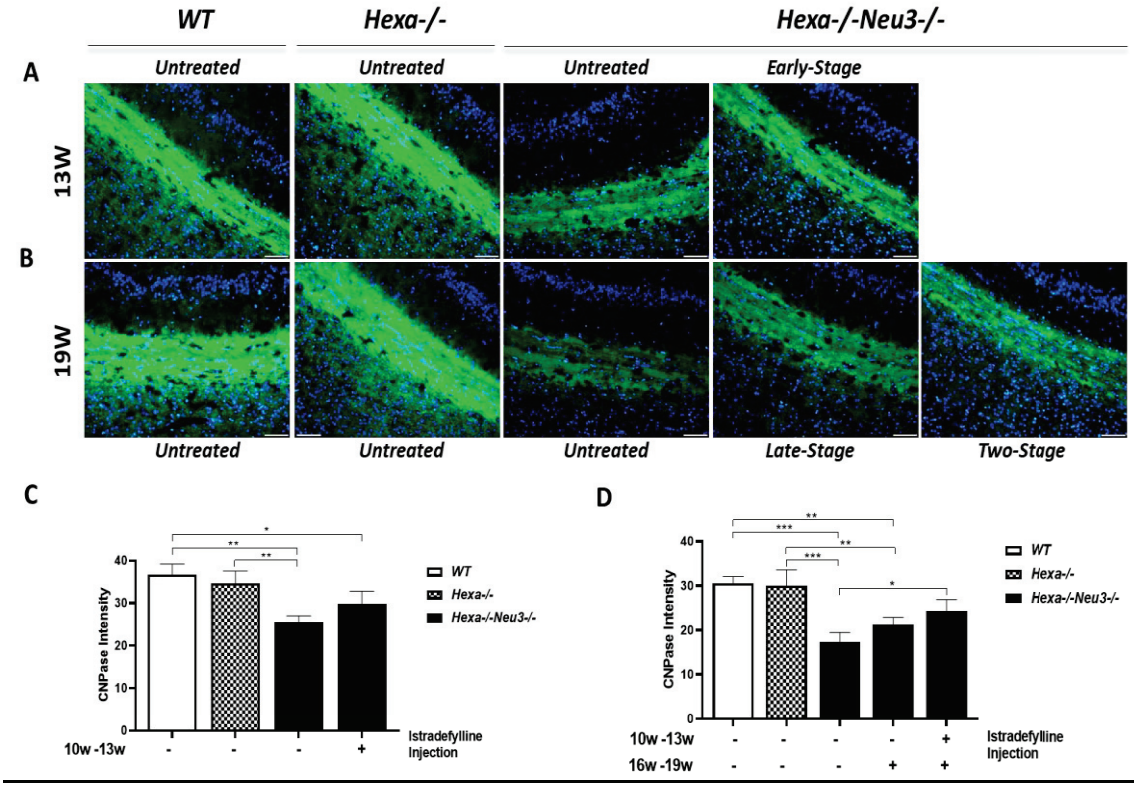

Figure 3.23. CNPase staining in cortex region of WT, Hexa-/- and Hexa-/-Neu3-/- were represented. The 20μm coronal sections were stained in green by anti-CNPase antibody (oligodendriocyte marker) and in blue by DAPI (nucleus). Images for 13W-old controls and early-stage treated Hexa-/-Neu3-/- mice (A) and 19W-old controls, late-stage and two-stage treated Hexa-/-Neu3-/- mice (B) were represented. GFAP intensity analyses performed by NIH Image J program and histographic representation for 13W-old (C) and 19W-old groups (D) were shown. Scale bar indicates 50μm of cortex. Data is representative of mean ± SEM of measurements. one-way ANOVA was used for statistical analysis (*$p<0.05$ and **$p<0.025$)

When we analyzed the CNPase level; it can be observed that untreated *Hexa-/-Neu3-/-* mice displayed significantly reduced CNPase levels in both cortex and cerebellum region when compared to age-matched *WT* and *Hexa-/-* mice (Figure 3.23 and

24). This reduction was significantly reversed in cortex region of *Hexa-/-Neu3-/-* by two-stage treatment strategy (Figure 3.23D) compared to age-matched untreated condition. Early and late-stage treatment strategies did not significantly change CNPase level in the cortex of *Hexa-/-Neu3-/-* mice. On the other hand, CNPase level were significantly increased in the cerebellum region of *Hexa-/-Neu3-/-* by all three different istradefylline administration strategies when compared to age-matched untreated *Hexa-/-Neu3-/-* mice (Figure 3.24 C, D).

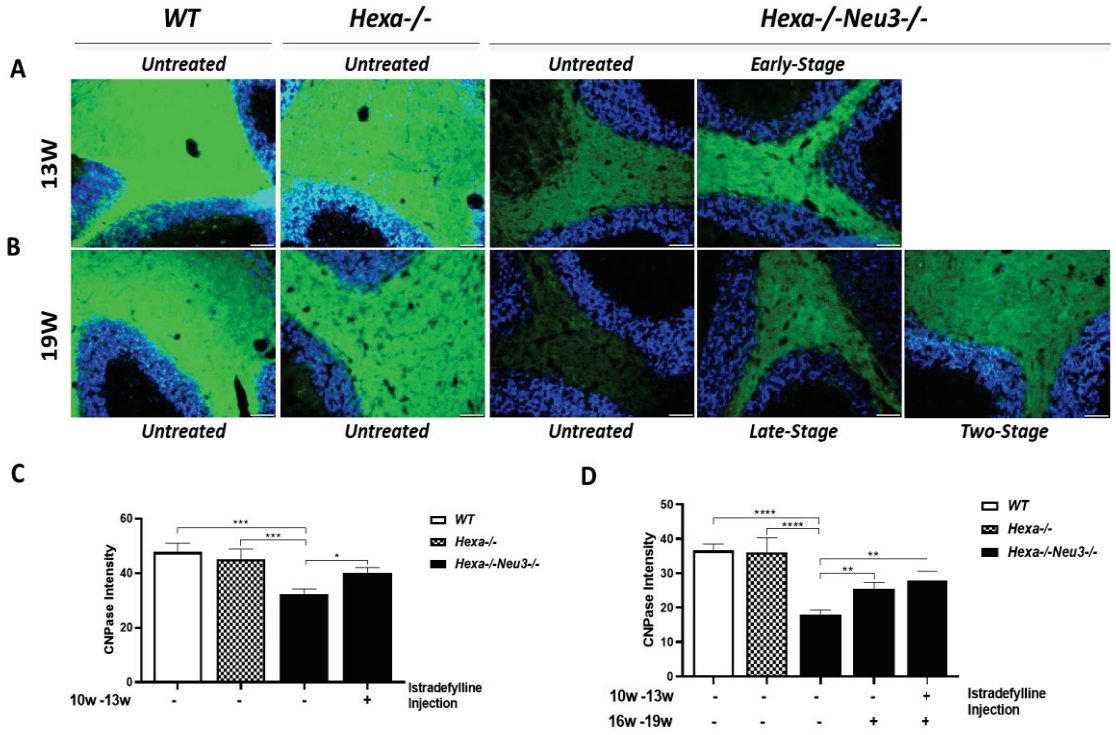

Figure 3.24. CNPase staining in cerebellum region of WT, Hexa-/- and Hexa-/-Neu3-/- were represented. The 20μm coronal sections were stained in green by anti-CNPase antibody (oligodendriocyte marker) and in blue by DAPI (nucleus). Images for 13W-old controls and early-stage treated Hexa-/-Neu3-/- mice (A) and 19W-old controls, late-stage and two-stage treated Hexa-/-Neu3-/- mice (B) were represented. GFAP intensity analyses performed by NIH Image J program and histographic representation for 13W-old (C) and 19W-old groups (D) were shown. Scale bar indicates 50μm of cortex. Data is representative of mean ± SEM of measurements. one-way ANOVA was used for statistical analysis (*$p<0.05$ and **$p<0.025$)

3.3.3.4. IL-6 Staining

Interleukin-6 level was also measured in cortex, cerebellum, thalamus and hippocampus regions of untreated *WT*, *Hexa-/-*, *Hexa-/-Neu3-/-* control groups and early-stage (10w-13w), late-stage (16w-19w) and two-stage (10w-13w & 16w-19w) treatment groups of *Hexa-/-Neu3-/-* by anti-IL-6 antibody staining.

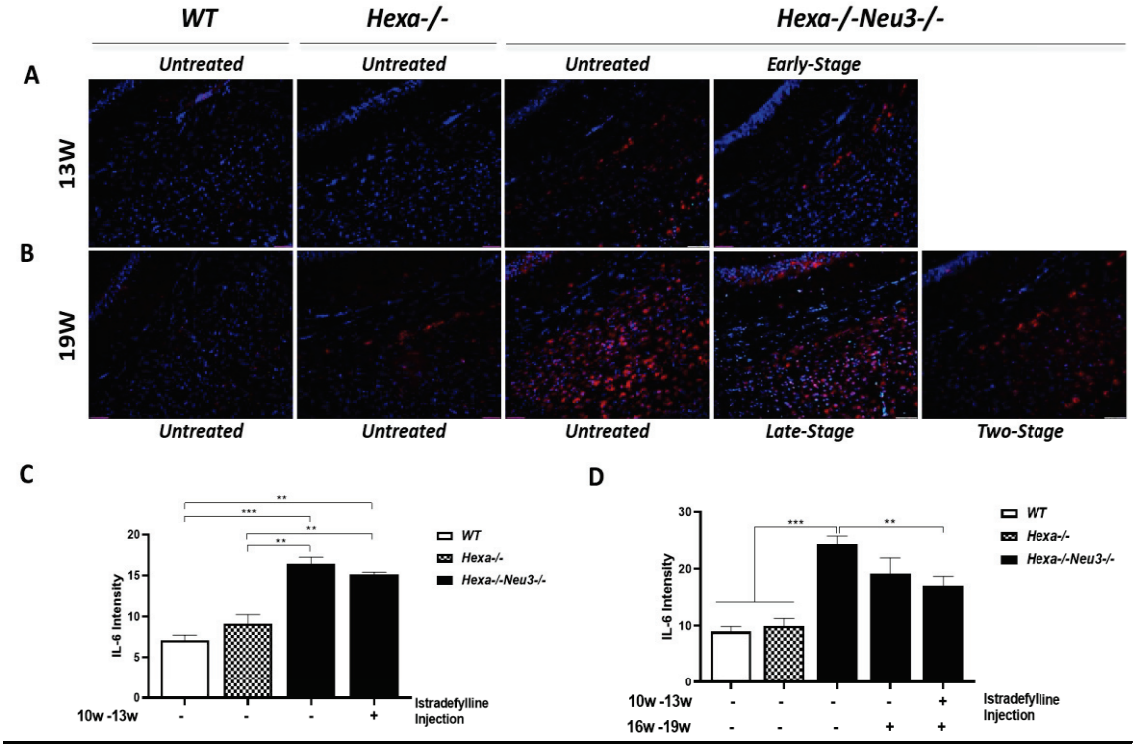

Figure 3.25. IL-6 staining in cortex region of WT, Hexa-/- and Hexa-/-Neu3-/- were represented. The 20μm coronal sections were stained in red by anti-IL-6 antibody (interleukin-6 marker) and in blue by DAPI (nucleus). Images for 13W-old controls and early-stage treated Hexa-/-Neu3-/- mice (A) and 19W-old controls, late-stage and two-stage treated Hexa-/-Neu3-/- mice (B) were represented. GFAP intensity analyses performed by NIH Image J program and histographic representation for 13W-old (C) and 19W-old groups (D) were shown. Scale bar indicates 50μm of cortex. Data is representative of mean ± SEM of measurements. one-way ANOVA was used for statistical analysis (*p<0.05 and **p<0.025)

Interleukin-6 level was significantly increased in all of the brain regions (cortex, cerebellum, thalamus and hippocampus) of untreated *Hexa-/-Neu3-/-* mice compared to age-matched *WT* and *Hexa-/-* controls. In cortex region this increased IL-6 level in *Hexa-*

/-Neu3-/- mice was significantly reduced by two-stage treatment of istradefylline when compared to untreated conditions (Figure 3.25). Early and late-stage treatment did not affect IL-6 level in cortex even if late stage treatment enabled slight decrease (Figure 3.25D).

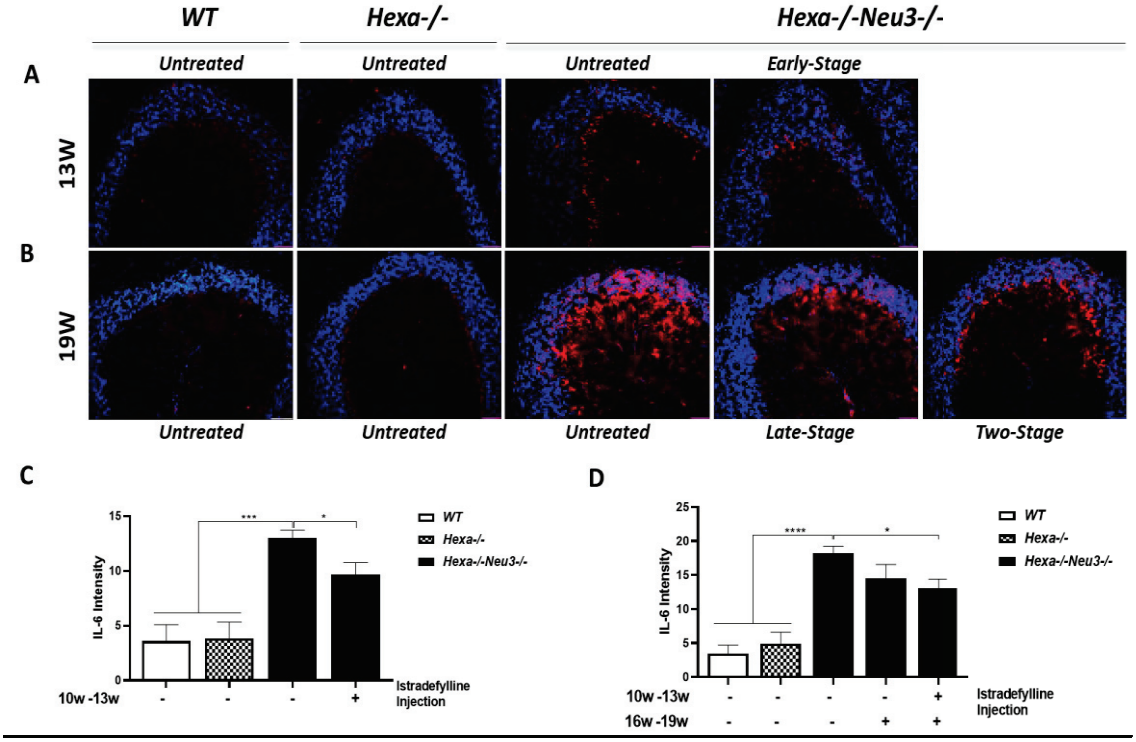

Figure 3.26. IL-6 staining in cerebellum region of WT, Hexa-/- and Hexa-/-Neu3-/- were represented. The 20μm coronal sections were stained in red by anti-IL-6 antibody (interleukin-6 marker) and in blue by DAPI (nucleus). Images for 13W-old controls and early-stage treated Hexa-/-Neu3-/- mice (A) and 19W-old controls, late-stage and two-stage treated Hexa-/-Neu3-/- mice (B) were represented. GFAP intensity analyses performed by NIH Image J program and histographic representation for 13W-old (C) and 19W-old groups (D) were shown. The scale bar indicates 50μm of cortex. Data is representative of mean ± SEM of measurements. one-way ANOVA was used for statistical analysis (*p<0.05 and **p<0.025)

In cerebellum region, IL-6 level in 13W-old *Hexa-/-Neu3-/-* was significantly decreased by early-stage treatment of istradefylline (Figure 3.26C). In the 19W-old group; two-stage treatment significantly reduced IL-6 level in cerebellum of *Hexa-/-Neu3-/-* when compared to untreated condition. In addition, late stage treatment led to slight decrease in IL-6 level as well but it was not statistically significant (Figure 3.26D).

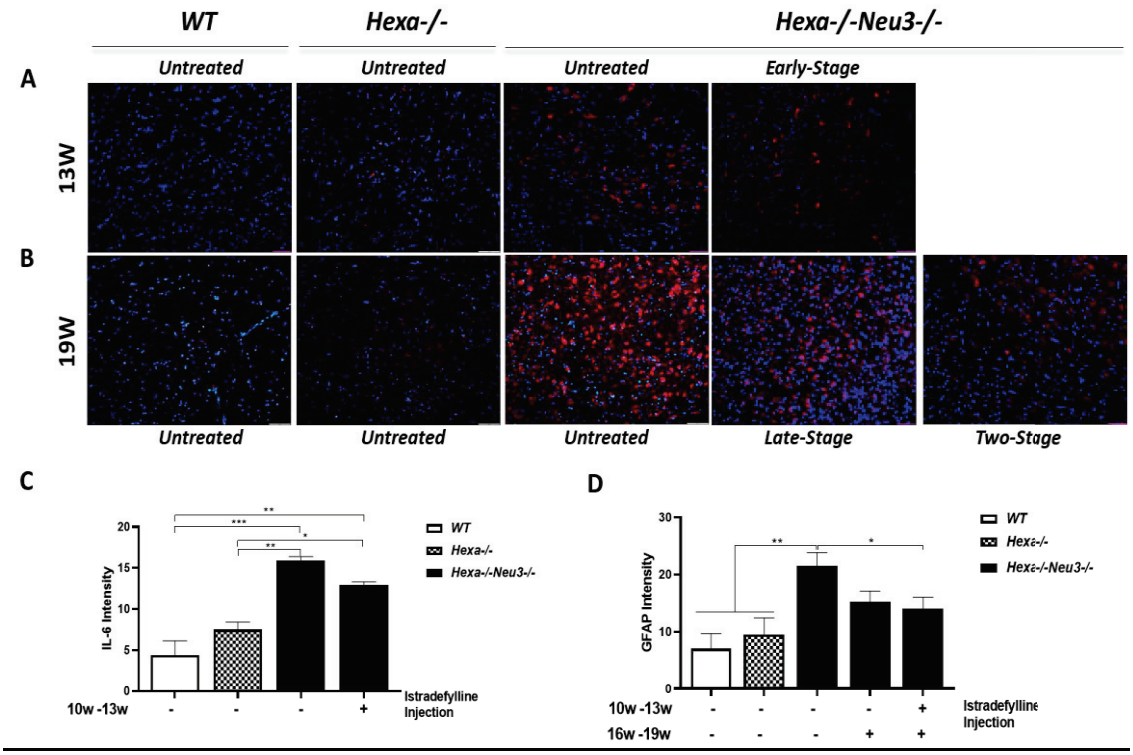

Figure 3.27. IL-6 staining in thalamus region of WT, Hexa-/- and Hexa-/-Neu3-/- were represented. The 20μm coronal sections were stained in red by anti-IL-6 antibody (interleukin-6 marker) and in blue by DAPI (nucleus). Images for 13W-old controls and early-stage treated Hexa-/-Neu3-/- mice (A) and 19W-old controls, late-stage and two-stage treated Hexa-/-Neu3-/- mice (B) were represented. GFAP intensity analyses performed by NIH Image J program and histographic representation for 13W-old (C) and 19W-old groups (D) were shown. Scale bar indicates 50μm of cortex. Data is representative of mean ± SEM of measurements. one-way ANOVA was used for statistical analysis (*p<0.05 and **p<0.025)

Similar to cortex region, IL-6 level was significantly decreased in thalamus region of *Hexa-/-Neu3-/-* mice by two-stage treatment of istradefylline when compared to untreated condition (Figure 3.27D). When we look at the other strategies (early and late), there was not any significant change in IL-6 levels in thalamus except for a slight decrease in late stage treatment group (Figure 3.27C, D).

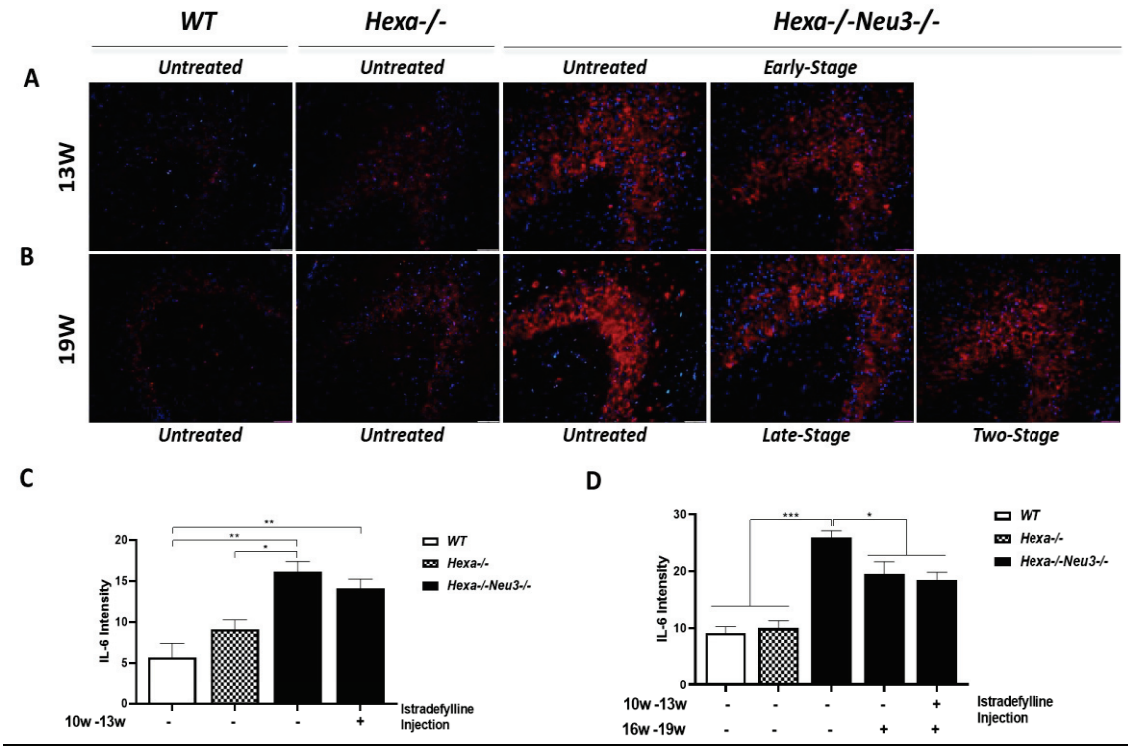

Figure 3.28. IL-6 staining in hippocampus region of WT, Hexa-/- and Hexa-/-Neu3-/- were represented. The 20μm coronal sections were stained in red by anti-IL-6 antibody (interleukin-6 marker) and in blue by DAPI (nucleus). Images for 13W-old controls and early-stage treated Hexa-/-Neu3-/- mice (A) and 19W-old controls, late-stage and two-stage treated Hexa-/-Neu3-/- mice (B) were represented. GFAP intensity analyses performed by NIH Image J program and histographic representation for 13W-old (C) and 19W-old groups (D) were shown. Scale bar indicates 50μm of cortex. Data is representative of mean ± SEM of measurements. one-way ANOVA was used for statistical analysis (*p<0.05 and **p<0.025)

Finally, in hippocampus region IL-6 level did not significantly changed by early stage treatment (Figure 3.28C) however late and two-stage treatment of istradefylline were led to significant decrease in IL-6 level in *Hexa-/-Neu3-/-* mice when compared to untreated condition (Figure 3.28D).

3.4. Oxidative Stress Analysis

Oxidative stress markers were analyzed by RTPCR and western blot by the support of TUBİTAK-123Z180 project.

3.4.1. Real-Time PCR

The effects of anti-inflammatory therapy on redox homeostasis were analyzed in cortex and cerebellum region by RTPCR analysis for markers involving in antioxidant defense mechanism: SOD2, TTase1, and Catalase. In the cortex region, the gene expression level of SOD2 was significantly higher in 13W-old and 19W-old *Hexa-/-Neu3-/-* compared to age-matched *WT* and *Hexa-/-* mice. Istradefylline administration reduced the SOD2 gene expression level in the cortex of *Hexa-/-Neu3-/-* slightly by early-stage treatment (Figure 3.29A) and significantly by late and two-stage treatment strategies compared to untreated condition (Figure 3.29B). Catalase expression level did not change in the 13W-old group (Figure 3.29C) however it was significantly increased in 19W-old untreated *Hexa-/-Neu3-/-* compared to age-matched *Hexa-/-* and significantly decreased by two-stage treatment (Figure 3.29D). In addition, significant overexpression of the TTase-1 gene was observed in 13W-old and 19W-old *Hexa-/-Neu3-/-* compared to age-matched controls (Figure 3.29E,F) and early-stage (Figure 3.29E) and two-stage treatment (Figure 3.29F) significantly reduced the TTase-1 expression in the cortex of *Hexa-/-Neu3-/-* compared to untreated condition. Late-stage treatment also slightly reduced the expression level of TTase-1 in cortex of *Hexa-/-Neu3-/-* but it was not statistically significant (Figure 3.29F).

The effect of three different strategies on gene expression levels of oxidative stress markers in the cortex region was also normalized to age-matched *WT* and compared with each other and untreated conditions for SOD2 (Figure 3.29G), Catalase (Figure 3.29H) and TTase-1 (Figure 3.29I). The gene expression levels of SOD2 were significantly decreased in the cortex region of 19W-old untreated *Hexa-/-Neu3-/-* mice compared to 13W-old untreated *Hexa-/-Neu3-/-* mice (Figure 3.29G). Two-stage treatment was the most effective strategy of istradefylline administration to reduce the expression levels of SOD2 (Figure 3.29G), Catalase (Figure 3.29H) and TTase-1 (Figure 3.29I).

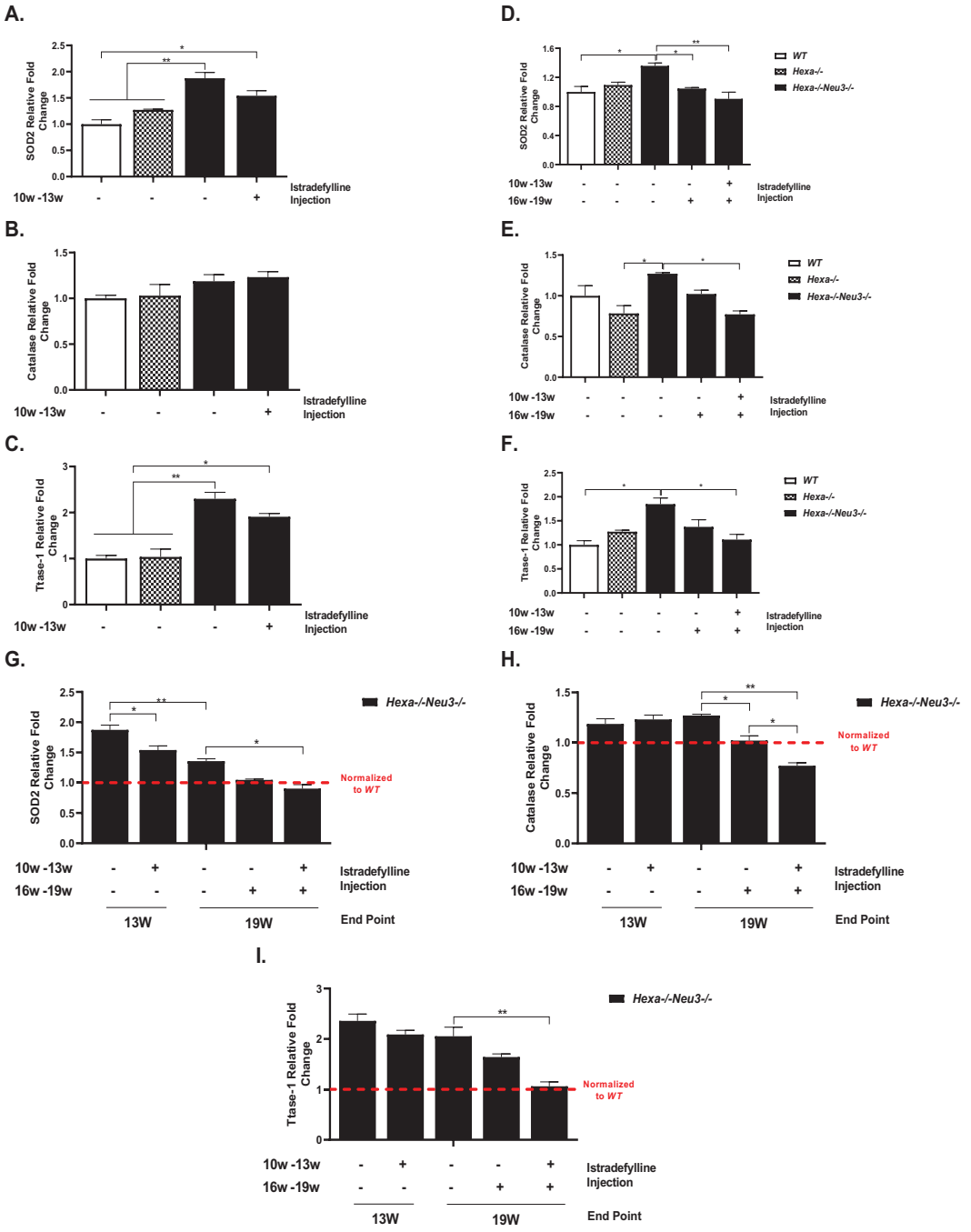

Figure 3.29. The expression levels of SOD2, Catalase and TTase-1 in cortex region of WT, Hexa-/- and Hexa-/-Neu3-/- were represented. The expression levels of SOD2 (A,B), Catalase (C,D) and TTase-1(E,F) in age-matched controls and early-stage (10w-13w), late-stage and two stage treatment groups (10w-13w & 16w-19w) were indicated respectively. SOD2 (G), Catalse (H) and TTase-1 (I) gene expression levels in cortex region of untreated and treated Hexa-/-Neu3-/- were represented as normalized to age-matched WT that are compared based on untreated, early-stage late-stage and two-stage treatment conditions Expression ratio calculations were performed by ΔCT method and data was normalized to expression levels of age-matched WT mice. Significant levels in the data were presented by using the one-way ANOVA (*p<0.05, **p<0.01, ***p<0.001, and ****p<0.0001).

When we look at the expression levels of oxidative stress markers in the cerebellum region; SOD2, Catalase, and TTase-1 gene expression levels were significantly increased in the cerebellum region of both 13W-old and 19W-old untreated *Hexa-/-Neu3-/-* mice compared to untreated *WT* and *Hexa-/-* counterparts except for catalase expression at 13W-old stage (Figure 3.30).

Istradefylline administration significantly reduced the SOD2 gene expression level in the cerebellum of *Hexa-/-Neu3-/-* by early-stage (Figure 3.30A) late-stage and two-stage treatment strategies compared to untreated condition (Figure 3.30B). Catalase expression level did not change by early-stage and late stage treatment (Figure 3.30C, D) however it was significantly decreased by two-stage treatment in the cerebellum of *Hexa-/-Neu3-/-* compared to untreated condition (Figure 3.30D). Additionally, the TTase-1 gene expression level was reduced slightly by early (Figure 3.30E) and late-stage treatment and significantly by two-stage treatment in the *Hexa-/-Neu3-/-* cerebellum compared to untreated condition (Figure 3.30F). The effect of three different strategies on gene expression levels of oxidative stress markers in cerebellum region was also normalized to age-matched *WT* and compared with each other and untreated conditions for SOD2 (Figure 3.30G), Catalase (Figure 3.30H) and TTase-1 (Figure 3.30I). The gene expression levels of Catalase were significantly increased in the cortex region of 19W-old untreated *Hexa-/-Neu3-/-* mice compared to 13W-old untreated *Hexa-/-Neu3-/-* mice (Figure 3.30H). SOD2 (Figure 3.30G) and TTase-1 (Figure 3.30I) expression did not change in cerebellum of HexaNeu3 mice in an age dependent way. Similar to cortex region, two-stage treatment was the most effective strategy of istradefylline administration to reduce the expression levels of SOD2 (Figure 3.30G), Catalase (Figure 3.30H) and TTase-1 (Figure 3.30I) in cerebellum region.

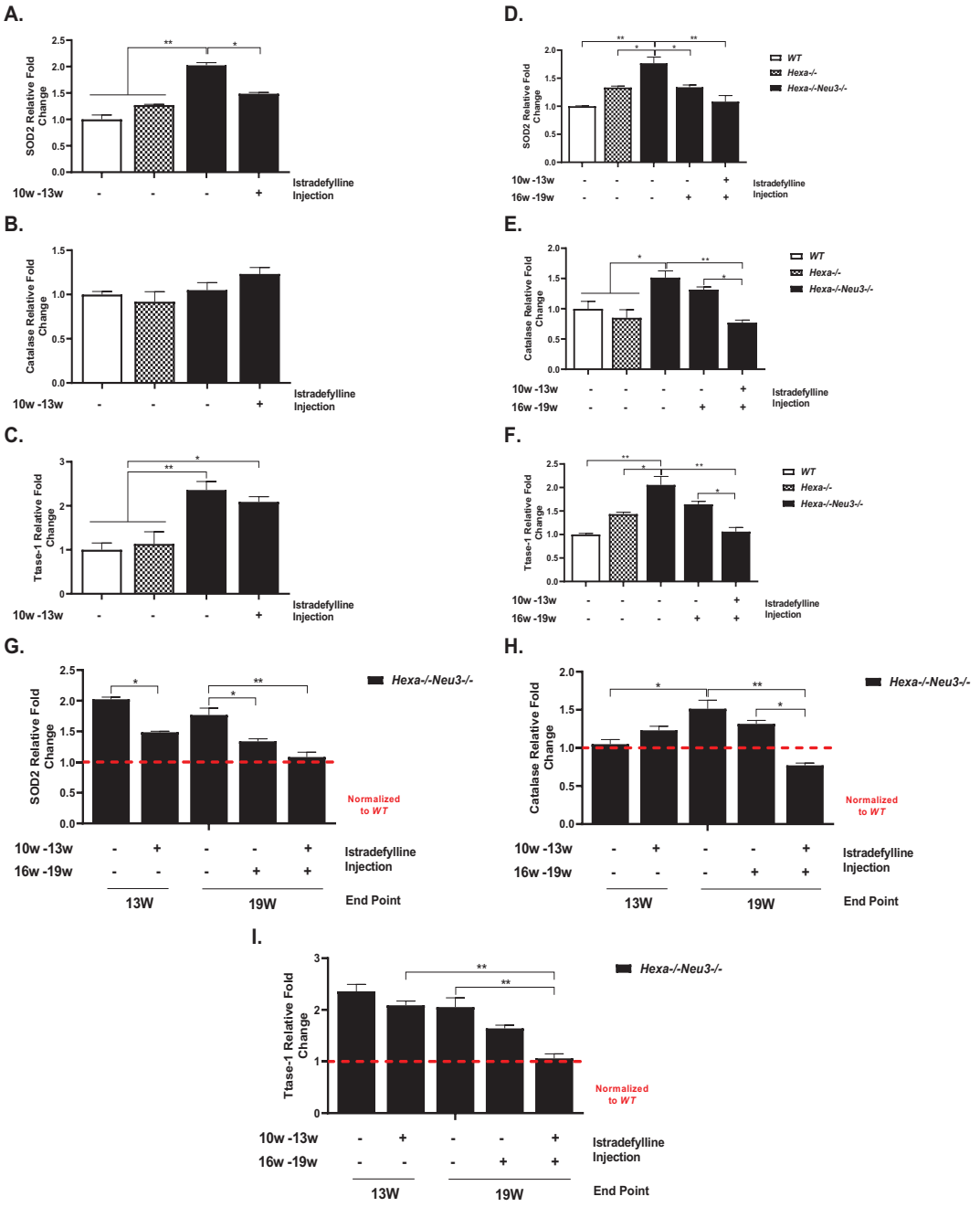

Figure 3.30. The expression levels of SOD2, Catalase and TTase-1 in cerebellum region of WT, Hexa-/- and Hexa-/-Neu3-/- were represented. The expression levels of SOD2 (A,B), Catalase (C,D) and TTase-1(E,F) in age-matched controls and early-stage (10w-13w), late-stage and two stage treatment groups (10w-13w & 16w-19w) were indicated respectively. SOD2 (G), Catalse (H) and TTase-1 (I) gene expression levels in cerebellum region of untreated and treated Hexa-/-Neu3-/- were represented as normalized to age-matched WT that are compared based on untreated, early-stage late-stage and two-stage treatment conditions Expression ratio calculations were performed by ΔCT method and data was normalized to expression levels of age-matched WT mice. Significant levels in the data were presented by using the one-way ANOVA (*p<0.05, **p<0.01, ***p<0.001, and ****p<0.0001).

3.4.2. Western Blot

APE1 protein expression were analyzed by Western Blot in cortex and cerebellum region of untreated *WT*, *Hexa-/-*, *Hexa-/-Neu3-/-* control groups and early-stage (10w-13w), late-stage (16w-19w) and two-stage (10w-13w & 16w-19w) treated *Hexa-/-Neu3-/-*. In the cortex region, APE1 protein level did not change in 13W-old untreated *WT, Hexa-/-* and *Hexa-/-Neu3-/-* however early-stage treatment increased the APE1 protein expression in *Hexa-/-Neu3-/-* mice compared to untreated condition (Figure 3.31A, B). In 19W-old group there was no significant change in untreated conditions however two-stage treatment significantly increased APE1 protein expression in cortex region of *Hexa-/-Neu3-/-* compared to untreated condition (Figure 3.31C, D).

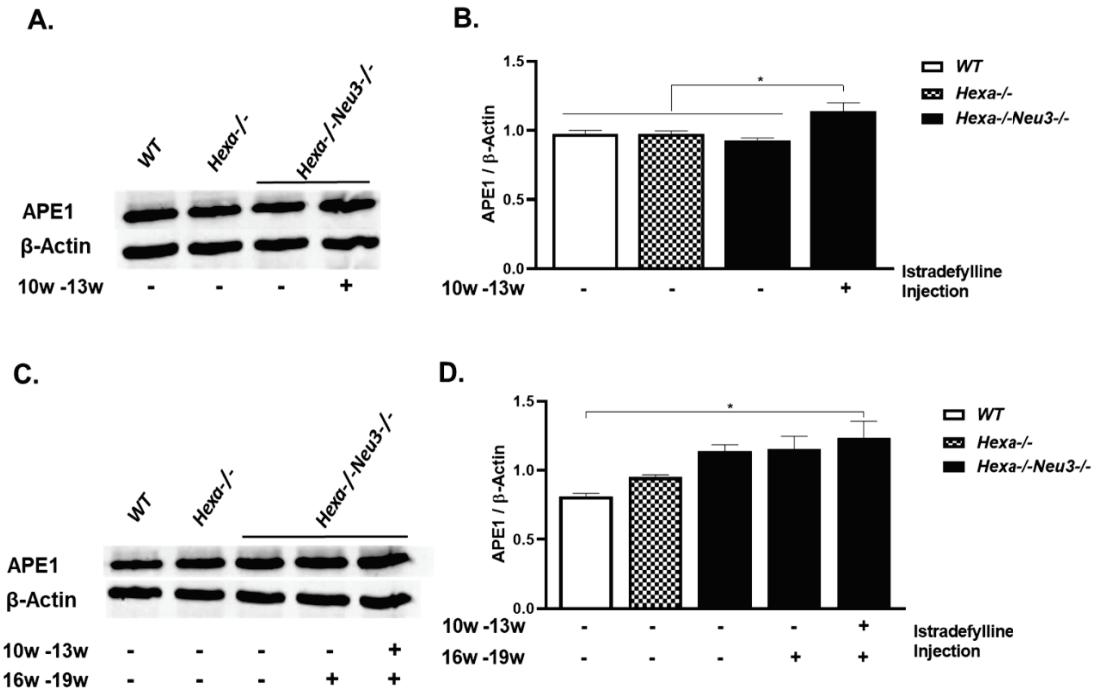

Figure 3.31. Western-blot analysis for APE1 protein in cortex region of WT, Hexa-/- and Hexa-/-Neu3-/- were represented. Western blot images and histographic representation were indicated for early-stage(10w-13w) (A, B), Late-stage (16w-19w) (C,D) and two-stage treatment (10w-13w & 16w-19w)(C,D,) groups were indicated respectively.

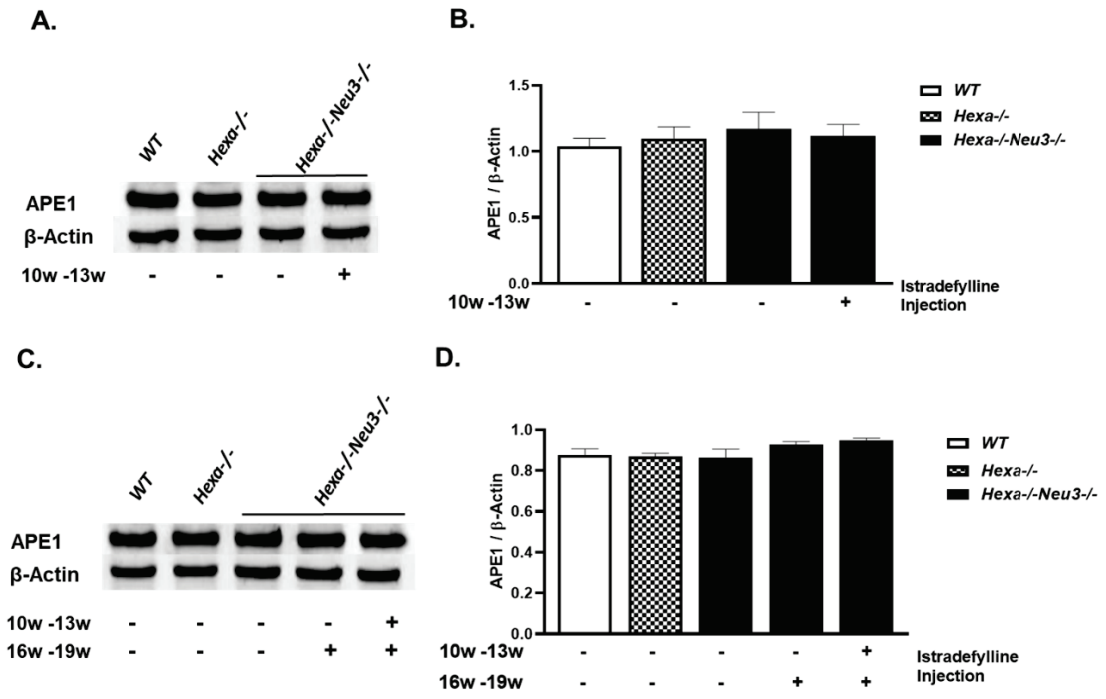

Figure 3.32. Western-blot analysis for APE1 protein in cerebellum region of WT, Hexa-/- and Hexa-/-Neu3-/- were represented. Western blot images and histographic representation were indicated for early-stage(10w-13w) (A,B), Late-stage (16w-19w) (C,D) and two-stage treatment (10w-13w & 16w-19w)(C,D,) groups were indicated respectively.

Moreover, APE1 protein expression did not significantly change in cerebellum region depending on the genotypes, age-group or any of istradefylline administration strategies (Figure3.32).

3.5. Disease Pathology Analysis

The markers related with the Tay-Sachs Disease pathology was analyzed by RT-PCR, thin layer chromatography and NeuN staing for cortex and cerebellum regions of control and treatment groups.

3.5.1. RT-PCR Analysis

To determine the effect of istradefylline administration on gene expression levels of enzymes involving in ganglioside synthesis and degradation pathway in cortex and

cerebellum regions of untreated *WT*, *Hexa-/-* , *Hexa-/-Neu3-/-* control groups and early-stage (10w-13w), late-stage (16w-19w) and two stage treatment groups (10w-13w & 16w-19w). In cortex region HexB gene expression levels of HexB were significantly increased in untreated *Hexa-/-Neu3-/-* mice compared to untreated age-matched *WT* and *Hexa-/-* counterparts. In addition, early and two-stage treatment led to significant increase in HexB gene expression level in *Hexa-/-Neu3-/-* mice compared to untreated counterparts (Figure 3.33 A, B).-The effect of three different strategies on gene expression level of HexB was normalized to age-matched *WT* and compared with each other and untreated conditions. Accordingly, two-stage administration strategy was most prominently increased HexB gene expression level in cortex of *Hexa-/-Neu3-/-* mice when compared to age matched controls, early- and late-stage treatment groups (Figure 3.33 C). When we look at the GM2AP expression level in cortex region, we did not observe any significant change in expression level of GM2AP between control groups or upon treatments (Figure 3.33 D, E, and F).

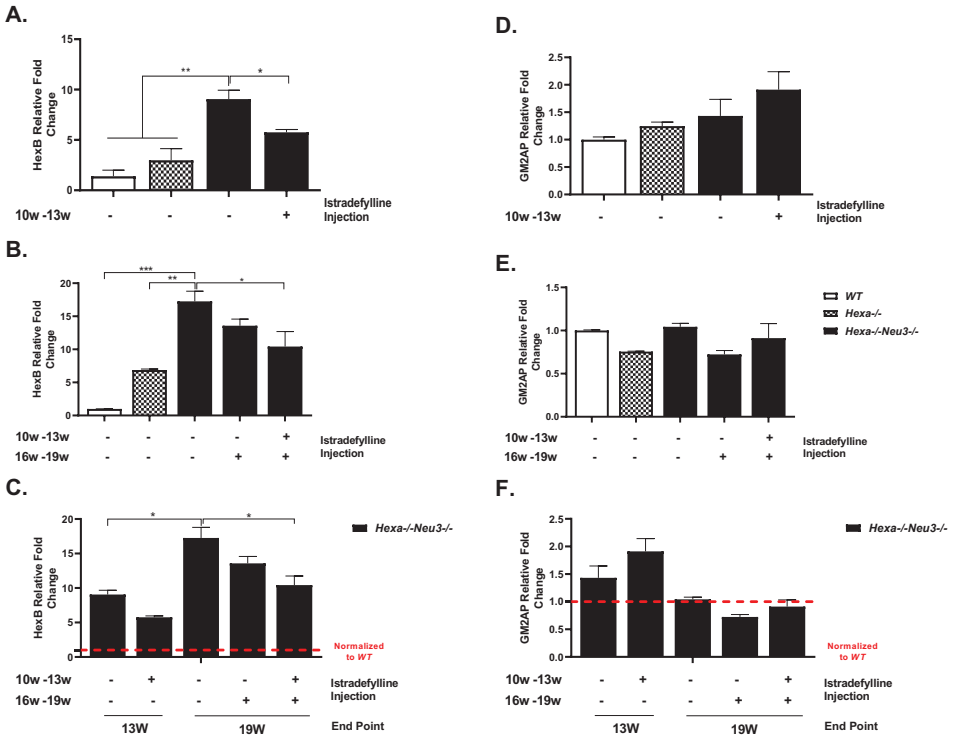

Figure 3.33. The expression levels of HexB and GM2AP in cortex region of WT, Hexa-/- and Hexa-/-Neu3-/- were represented. The expression levels of HexB (A,B) and GM2AP (D,E) in age-matched controls and early-stage (10w-13w), late-stage and two stage treatment groups (10w-13w & 16w-19w) were indicated respectively. HExB (C) and GM2AP (F) gene expression levels in cortex region of untreated and treated Hexa-/-Neu3-/- were represented as normalized to age-matched WT that are compared based on untreated, early-stage late-stage and two-stage treatment conditions Expression ratio calculations were performed by ΔCT method and data

was normalized to expression levels of age-matched WT mice. Significant levels in the data were presented by using the one-way ANOVA (*p<0.05, **p<0.01, ***p<0.001, and ****p<0.0001).

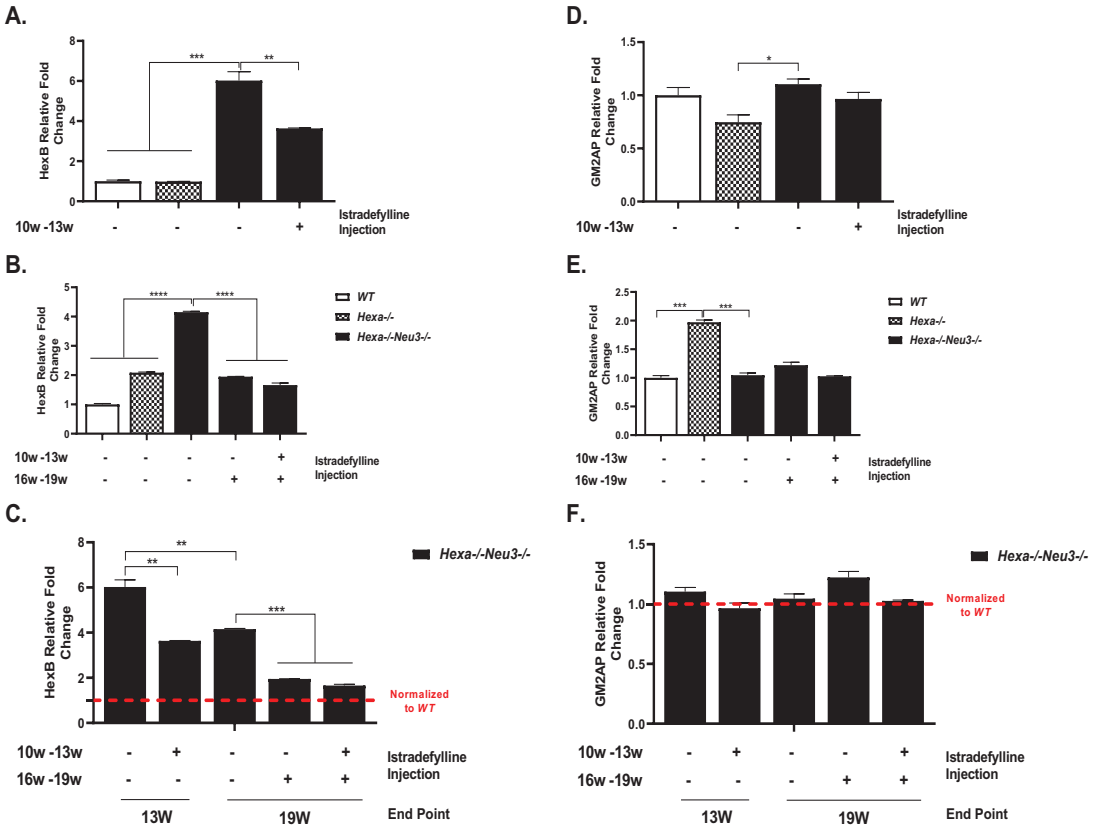

Figure 3.34. The expression levels of HexB and GM2AP in cerebellum region of WT, Hexa-/- and Hexa-/-Neu3-/- were represented. The expression levels of HexB (A, B) and GM2AP (D,E) in age-matched controls and early-stage (10w-13w), late-stage(16w-19w) and two stage treatment groups (10w-13w & 16w-19w) were indicated respectively. HExB (C) and GM2AP (F) gene expression levels in cerebellum region of untreated and treated Hexa-/-Neu3-/- were represented as normalized to age-matched WT that are compared based on untreated, early-stage late-stage and two-stage treatment conditions Expression ratio calculations were performed by ΔCT method and data was normalized to expression levels of age-matched WT mice. Significant levels in the data were presented by using the one-way ANOVA (*p<0.05, **p<0.01, ***p<0.001, and ****p<0.0001).

HexB gene expression level was significantly increased in cerebellum region of untreated *Hexa-/-Neu3-/-* mice compared to age-matched *WT* and *Hexa-/-* controls. The increased HexB expression level was reduced in cerebellum of *Hexa-/-Neu3-/-* mice by all early, late and two-stage treatment strategies (Figure 3.34 A, B). When we compare

the effectiveness of the 3 different strategies, it can be said that late and two-stage treatment reduced HexB expression more evidently (Figure 3.34 C). GM2AP expression in cerebellum of 13W-old *Hexa-/-Neu3-/-* was significantly higher than age matched Hexa-/- (Figure 3.34 D) and significant increase in GM2AP expression was also observed in cerebellum of 19W-old *Hexa-/-* compared to age matched *WT* and *Hexa-/-Neu3-/-* (Figure 3.34 E).Additionally, istradefylline administration by three different strategies did not affect GM2AP expression in cerebellum of *Hexa-/-Neu3-/-* (Figure 3.34F).

3.5.2. Thin Layer Chromatography

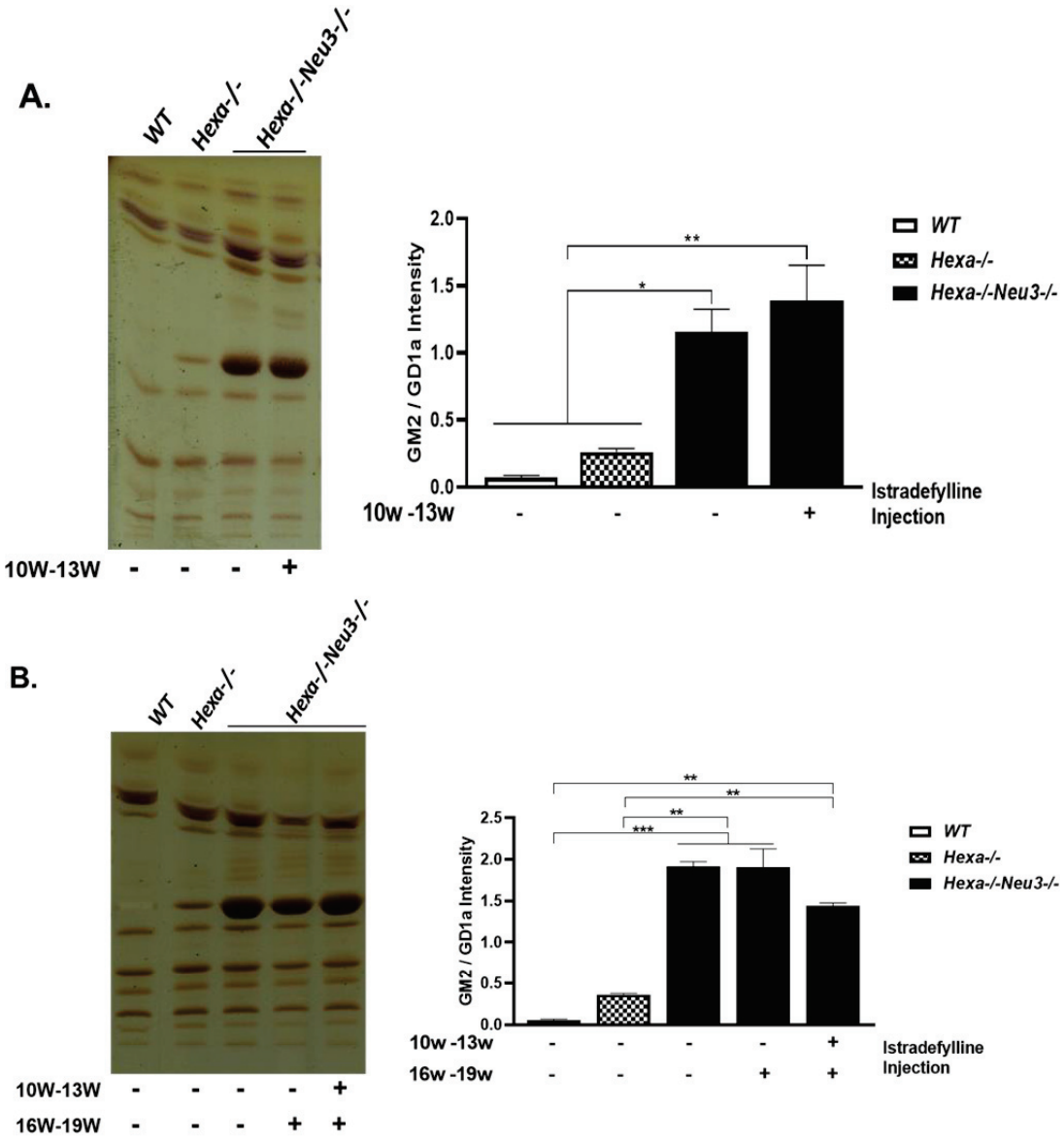

Figure 3.35. TLC plate images and histograps of GM2 intensity in cortex of early-stage (A), late-stage and two-stage treatment (B) groups were represented for acidic GSLs. The

levels of GM2 ganglioside normalized to GD1a level in the cerebellum region were indicated in histographs. Data is representative of mean ± SEM of measurements. Significant levels in the data were presented by using the one-way ANOVA (*p<0.05, ***p<0.001 and ****p<0.0001).

To determine the effect of istradefylline administration on GM2 accumulation, which is a hallmark of TSD pathology, thin layer chromatography analysis was performed for cortex and cerebellum regions of untreated *WT*, *Hexa-/-* , *Hexa-/-Neu3-/-* control groups and early-stage (10w-13w), late-stage (16w-19w) and two stage treatment groups (10w-13w & 16w-19w). TLC analyses on cortex and cerebellum regions were generated by optimized TLC procedure in our lab to isolate and separate acidic gangliosides. The GM2 ganglioside band intensity was normalized to GD1a intensity.

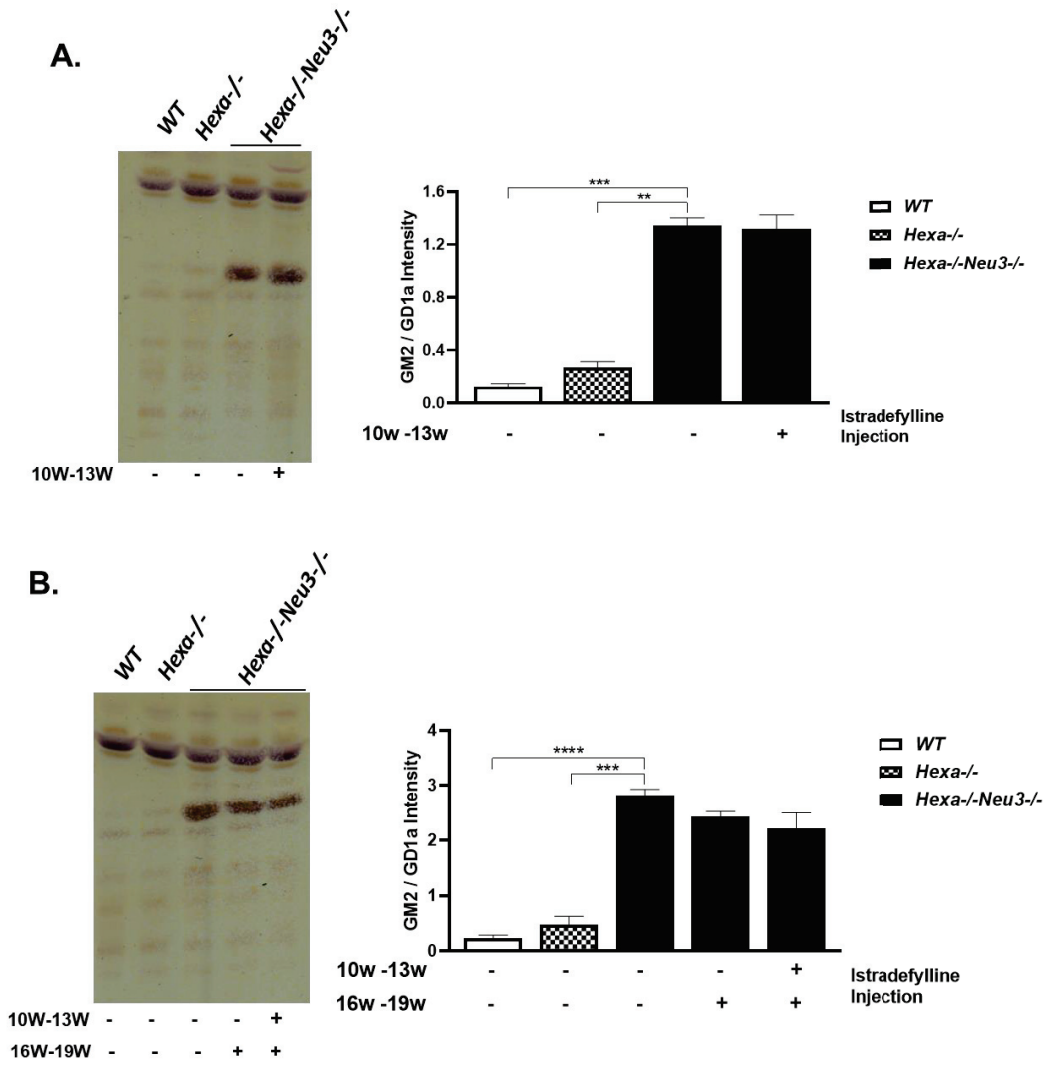

Figure 3.36. TLC plate images and histograps of GM2 intensity in cerebellum of early-stage (A), late-stage and two-stage treatment (B) groups were represented for acidic GSLs.

The levels of GM2 ganglioside normalized to GD1a level in the cerebellum region were indicated in histographs. Data is representative of mean ± SEM of measurements. Significant levels in the data were presented by using the one-way ANOVA (*p<0.05, ***p<0.001 and ****p<0.0001).

In both cortex and cerebellum region, severe GM2 ganglioside accumulation was observed in untreated *Hexa-/-Neu3-/-* mice compared to age-matched *WT* and *Hexa-/-* (Figure 3.35 and 36). Early stage treatment slightly increased but two stage treatment of istradefylline slightly reduced the accumulation level of GM2 ganglioside in cortex of *Hexa-/-Neu3-/-* mice compared to untreated condition (Figure 3.35). On the other hand, istradefylline administration did not affect GM2 accumulation level in cerebellum of *Hexa-/-Neu3-/-* mice independent of the strategy of the administration (Figure 3.36).

3.5.3. Immunohistochemical Analysis

Neurodegeneration degree of control and treatment groups were analyzed by staining cortex and cerebellum regions by anti-NeuN which is a neuronal marker.

3.5.3.1. NeuN Staining

To determine the effect of istradefylline administration on neuronal density, cortex, cerebellum, hippocampus and thalamus regions of untreated *WT*, *Hexa-/-*, *Hexa-/-Neu3-/-* control groups and early-stage (10w-13w), late-stage (16w-19w) and two-stage (10w-13w & 16w-19w) treatment groups of *Hexa-/-Neu3-/-* were stained with anti-NeuN which is a neuronal marker. *Hexa-/-Neu3-/-* mice displayed significantly decreased NeuN density in cortex, cerebellum, thalamus and hippocampus region in untreated condition compared to age-matched *WT* and *Hexa-/-* mice (Figure 3.37, 38, 39 and 40).

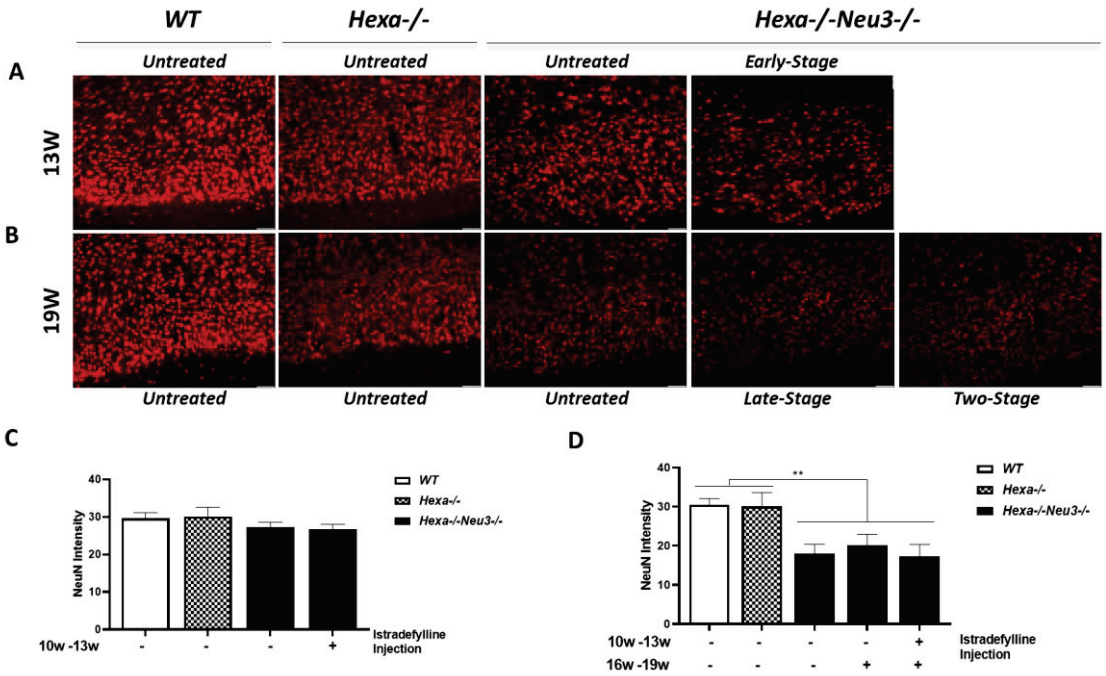

Figure 3.37. Anti-NeuN staining in cortex region of WT, Hexa-/- and Hexa-/-Neu3-/- were represented. The 20μm coronal sections were stained in red by anti-NeuN antibody (neuron marker). Images for 13W-old controls and early-stage treated Hexa-/-Neu3-/- mice (A) and 19W-old controls, late-stage and two-stage treated Hexa-/-Neu3-/- mice (B) were represented. NeuN intensity analyses performed by NIH Image J program and histographic representation for 13W-old (C) and 19W-old groups (D) were shown. Scale bar indicates 50μm of cortex. Data is representative of mean ± SEM of measurements. one-way ANOVA was used for statistical analysis (*$p<0.05$ and **$p<0.025$)

Istradefylline administration did not significantly affect NeuN density in cortex (Figure3.37), cerebellum (Figure3.38), thalamus (Figure3.39) and hippocampus (Figure3.40) of *Hexa-/-Neu3-/-* mice compared to untreated condition. Nevertheless, in cerebellum, thalamus and hippocampus region the NeuN intensity was slightly increased by late and two-stage treatment of istradefylline.

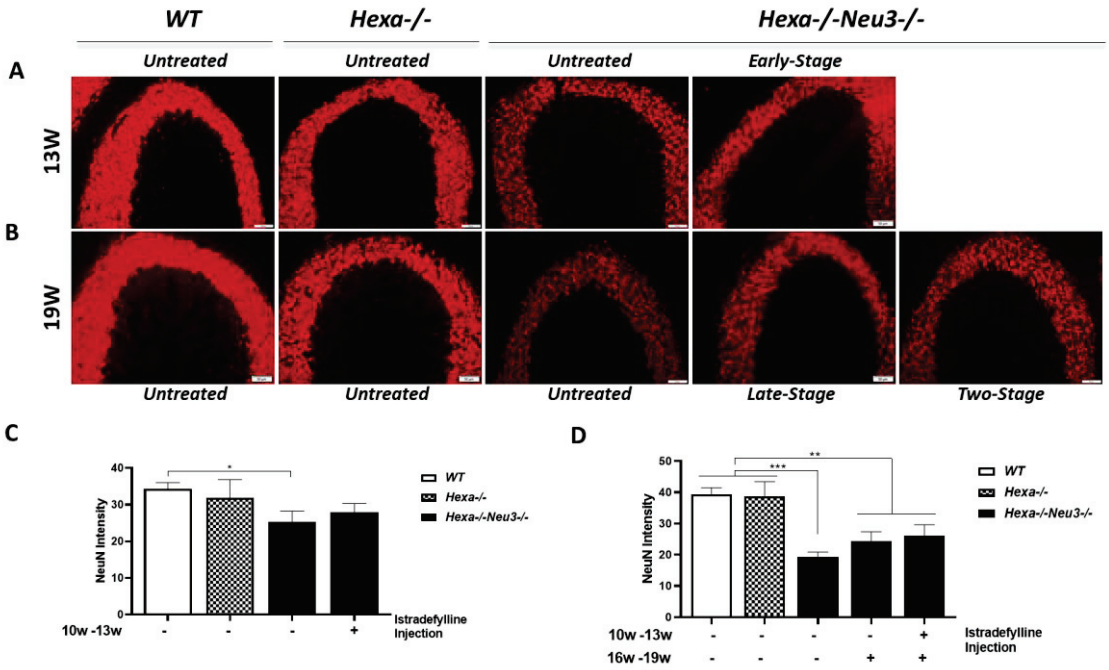

Figure 3.38. Anti-NeuN staining in cerebellum region of WT, Hexa-/- and Hexa-/-Neu3-/- were represented. The 20μm coronal sections were stained in red by anti-NeuN antibody (neuron marker). Images for 13W-old controls and early-stage treated Hexa-/-Neu3-/- mice (A) and 19W-old controls, late-stage and two-stage treated Hexa-/-Neu3-/- mice (B) were represented. NeuN intensity analyses performed by NIH Image J program and histographic representation for 13W-old (C) and 19W-old groups (D) were shown. Scale bar indicates 50μm of cortex. Data is representative of mean ± SEM of measurements. one-way ANOVA was used for statistical analysis (*$p<0.05$ and **$p<0.025$)

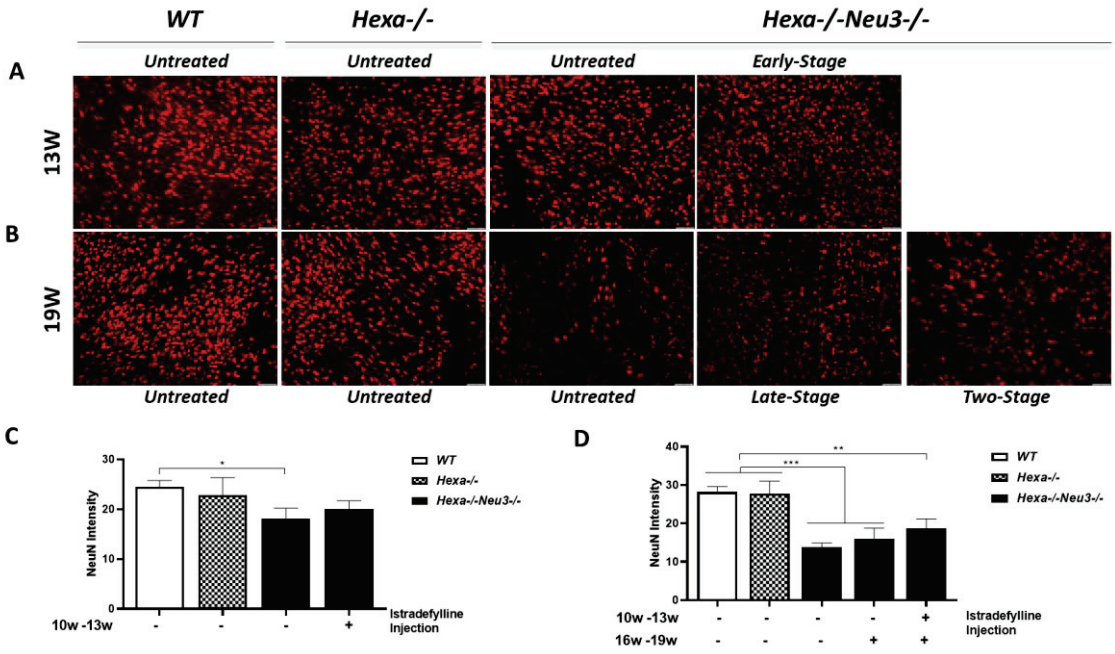

Figure 3.39. Anti-NeuN staining in thalamus region of WT, Hexa-/- and Hexa-/-Neu3-/- were represented. The 20μm coronal sections were stained in red by anti-NeuN antibody (neuron marker). Images for 13W-old controls and early-stage treated Hexa-/-Neu3-/- mice (A) and 19W-old controls, late-stage and two-stage treated Hexa-/-Neu3-/- mice (B) were represented. NeuN intensity analyses performed by NIH Image J program and histographic representation for 13W-old (C) and 19W-old groups (D) were shown. Scale bar indicates 50μm of cortex. Data is representative of mean ± SEM of measurements. one-way ANOVA was used for statistical analysis (*$p<0.05$ and **$p<0.025$)

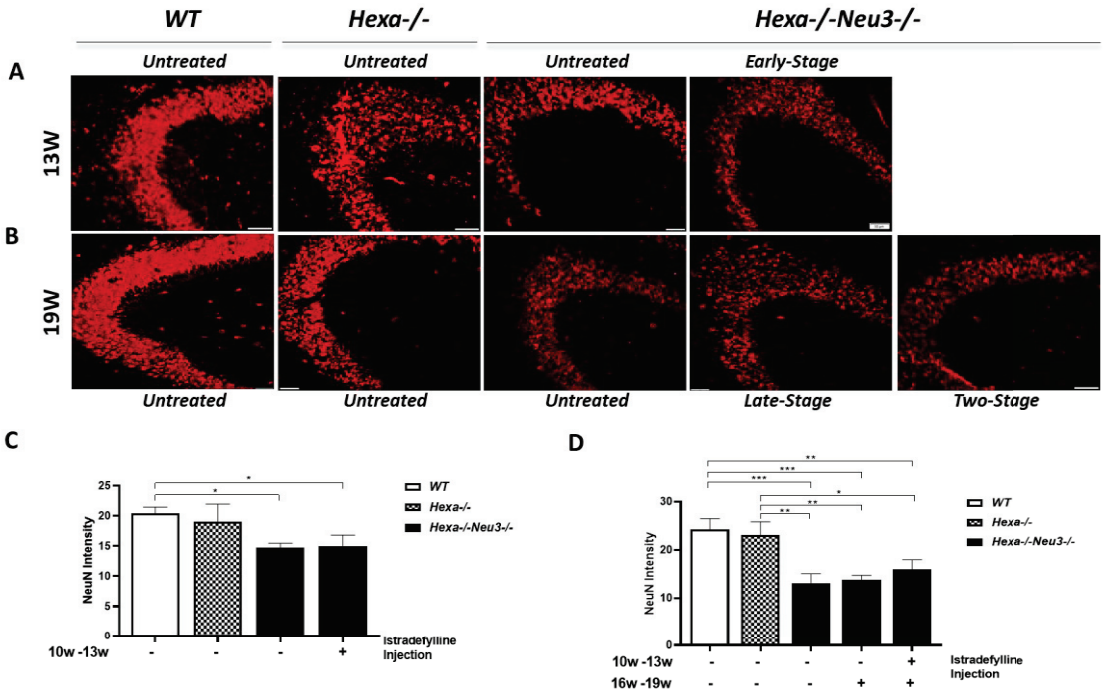

Figure 3.40. Anti-NeuN staining in hippocampus region of WT, Hexa-/- and Hexa-/-Neu3-/- were represented. The 20μm coronal sections were stained in red by anti-NeuN antibody (neuron marker). Images for 13W-old controls and early-stage treated Hexa-/-Neu3-/- mice (A) and 19W-old controls, late-stage and two-stage treated Hexa-/-Neu3-/- mice (B) were represented. NeuN intensity analyses performed by NIH Image J program and histographic representation for 13W-old (C) and 19W-old groups (D) were shown. Scale bar indicates 50μm of cortex. Data is representative of mean ± SEM of measurements. one-way ANOVA was used for statistical analysis (*p<0.05 and **p<0.025)

CHAPTER 4

DISCUSSION

Tay-Sachs disease is a severe genetic disorder that affects the central nervous system due to mutations in the HEXA gene, leading to the accumulation of GM2 ganglioside in neurons and progressive neurodegeneration. Babies with this disease appear healthy at birth but typically die at a young age without a cure. Researchers have developed a mouse model called *Hexa-/-* to study the disease and recent findings suggested the involvement of the Neu3 sialidase enzyme in ganglioside degradation, leading to the creation of the *Hexa-/-Neu3-/-* mouse model, which closely mimics the disease's symptoms for research purposes.(Seyrantepe, Demir, Timur, Gerichten, et al., 2018)

Neuroinflammation is generally observed in lysosomal storage disorders mainly affecting central nervous system(Bosch & Kielian, 2015b). Previously we showed that abnormal GM2 accumulation in *Hexa-/-Neu3-/-* TSD mouse model triggered the activation of the microglial and macrophage systems within the brain. This activation, in turn, caused a notable shift in the pattern of expression of various cytokines and chemokines in both the cortex and cerebellum regions. Specifically, it was demonstrated that in the cortex and cerebellum regions of the brain, there was a significant increase in the expression of pro-inflammatory cytokines and chemokines such as Ccl2, Ccl3, Ccl4, and Cxcl10. Pro-inflammatory cytokines and chemokines are typically associated with promoting inflammation and immune responses, which are essential for combating infections and injuries. On the flip side, there was a marked decrease in the expression of anti-inflammatory cytokines and chemokines, including IL10, IL13, IL11, and IL24. Anti-inflammatory cytokines and chemokines are generally responsible for dampening or resolving inflammatory responses and maintaining tissue homeostasis. In essence, this research suggests that the accumulation of GM2 ganglioside in the brain of *Hexa−/−Neu3−/−* mice had a profound effect on the immune and inflammatory balance within the brain. The activation of the microglial/macrophage system led to an imbalance favoring pro-inflammatory responses while reducing the presence of molecules that typically mitigate inflammation. (Demir et al., 2020; Ramesh et al., 2013)

Research has shown that increase in the proinflammatory cytokines like Ccl2, Ccl3, and Ccl5 levels in the brains of mice correlated with the development of epileptic seizures (Arisi et al., 2015). Previously we suggested that the elevation in these cytokines is connected to the occurrence of neuroinflammation and seizures seen in the *Hexa-/-Neu3-/-* TSD mouse model(Demir et al., 2020). Importantly, these cytokines also have a role in attracting, mobilizing, and activating various immune cells like monocytes, lymphocytes, and neutrophils within the central nervous system (Duque & Descoteaux, 2014). An infiltration of peripheral blood mononuclear cells (PBMC) in response to these heightened cytokine levels was observed in *Hexa-/-Neu3-/-* model as in Hexb-/- mice (Kyrkanides et al., 2008).

Glial cells of the central nervous system like monocytes, macrophage, oligodendrocytes microglia and astrocytes are types of immune cells that express wide range of chemokine receptors, one of which is CCR2 (CC-chemokine receptor 2)(Baaklini et al., 2019; Charo & Ransohoff, 2006). It has been found that CCR2 have a role in the infiltration of peripheral blood mononuclear cells into the brain (Cui et al., 2020; Izikson et al., 2000). Additionally, research demonstrated that mice with deficiency of CCR2 was resistant to experimental autoimmune encephalitis (Fife et al., 2000; Gaupp et al., 2003). Furthermore, in Alzheimer's disease brains, the CCL2, which is the primary ligand for CCR2, is found to be upregulated. This provides more evidence that CCR2 have a crucial role in facilitating the trafficking of microglial precursor cells into the brain affected by Alzheimer's disease (Azizi et al., 2014). These findings have implications for our understanding of neurological conditions and may offer insights into potential therapeutic strategies targeting CCR2-CCL2 axis to modulate the immune response in the brain. In this thesis study, we aimed to target CCR2 receptor to reduce neuroinflammation in *Hexa-/-Neu3-/-* mouse model. Previously, researchers have shown that astrocytes of Hexb-/- mice model overexpresses adenosine A_{2A} receptor which in turn increases ccl2 expression in astrocytes (Ogawa et al., 2018). A_{2A} receptors are key modulators in adenosine signaling in brain and increased activity of them led to neurodegenerative effects (Stockwell et al., 2017). It has been implicated in several neurodegenerative disorders and antagonism against this receptor have been studied in clinical research(Kondo & Mizuno, 2015; Yuzlenko & Kiec-Kononowicz, 2006). Istradefylline is an FDA approved nondopaminergic drug which works as an antagonist of A_{2A} receptor and widely used for Parkinson disease along with L-DOPA to reduce “off” episodes observed in patients(Cummins & Cates, 2022). Accordingly, in this study, the aim was to

reduce neuroinflammation pathology and neurodegenerative effects of A2A receptors in *Hexa-/-Neu3-/-* mouse model by istradefylline administration. For this purpose three different strategies were applied as early-stage (10w-13w), late-stage(16w-19w) and two stage treatment (10w-13w & 16w-19w). Firstly, the effect of istradefylline on motor coordination was analyzed by rotarod analysis and open field analysis; early-stage and two-stage treatment strategies increased the motor function of *Hexa-/-Neu3-/-* mice with increased activity on rod and total distance traveled in open field analysis. When we look at the time spent in the center of open field, increased anxiety level is observed in istradefylline treatment groups and this situation may be related with the daily intraperitoneal injection of the drug. After sacrification of mice at the end point of interest (13W-old for earl-stage group, 19W-old for late and two-stage group), to analyze the expression levels of neuroinflammatory markers in cortex and cerebellum region RT-PCR was performed. In cortex neuroinflammatory markers, like chemokines CCL2, CCL3 and also interleukins like IL-1β, displayed decreased expression pattern mostly in two-stage treatment strategy and contrarily early stage and late stage treatment strategies were not as effective; even early stage treatment led to increased expression of some of neuroinflammatory markers like GFAP and CXCL10. A2A receptors are highly expressed in astrocytes and treatment at 10W of age interestingly led to increased astrogliosis in cortex region. In cerebellum, expectedly and similar to cortex; two stage treatment strategy was the most effective one reducing the neuroinflammatory response in Hexa-/-Neu3 mice. As direct target of istradefylline is CCR2; CCL2 expression was significantly reduced in both cortex and cerebellum region of *Hexa-/-Neu3-/-* by all three different administration strategies of istradefylline. The chemokines studied in this thesis project are all pro-inflammatory chemokines and anti-inflammatory therapy by istradefylline was able to reduce the gene expression levels of these chemokines in brain tissue of Tay-Sachs disease mouse model.

NFκB and IκB protein expression levels were also analyzed after istradefylline administration in cortex and cerebellum regions of *Hexa-/-Neu3-/-* mice and control groups. IκB expression did not display any difference between genotypes or in *Hexa-/-Neu3-/-* mice after istradefylline administration. Contrarily, NFκB protein expression was drastically reduced in both cortex and cerebellum of *Hexa-/-Neu3-/-* mice after two-stage treatment of istradefylline. Early-stage treatment does not affect the NFκB expression and late stage treatment also reduced NFκB level in both cortex and cerebellum. It has been demonstrated that adenosine signaling through A2aR inhibits NFκB pathways in T-cells

(Bradley & Bradley, 2001). On the other hand, A2A receptors have been shown to involve in the activation of MAPK/ NFκB pathway which have role as neuromodulator. It is also known that NFκB is triggered by wide range of factors including cytokine release and cellular stress and the activation of NFκB promotes the expression of neuroinflammatory factors (Ko et al., 2021; J. N. Wang et al., 2023). Based on this information; A2AR antagonism by istradefylline led to inhibition of NFκB signaling in brain tissue of TSD model and this inhibition may have an additive role in anti-inflammatory effect of istradefylline. IκB is the inhibitor of NFκB as it is bound to NFκB preventing its binding to DNA and activation of NFκB requires degradation of IκB. While we understand how external stimuli trigger NF-κB signaling, the processes governing IκB degradation without stimulation are less clear. Early studies had conflicting findings regarding the role of specific serine sites, the C-terminal PEST domain, and poly-ubiquitination in basal IκB turnover. Recent research found that bound IκB lasts much longer in unstimulated cells compared to free IκB. However, despite this, free IκB is not a strong substrate for IKK, even though it's commonly used in experiments to measure IKK activity. (O'Dea et al., 2007) The reason behind constant level of IκB despite the decreasing level of NFκB may be related with the basal IκB turnover.

After that, the neuroinflammatory markers were analyzed by immunohistochemical analysis to localize the neuroinflammatory modulators. GFAP localization in early-stage (10w-13w), late-stage(16w-19w) and two stage treatment (10w-13w & 16w-19w) group displayed decreased intensity in cortex region of *Hexa-/-Neu3-/-* when treated with all three different strategies of istradefylline administration. In cerebellum region only two stage treatment was effective to reduce GFAP. Additionally, in hippocampus and thalamus region GFAP expression did not change when compared to untreated *Hexa-/-Neu3-/-*. These results can be correlated with the increased mRNA expression of GFAP in RT-PCR results by which we can deduce that istradefylline administration does not significantly affect astrogliosis condition *Hexa-/-Neu3-/-* mice brain.

In order to analyze the activation of microglia samples were stained by MOMA-2 and LAMP1 colocalization. Untreated *Hexa-/-Neu3-/-* mice displayed strong microgliosis compared to healthy controls when we look at the immunohistochemistry results. MOMA-2 positive cells were colocalized with lysosomal associated membrane protein displaying correlation between lysosomal accumulation and microgliosis. Moreover, in MPS mouse model, it has been previously demonstrated that an unidentified

antigen associated with MOMA-2 is likely a protein located within the lysosomes(K. Ohmi et al., 2003). In the present study, it has been demonstrated that istradefylline administration enabled significant reduction in strong microglial activation in cortex cerebellum, thalamus and hippocampus region of *Hexa-/-Neu3-/-* mice. All three different strategies reduced microgliosis but two-stage treatment was the most effective istradefylline administration strategy to reverse microglial activation. This result is correlated with the previous results in which istradefylline decreases microgliosis in Hexb-/- mice model (Ogawa et al., 2018), in retinal ischemia model (Boia et al., 2017), experimental glaucoma (X. Liu et al., 2016) and neurodegenerative disorders like Parkinson's disease (Berger et al., 2020; P. Z. Chen et al., 2018).

By CNPase staining, oligodendriocyte level was measured and in untreated *Hexa-/-Neu3-/-* mice model oligodendriocyte level was strongly reduced in cortex and cerebellum regions. In cortex region of *Hexa-/-Neu3-/-* mice, only two-stage treatment of istradefylline provide increase in oligodendrocyte level however all three different strategies for istradefylline administration enabled elevation in oligodendrocytes in *Hexa-/-Neu3-/-* TSD model. It has been previously demonstrated that oligodendrocyte progenitor cells negatively regulated by adenosine signaling (Coppi et al., 2015)and inhibition of OPC maturation through A2A receptor activation is linked to the activation of this specific receptor subtype hindering the deposition of myelin (Coppi et al., 2013). Thus, increasing oligodendrocyte level in brain of *Hexa-/-Neu3-/-* mice by istradefylline administration may be associated with the interrelation between OPC maturation and adenosine signaling.

Interleukin-6 level was measured by immunohistochemistry as well as RT-PCR. As mentioned, IL-6 is a pro-inflammatory cytokine and the gene expression level was reduced in cortex and cerebellum region of *Hexa-/-Neu3-/-* mice by two-stage treatment of istradefylline. Accordingly, IHC results demonstrated that IL-6 release was reduced in cortex, cerebellum, thalamus and hippocampus regions of *Hexa-/-Neu3-/-* mice after two-stage treatment. Growing evidence indicates that adenosine signaling contributes to the control of inflammatory cytokine and chemokine network processes (Haskó et al., 2008). Adenosine has been shown to enhance the secretion of proinflammatory cytokines including IL-6 in various cell types (Rees et al., 2003; Schwaninger et al., 1997).

After analyzing neuroinflammatory markers by RT-PCR, Western Blot and immunohistochemistry, oxidative stress markers were analyzed in order to investigate the effect of anti-inflammatory therapy on oxidative stress condition in *Hexa-/-Neu3-/-* mice.

The gene expression levels of the players involving in antioxidant defense mechanism like SOD2, Catalase and TTase1 were analyzed by RT-PCR and overexpression of these genes was observed in untreated *Hexa-/-Neu3-/-* mice suggesting increased oxidative stress condition in these mice. Oxidative stress condition has been reported in certain LSDs. Decreased SOD2 protein expression in NPC human fibroblasts (Woš et al., 2016) and Hexb-/- GM2 gangliosidosis mouse brains (Suzuki et al., 2016), which is a mitochondrial antioxidant enzyme. Additionally, catalase which is responsible for breaking down hydrogen peroxide, displayed increased activity in blood samples of GD patients (Mello et al., 2015) but decreased activity in NCL human fibroblasts (Vidal-Donet et al., 2013). In addition, Thioltransferase-1 (Ttase1), a member of the glutaredoxin family, was upregulated in fibroblasts from various LSDs like GM1 gangliosidosis, GD patients and Tay-Sachs; indicating its role in antioxidant defense (Wei et al., 2008). In the present study; istradefylline treatment reduced the expression levels of these oxidative stress markers in both cortex and cerebellum region of *Hexa-/-Neu3-/-* mice, most effectively by two-stage treatment strategy. It has been previously reported that adenosine receptors have a cytoprotective effect against hypoxia and ischemia (Kobayashi & Millhorn, 1999; von Lubitz, 1999), and the protective effect of these adenosine receptors is provided by the regulation of oxidative stress through the antioxidant defense mechanism (Huang, 2003). It was reported that adenosine reduces oxidative stress in neural stem cells under induced oxidative stress conditions (Gholinejad et al., 2018). Thus, the decrease of oxidative stress markers by two-stage anti-inflammatory therapy may be related with the regulation of oxidative stress by adenosine signaling. Oxidative stress is harmful for macromolecules like lipids, proteins or DNA. APE1 protein is a DNA repair enzyme involving in repairment in oxidative DNA damages and controlling redox-dependent mechanism for regulation of target gene expression (McNeill et al., 2020). APE1 protein expression was analyzed by western blot after istradefylline treatment. In cortex region early stage and two-stage treatment of istradefylline caused increase in APE1 protein level and in cerebellum region there was no difference in the level of APE1. Therefore, we can suggest that istradefylline administration starting from early stage enables increased defense against oxidative DNA damages.

As final question of the thesis study, the effect of istradefylline on hallmarks of Tay-Sachs disease pathology was analyzed. HexB and GM2AP gene expression levels were analyzed by RT-PCR. GM2AP is the activator protein involving in the synthesis and degradation pathway catalyzing recruitment of GM2 ganglioside to β-

hexosaminidase-A enzyme (Wendeler et al., 2006). The expression level of GM2AP was not affected in neither cortex nor cerebellum region of *Hexa-/-Neu3-/-* mice by istradefylline administration. On the other hand, HexB gene expression level was strongly decreased after istradefylline administration independent of the administration strategy. The previous research demonstrated that HEXB is highly expressed in microglia compared to other brain cell types thus hexb is associated with microgliosis (Bennett et al., 2018; Butovsky et al., 2014). Since microglia are known for their strong phagocytic activity, the functioning of lysosomes is crucial for breaking down materials they ingest, and HEXB likely plays a significant role in microglial function as well (Kuil et al., 2019). As mentioned above, MOMA-2 / LAMP1 immunohistochemistry analysis demonstrated decreased microgliosis in all brain regions of *Hexa-/-Neu3-/-* mice and accordingly HexB expression, which is one of the signature genes of microglia, was also strongly reduced by istradefylline treatment in both cortex and cerebellum region. The level of GM2 accumulation was measured in cortex and cerebellum region by thin layer chromatography analysis after istradefylline treatment. The anti-inflammatory therapy did not significantly affect the GM2 accumulation in neither cortex nor cerebellum region however in cortex region two stage treatment enabled slight decrease in GM2 accumulation in *Hexa-/-Neu3-/-* mice compared to untreated condition. Based on these results anti-inflammatory therapy by istradefylline provide deceleration in progressive accumulation of GM2.

Neurodegeneration is another hallmark of Tay-Sachs disease pathology and in the study the effect of anti-inflammatory therapy on neurodegeneration was analyzed by anti-NeuN staining. Untreated *Hexa-/-Neu3-/-* mice displayed strong neurodegeneration with significantly decreased NeuN density in cortex and cerebellum region compared to age matched *WT* and *Hexa-/-* mice. Early stage treatment of istradefylline did not affect the neurodegeneration pathology however late and two stage treatment slightly elevate neuronal density in cerebellum, thalamus and hippocampus region of *Hexa-/-Neu3-/-* mouse model. Therefore, it can be said that istradefylline treatment did not affect neurodegeneration pathology in TSD mouse model.

4.1. Conclusion

In the present thesis study, it was aimed to reduce neuroinflammation pathology in *Hexa-/-Neu3-/-* Tay-Sachs disease mouse model by using istradefylline as an anti-inflammatory drug. For anti-inflammatory therapy three different strategies of istradefylline administration as early, late and two stage treatment. The purpose of the three different strategies was to determine the effect of the drug treatment in early or late stage of the disease and whether treatment starting from early stage followed by late stage as well would make a difference in pathology. Istradefylline indirectly targets CCR2-CCL2 pathway and all three different strategies enabled reduction in CCL2 gene expression level in cortex and cerebellum region besides other pro-inflammatory cytokines. Western Blot and immunohistochemistry against neuroinflammatory markers demonstrated that two-stage treatment of istradefylline were the most effective strategy in reducing the neuroinflammation pathology in TSD mouse model. Besides neuroinflammation, the effect of istradefylline on oxidative stress was also analyzed and the treatment reduced expression levels of oxidative stress markers in cortex and cerebellum region of TSD mouse model, with two stage treatment being the most effective strategy of administration. The reason behind why the two-stage treatment is the most effective strategy may be starting from early stage and continuing in the late stage as well. Tay-sachs disease is a progressive disease and two stage treatment may slow down the progression of the neuroinflammation pathology. On the other hand, istradefylline did not affect the GM2 accumulation level and neurodegeneration significantly. Therefore, anti-inflammatory therapy may provide an additive treatment strategy along with more influential therapeutical approaches like gene therapy.

REFERENCES

Abed Rabbo, M., Khodour, Y., Kaguni, L. S., & Stiban, J. (2021). Sphingolipid lysosomal storage diseases: from bench to bedside. In *Lipids in Health and Disease* (Vol. 20, Issue 1). https://doi.org/10.1186/s12944-021-01466-0

Abou-Ghali, M., & Stiban, J. (2015). Regulation of ceramide channel formation and disassembly: Insights on the initiation of apoptosis. *Saudi Journal of Biological Sciences*, *22*(6). https://doi.org/10.1016/j.sjbs.2015.03.005

Aerts, J. M. F. G., Hollak, C. E. M., Boot, R. G., Groener, J. E. M., & Maas, M. (2006). Substrate reduction therapy of glycosphingolipid storage disorders. *Journal of Inherited Metabolic Disease*, *29*(2–3). https://doi.org/10.1007/s10545-006-0272-5

Albeituni, S., & Stiban, J. (2019). Roles of Ceramides and Other Sphingolipids in Immune Cell Function and Inflammation. In *Advances in Experimental Medicine and Biology* (Vol. 1161). https://doi.org/10.1007/978-3-030-21735-8_15

Allan, S. M., Tyrrell, P. J., & Rothwell, N. J. (2005). Interleukin-1 and neuronal injury. In *Nature Reviews Immunology* (Vol. 5, Issue 8). https://doi.org/10.1038/nri1664

Americo, J., Filho, F., & Shapiro, B. E. (2010). Tay-Sachs disease. *Arch Neurol*, *61*(11), 1466–1468. https://doi.org/10.1001/archneur.61.9.1466

Amor, S., Peferoen, L. A. N., Vogel, D. Y. S., Breur, M., van der Valk, P., Baker, D., & Van Noort, J. M. (2014). Inflammation in neurodegenerative diseases - an update. In *Immunology* (Vol. 142, Issue 2). https://doi.org/10.1111/imm.12233

Arisi, G. M., Foresti, M. L., Katki, K., & Shapiro, L. A. (2015). Increased CCL2, CCL3, CCL5, and IL-1β cytokine concentration in piriform cortex, hippocampus, and neocortex after pilocarpine-induced seizures. *Journal of Neuroinflammation*, *12*(1). https://doi.org/10.1186/s12974-015-0347-z

Arroyo, D. S., Gaviglio, E. A., Peralta Ramos, J. M., Bussi, C., Rodriguez-Galan, M. C., & Iribarren, P. (2014). Autophagy in inflammation, infection, neurodegeneration and cancer. In *International Immunopharmacology* (Vol. 18, Issue 1). https://doi.org/10.1016/j.intimp.2013.11.001

Azizi, G., Khannazer, N., & Mirshafiey, A. (2014). The potential role of chemokines in alzheimer's disease pathogenesis. In *American Journal of Alzheimer's Disease and other Dementias* (Vol. 29, Issue 5). https://doi.org/10.1177/1533317513518651

Baaklini, C. S., Rawji, K. S., Duncan, G. J., Ho, M. F. S., & Plemel, J. R. (2019). Central Nervous System Remyelination: Roles of Glia and Innate Immune Cells. In *Frontiers in Molecular Neuroscience* (Vol. 12). https://doi.org/10.3389/fnmol.2019.00225

Bardaweel, S. K., Gul, M., Alzweiri, M., Ishaqat, A., Alsalamat, H. A., & Bashatwah, R. M. (2018). Reactive oxygen species: The dual role in physiological and pathological conditions of the human body. In *Eurasian Journal of Medicine* (Vol. 50, Issue 3). https://doi.org/10.5152/eurasianjmed.2018.17397

Batista, C. R. A., Gomes, G. F., Candelario-Jalil, E., Fiebich, B. L., & de Oliveira, A. C. P. (2019). Lipopolysaccharide-induced neuroinflammation as a bridge to understand neurodegeneration. In *International Journal of Molecular Sciences* (Vol. 20, Issue 9). https://doi.org/10.3390/ijms20092293

Bennett, F. C., Bennett, M. L., Yaqoob, F., Mulinyawe, S. B., Grant, G. A., Hayden Gephart, M., Plowey, E. D., & Barres, B. A. (2018). A Combination of Ontogeny and CNS Environment Establishes Microglial Identity. *Neuron*, *98*(6). https://doi.org/10.1016/j.neuron.2018.05.014

Berger, A. A., Winnick, A., Welschmeyer, A., Kaneb, A., Berardino, K., Cornett, E. M., Kaye, A. D., Viswanath, O., & Urits, I. (2020). Istradefylline to treat patients with parkinson's disease experiencing "off" episodes: A comprehensive review. In *Neurology International* (Vol. 12, Issue 3). https://doi.org/10.3390/neurolint12030017

Block, M. L., & Hong, J. S. (2007). Chronic microglial activation and progressive dopaminergic neurotoxicity. *Biochemical Society Transactions*, *35*(5). https://doi.org/10.1042/BST0351127

Boche, D., Perry, V. H., & Nicoll, J. A. R. (2013). Review: Activation patterns of microglia and their identification in the human brain. In *Neuropathology and Applied Neurobiology* (Vol. 39, Issue 1). https://doi.org/10.1111/nan.12011

Boia, R., Elvas, F., Madeira, M. H., Aires, I. D., Rodrigues-Neves, A. C., Tralhão, P., Szabó, E. C., Baqi, Y., Müller, C. E., Tomé, Â. R., Cunha, R. A., Ambrósio, A. F., & Santiago, A. R. (2017). Treatment with A2A receptor antagonist KW6002 and caffeine intake regulate microglia reactivity and protect retina against transient ischemic damage. *Cell Death and Disease*, *8*(10). https://doi.org/10.1038/cddis.2017.451

Bosch, M. E., & Kielian, T. (2015a). Neuroinflammatory paradigms in lysosomal storage diseases. In *Frontiers in Neuroscience* (Vol. 9, Issue OCT). https://doi.org/10.3389/fnins.2015.00417

Bosch, M. E., & Kielian, T. (2015b). Neuroinflammatory paradigms in lysosomal storage diseases. In *Frontiers in Neuroscience* (Vol. 9, Issue OCT). https://doi.org/10.3389/fnins.2015.00417

Bouma, H. R., Ploeg, R. J., & Schuurs, T. A. (2009). Signal transduction pathways involved in brain death-induced renal injury. In *American Journal of Transplantation* (Vol. 9, Issue 5). https://doi.org/10.1111/j.1600-6143.2009.02587.x

Bradley, K. K., & Bradley, M. E. (2001). Phosphodiesterase 4 inhibitors prevent cytokine secretion by T lymphocytes by inhibiting nuclear factor-κB and nuclear factor of

activated T cells activation. *Journal of Pharmacology and Experimental Therapeutics*, *299*(2).

Butovsky, O., Jedrychowski, M. P., Moore, C. S., Cialic, R., Lanser, A. J., Gabriely, G., Koeglsperger, T., Dake, B., Wu, P. M., Doykan, C. E., Fanek, Z., Liu, L., Chen, Z., Rothstein, J. D., Ransohoff, R. M., Gygi, S. P., Antel, J. P., & Weiner, H. L. (2014). Identification of a unique TGF-β-dependent molecular and functional signature in microglia. *Nature Neuroscience*, *17*(1). https://doi.org/10.1038/nn.3599

Cappellano, G., Carecchio, M., Fleetwood, T., Magistrelli, L., Cantello, R., Dianzani, U., & Comi, C. (2013). Immunity and inflammation in neurodegenerative diseases. In *American Journal of Neurodegenerative Diseases* (Vol. 2, Issue 2).

Carson, M. J., Bilousova, T. V., Puntambekar, S. S., Melchior, B., Doose, J. M., & Ethell, I. M. (2007). A Rose by Any Other Name? The Potential Consequences of Microglial Heterogeneity During CNS Health and Disease. *Neurotherapeutics*, *4*(4). https://doi.org/10.1016/j.nurt.2007.07.002

Carson, M. J., Cameron Thrash, J., & Walter, B. (2006). The cellular response in neuroinflammation: The role of leukocytes, microglia and astrocytes in neuronal death and survival. *Clinical Neuroscience Research*, *6*(5). https://doi.org/10.1016/j.cnr.2006.09.004

Cecerska-Heryć, E., Pękała, M., Serwin, N., Gliźniewicz, M., Grygorcewicz, B., Michalczyk, A., Heryć, R., Budkowska, M., & Dołęgowska, B. (2023). The Use of Stem Cells as a Potential Treatment Method for Selected Neurodegenerative Diseases: Review. In *Cellular and Molecular Neurobiology* (Vol. 43, Issue 6). https://doi.org/10.1007/s10571-023-01344-6

Charo, I. F., & Ransohoff, R. M. (2006). The Many Roles of Chemokines and Chemokine Receptors in Inflammation. *New England Journal of Medicine*, *354*(6). https://doi.org/10.1056/nejmra052723

Chen, P. Z., He, W. J., Zhu, Z. R., E, G. J., Xu, G., Chen, D. W., & Gao, Y. Q. (2018). Adenosine A2A receptor involves in neuroinflammation-mediated cognitive decline through activating microglia under acute hypobaric hypoxia. *Behavioural Brain Research*, *347*. https://doi.org/10.1016/j.bbr.2018.02.038

Chen, X., Guo, C., & Kong, J. (2012). Oxidative stress in neurodegenerative diseases. *Neural Regeneration Research*, *7*(5). https://doi.org/10.1146/annurev.pharmtox.36.1.83

Clarke, J. T. R., Mahuran, D. J., Sathe, S., Kolodny, E. H., Rigat, B. A., Raiman, J. A., & Tropak, M. B. (2011). An open-label Phase I/II clinical trial of pyrimethamine for the treatment of patients affected with chronic GM2 gangliosidosis (Tay-Sachs or Sandhoff variants). *Molecular Genetics and Metabolism*, *102*(1). https://doi.org/10.1016/j.ymgme.2010.09.004

Colombo, E., & Farina, C. (2016). Astrocytes: Key Regulators of Neuroinflammation. In *Trends in Immunology* (Vol. 37, Issue 9). https://doi.org/10.1016/j.it.2016.06.006

Coppi, E., Cellai, L., Maraula, G., Dettori, I., Melani, A., Pugliese, A. M., & Pedata, F. (2015). Role of adenosine in oligodendrocyte precursor maturation. *Frontiers in Cellular Neuroscience*, *9*(APR). https://doi.org/10.3389/fncel.2015.00155

Coppi, E., Cellai, L., Maraula, G., Pugliese, A. M., & Pedata, F. (2013). Adenosine A2A receptors inhibit delayed rectifier potassium currents and cell differentiation in primary purified oligodendrocyte cultures. *Neuropharmacology*, *73*. https://doi.org/10.1016/j.neuropharm.2013.05.035

Couchman, J. R., & Pataki, C. A. (2012). An Introduction to Proteoglycans and Their Localization. *Journal of Histochemistry and Cytochemistry*, *60*(12). https://doi.org/10.1369/0022155412464638

Cui, L. Y., Chu, S. F., & Chen, N. H. (2020). The role of chemokines and chemokine receptors in multiple sclerosis. In *International Immunopharmacology* (Vol. 83). https://doi.org/10.1016/j.intimp.2020.106314

Cummins, L., & Cates, M. E. (2022). Istradefylline: A novel agent in the treatment of ‘“off”’ episodes associated with levodopa/carbidopa use in Parkinson disease. In *Mental Health Clinician* (Vol. 12, Issue 1). https://doi.org/10.9740/MHC.2022.01.032

D’Azzo, A., & Bonten, E. (2010). Molecular mechanisms of pathogenesis in a glycosphingolipid and a glycoprotein storage disease. *Biochemical Society Transactions*, *38*(6). https://doi.org/10.1042/BST0381453

De Gioia, R., Biella, F., Citterio, G., Rizzo, F., Abati, E., Nizzardo, M., Bresolin, N., Comi, G. Pietro, & Corti, S. (2020). Neural stem cell transplantation for neurodegenerative diseases. In *International Journal of Molecular Sciences* (Vol. 21, Issue 9). https://doi.org/10.3390/ijms21093103

De la Fuente, M. (2019). Oxidation and Inflammation in the Immune and Nervous Systems, a Link Between Aging and Anxiety. In *Handbook of Immunosenescence*. https://doi.org/10.1007/978-3-319-99375-1_115

Demir, S. A., Timur, Z. K., Ateş, N., Martínez, L. A., & Seyrantepe, V. (2020). GM2 ganglioside accumulation causes neuroinflammation and behavioral alterations in a mouse model of early onset Tay-Sachs disease. *Journal of Neuroinflammation*, *17*(1). https://doi.org/10.1186/s12974-020-01947-6

Dinarello, C. A. (2010). Anti-inflammatory Agents: Present and Future. In *Cell* (Vol. 140, Issue 6). https://doi.org/10.1016/j.cell.2010.02.043

DiSabato, D. J., Quan, N., & Godbout, J. P. (2016a). Neuroinflammation: the devil is in the details. *Journal of Neurochemistry*, *139*. https://doi.org/10.1111/jnc.13607

DiSabato, D. J., Quan, N., & Godbout, J. P. (2016b). Neuroinflammation: the devil is in the details. *Journal of Neurochemistry*, *139*. https://doi.org/10.1111/jnc.13607

Duque, G. A., & Descoteaux, A. (2014). Macrophage cytokines: Involvement in immunity and infectious diseases. In *Frontiers in Immunology* (Vol. 5, Issue OCT). https://doi.org/10.3389/fimmu.2014.00491

Fife, B. T., Huffnagle, G. B., Kuziel, W. A., & Karpus, W. J. (2000). CC chemokine receptor 2 is critical for induction of experimental autoimmune encephalomyelitis. *Journal of Experimental Medicine*, *192*(6). https://doi.org/10.1084/jem.192.6.899

Forrester, S. J., Kikuchi, D. S., Hernandes, M. S., Xu, Q., & Griendling, K. K. (2018). Reactive oxygen species in metabolic and inflammatory signaling. In *Circulation Research* (Vol. 122, Issue 6). https://doi.org/10.1161/CIRCRESAHA.117.311401

Franco, R., & Navarro, G. (2018). Adenosine A2A receptor antagonists in neurodegenerative diseases: Huge potential and huge challenges. In *Frontiers in Psychiatry* (Vol. 9, Issue MAR). https://doi.org/10.3389/fpsyt.2018.00068

Fuller, M., Meikle, P. J., & Hopwood, J. J. (2014). Epidemiology of lysosomal storage diseases : an overview. In *Fabry Disease: Perspectives from 5 Years of FOS*. (p. Chapter 2, Table 1 (Australian Dataset)). https://doi.org/10.1146/annurev.neuro.29.051605.112824

Gaupp, S., Pitt, D., Kuziel, W. A., Cannella, B., & Raine, C. S. (2003). Experimental autoimmune encephalomyelitis (EAE) in CCR2-/- mice: Susceptibility in multiple strains. *American Journal of Pathology*, *162*(1). https://doi.org/10.1016/S0002-9440(10)63805-9

Gholinejad, M., Anarkooli, I. J., Taromchi, A., & Abdanipour, A. (2018). Adenosine decreases oxidative stress and protects H2O2-treated neural stem cells against apoptosis through decreasing Mst1 expression. *Biomedical Reports*, *8*(5). https://doi.org/10.3892/br.2018.1083

Ghosh, N., Das, A., Chaffee, S., Roy, S., & Sen, C. K. (2017). Reactive oxygen species, oxidative damage and cell death. In *Immunity and Inflammation in Health and Disease: Emerging Roles of Nutraceuticals and Functional Foods in Immune Support*. https://doi.org/10.1016/B978-0-12-805417-8.00004-4

Giovannoni, F., & Quintana, F. J. (2020). The Role of Astrocytes in CNS Inflammation. In *Trends in Immunology* (Vol. 41, Issue 9). https://doi.org/10.1016/j.it.2020.07.007

Goldsteins, G., Hakosalo, V., Jaronen, M., Keuters, M. H., Lehtonen, Š., & Koistinaho, J. (2022). CNS Redox Homeostasis and Dysfunction in Neurodegenerative Diseases. In *Antioxidants* (Vol. 11, Issue 2). https://doi.org/10.3390/antiox11020405

Gorji, A. (2022). Neuroinflammation: The Pathogenic Mechanism of Neurological Disorders. In *International Journal of Molecular Sciences* (Vol. 23, Issue 10). https://doi.org/10.3390/ijms23105744

Gravel, R. A., Kaback, M. M., Proia, R. L., Sandhoff, K., Suzuki, K., & Suzuki, K. (2014). The GM2 Gangliosidoses. In *The Online Metabolic and Molecular Bases of Inherited Diseases* (pp. 3827–3876). https://doi.org/10.1036/ommbid.184

Harry, G. J., & Kraft, A. D. (2008). Neuroinflammation and microglia: Considerations and approaches for neurotoxicity assessment. In *Expert Opinion on Drug Metabolism and Toxicology* (Vol. 4, Issue 10). https://doi.org/10.1517/17425255.4.10.1265

Haskó, G., Linden, J., Cronstein, B., & Pacher, P. (2008). Adenosine receptors: Therapeutic aspects for inflammatory and immune diseases. In *Nature Reviews Drug Discovery* (Vol. 7, Issue 9). https://doi.org/10.1038/nrd2638

Haskó, G., Pacher, P., Vizi, E. S., & Illes, P. (2005). Adenosine receptor signaling in the brain immune system. In *Trends in Pharmacological Sciences* (Vol. 26, Issue 10). https://doi.org/10.1016/j.tips.2005.08.004

Haynes, N. S., O'Neill, C. E., Hobson, B. D., & Bachtell, R. K. (2019). Effects of adenosine A 2A receptor antagonists on cocaine-induced locomotion and cocaine seeking. *Psychopharmacology*, *236*(2). https://doi.org/10.1007/s00213-018-5097-z

Huang, N. K. (2003). Adenosine A2A receptors regulate oxidative stress formation in rat pheochromocytoma PC12 cells during serum deprivation. *Neuroscience Letters*, *350*(2). https://doi.org/10.1016/S0304-3940(03)00860-7

Ibrisimovic, E., Drobny, H., Yang, Q., Höfer, T., Boehm, S., Nanoff, C., & Schicker, K. (2012). Constitutive activity of the A 2A adenosine receptor and compartmentalised cyclic AMP signalling fine-tune noradrenaline release. *Purinergic Signalling*, *8*(4). https://doi.org/10.1007/s11302-012-9298-3

Igdoura, S. A., Mertineit, C., Trasler, J. M., & Gravel, R. A. (1999). Sialidase-mediated depletion of G(M2) ganglioside in Tay-Sachs neuroglia cells. *Human Molecular Genetics*, *8*(6), 1111–1116. https://doi.org/10.1093/hmg/8.6.1111

Isik, S., Yeman Kiyak, B., Akbayir, R., Seyhali, R., & Arpaci, T. (2023). Microglia Mediated Neuroinflammation in Parkinson's Disease. In *Cells* (Vol. 12, Issue 7). https://doi.org/10.3390/cells12071012

Izikson, L., Klein, R. S., Charo, I. F., Weiner, H. L., & Luster, A. D. (2000). Resistance to experimental autoimmune encephalomyelitis in mice lacking the CC chemokine receptor (CCR)2. *Journal of Experimental Medicine*, *192*(7). https://doi.org/10.1084/jem.192.7.1075

Jacobs, J. F. M., Willemsen, M. A. A. P., Groot-Loonen, J. J., Wevers, R. A., & Hoogerbrugge, P. M. (2005). Allogeneic BMT followed by substrate reduction therapy in a child with subacute Tay-Sachs disease [5]. In *Bone Marrow Transplantation* (Vol. 36, Issue 10). https://doi.org/10.1038/sj.bmt.1705155

Jang, D. I., Lee, A. H., Shin, H. Y., Song, H. R., Park, J. H., Kang, T. B., Lee, S. R., & Yang, S. H. (2021). The role of tumor necrosis factor alpha (Tnf-α) in autoimmune disease and current tnf-α inhibitors in therapeutics. In *International Journal of Molecular Sciences* (Vol. 22, Issue 5). https://doi.org/10.3390/ijms22052719

Jenner, P. (2014). An Overview of adenosine A2A receptor antagonists in Parkinson's disease. In *International Review of Neurobiology* (Vol. 119). https://doi.org/10.1016/B978-0-12-801022-8.00003-9

Joshi, H. P., Jo, H. J., Kim, Y. H., An, S. B., Park, C. K., & Han, I. (2021). Stem cell therapy for modulating neuroinflammation in neuropathic pain. *International Journal of Molecular Sciences*, *22*(9). https://doi.org/10.3390/ijms22094853

Kaback, M., Lim-Steele, J., Dabholkar, D., Brown, D., Levy, N., & Zeiger, K. (1994). Tay-sachs disease—carrier screening, prenatal diagnosis and the molecular era: An international perspective, 1970 to 1993. *Obstetrical and Gynecological Survey*, *49*(5). https://doi.org/10.1097/00006254-199405000-00013

Kaback, M. M. (2001). Tay-Sachs Disease. In *Advances in Genetics* (Vol. 44). https://doi.org/10.1016/S0065-2660(01)44084-3

Kaback, M. M., & O'Brien, J. S. (1973). Tay-Sachs: Prototype for Prevention of Genetic Disease. *Hospital Practice*, *8*(3). https://doi.org/10.1080/21548331.1973.11706369

Kempuraj, D., Thangavel, R., Natteru, P. A., Selvakumar, G. P., Saeed, D., Zahoor, H., Zaheer, S., Iyer, S. S., & Zaheer, A. (2016). Neuroinflammation Induces Neurodegeneration. *Journal of Neurology, Neurosurgery and Spine*, *1*(1).

Kinney, J. W., Bemiller, S. M., Murtishaw, A. S., Leisgang, A. M., Salazar, A. M., & Lamb, B. T. (2018). Inflammation as a central mechanism in Alzheimer's disease. In *Alzheimer's and Dementia: Translational Research and Clinical Interventions* (Vol. 4). https://doi.org/10.1016/j.trci.2018.06.014

Kobayashi, S., & Millhorn, D. E. (1999). Stimulation of expression for the adenosine A2A receptor gene by hypoxia in PC12 cells. A potential role in cell protection. *Journal of Biological Chemistry*, *274*(29). https://doi.org/10.1074/jbc.274.29.20358

Ko, I. G., Jin, J. J., Hwang, L., Kim, S. H., Kim, C. J., Won, K. Y., Na, Y. G., Kim, K. H., & Kim, S. J. (2021). Adenosine A2a receptor agonist polydeoxyribonucleotide alleviates interstitial cystitis-induced voiding dysfunction by suppressing inflammation and apoptosis in rats. *Journal of Inflammation Research*, *14*. https://doi.org/10.2147/JIR.S287346

Kolter, T. (2012). Ganglioside Biochemistry. *ISRN Biochemistry*, *2012*. https://doi.org/10.5402/2012/506160

Kondo, T., & Mizuno, Y. (2015). A long-term study of istradefylline safety and efficacy in patients with parkinson disease. *Clinical Neuropharmacology*, *38*(2). https://doi.org/10.1097/WNF.0000000000000073

Kopp, K. O., Greer, M. E., Glotfelty, E. J., Hsueh, S. C., Tweedie, D., Kim, D. S., Reale, M., Vargesson, N., & Greig, N. H. (2023). A New Generation of IMiDs as Treatments for Neuroinflammatory and Neurodegenerative Disorders. In *Biomolecules* (Vol. 13, Issue 5). https://doi.org/10.3390/biom13050747

Krause, D. L., & Müller, N. (2010). Neuroinflammation, microglia and implications for anti-inflammatory treatment in Alzheimer's disease. In *International Journal of Alzheimer's Disease*. https://doi.org/10.4061/2010/732806

Kreher, C., Favret, J., Maulik, M., & Shin, D. (2021). Lysosomal functions in glia associated with neurodegeneration. In *Biomolecules* (Vol. 11, Issue 3). https://doi.org/10.3390/biom11030400

Kuil, L. E., López Martí, A., Carreras Mascaro, A., van den Bosch, J. C., van den Berg, P., van der Linde, H. C., Schoonderwoerd, K., Ruijter, G. J. G., & van Ham, T. J. (2019). Hexb enzyme deficiency leads to lysosomal abnormalities in radial glia and microglia in zebrafish brain development. *GLIA*, *67*(9). https://doi.org/10.1002/glia.23641

Kwon, H. S., & Koh, S. H. (2020). Neuroinflammation in neurodegenerative disorders: the roles of microglia and astrocytes. In *Translational Neurodegeneration* (Vol. 9, Issue 1). https://doi.org/10.1186/s40035-020-00221-2

Kyrkanides, S., Brouxhon, S. M., Tallents, R. H., Miller, J. nie H., Olschowka, J. A., & O'Banion, M. K. (2012). Conditional expression of human β-hexosaminidase in the neurons of Sandhoff disease rescues mice from neurodegeneration but not neuroinflammation. *Journal of Neuroinflammation*, *9*. https://doi.org/10.1186/1742-2094-9-186

Kyrkanides, S., Miller, A. W., Miller, J. nie H., Tallents, R. H., Brouxhon, S. M., Olschowka, M. E., O'Banion, M. K., & Olschowka, J. A. (2008). Peripheral blood mononuclear cell infiltration and neuroinflammation in the HexB-/- mouse model of neurodegeneration. *Journal of Neuroimmunology*, *203*(1). https://doi.org/10.1016/j.jneuroim.2008.06.024

Lachmann, R. H. (2009). Substrate-reduction therapy with miglustat for glycosphingolipid storage disorders affecting the brain. In *Expert Review of Endocrinology and Metabolism* (Vol. 4, Issue 3). https://doi.org/10.1586/eem.09.8

Lahiri, S., & Futerman, A. H. (2007). The metabolism and function of sphingolipids and glycosphingolipids. In *Cellular and Molecular Life Sciences* (Vol. 64, Issue 17). https://doi.org/10.1007/s00018-007-7076-0

Lamkanfi, M., & Dixit, V. M. (2012). Inflammasomes and their roles in health and disease. In *Annual Review of Cell and Developmental Biology* (Vol. 28). https://doi.org/10.1146/annurev-cellbio-101011-155745

Lawson, C. A., & Martin, D. R. (2016). Animal models of GM2 gangliosidosis: Utility and limitations. In *Application of Clinical Genetics* (Vol. 9). https://doi.org/10.2147/TACG.S85354

Leal, A. F., Benincore-Flórez, E., Solano-Galarza, D., Jaramillo, R. G. G., Echeverri-Peña, O. Y., Suarez, D. A., Alméciga-Díaz, C. J., & Espejo-Mojica, A. J. (2020). Gm2 gangliosidoses: Clinical features, pathophysiological aspects, and current

therapies. In *International Journal of Molecular Sciences* (Vol. 21, Issue 17). https://doi.org/10.3390/ijms21176213

Linnerbauer, M., Wheeler, M. A., & Quintana, F. J. (2020). Astrocyte Crosstalk in CNS Inflammation. In *Neuron* (Vol. 108, Issue 4). https://doi.org/10.1016/j.neuron.2020.08.012

Liu, P., Wang, Y., Sun, Y., & Peng, G. (2022). Neuroinflammation as a Potential Therapeutic Target in Alzheimer's Disease. *Clinical Interventions in Aging*, *17*. https://doi.org/10.2147/CIA.S357558

Liu, T., Zhang, L., Joo, D., & Sun, S. C. (2017). NF-κB signaling in inflammation. In *Signal Transduction and Targeted Therapy* (Vol. 2). https://doi.org/10.1038/sigtrans.2017.23

Liu, X., Huang, P., Wang, J., Yang, Z., Huang, S., Luo, X., Qi, J., Shen, X., & Zhong, Y. (2016). The effect of A2A receptor antagonist on microglial activation in experimental glaucoma. *Investigative Ophthalmology and Visual Science*, *57*(3). https://doi.org/10.1167/iovs.15-18024

Lopez, P. H., & Schnaar, R. L. (2009). Gangliosides in cell recognition and membrane protein regulation. In *Current Opinion in Structural Biology* (Vol. 19, Issue 5). https://doi.org/10.1016/j.sbi.2009.06.001

Lyman, M., Lloyd, D. G., Ji, X., Vizcaychipi, M. P., & Ma, D. (2014). Neuroinflammation: The role and consequences. In *Neuroscience Research* (Vol. 79, Issue 1). https://doi.org/10.1016/j.neures.2013.10.004

Maegawa, G. H. B., Banwell, B. L., Blaser, S., Sorge, G., Toplak, M., Ackerley, C., Hawkins, C., Hayes, J., & Clarke, J. T. R. (2009). Substrate reduction therapy in juvenile GM2 gangliosidosis. *Molecular Genetics and Metabolism*, *98*(1–2). https://doi.org/10.1016/j.ymgme.2009.06.005

Magnus, T., Chan, A., Savill, J., Toyka, K. V., & Gold, R. (2002). Phagocytotic removal of apoptotic, inflammatory lymphocytes in the central nervous system by microglia and its functional implications. In *Journal of Neuroimmunology* (Vol. 130, Issues 1–2). https://doi.org/10.1016/S0165-5728(02)00212-6

Mahuran, D. J. (1998). The GM2 activator protein, its roles as a co-factor in GM2 hydrolysis and as a general glycolipid transport protein. In *Biochimica et Biophysica Acta - Lipids and Lipid Metabolism* (Vol. 1393, Issue 1). https://doi.org/10.1016/S0005-2760(98)00057-5

Marques, A. R. A., & Saftig, P. (2019). Lysosomal storage disorders – challenges, concepts and avenues for therapy: Beyond rare diseases. *Journal of Cell Science*, *132*(2). https://doi.org/10.1242/jcs.221739

McNeill, D. R., Whitaker, A. M., Stark, W. J., Illuzzi, J. L., McKinnon, P. J., Freudenthal, B. D., & Wilson, D. M. (2020). Functions of the major abasic endonuclease (APE1)

in cell viability and genotoxin resistance. In *Mutagenesis* (Vol. 35, Issue 1). https://doi.org/10.1093/mutage/gez046

Meek, I. L., van de Laar, M. A. F. J., & Vonkeman, H. E. (2010). Non-steroidal anti-inflammatory drugs: An overview of cardiovascular risks. In *Pharmaceuticals* (Vol. 3, Issue 7). https://doi.org/10.3390/ph3072146

Mello, A. S., Garcia, C. D. S., Machado, F. D. S., Medeiros, N. D. S., Wohlenberg, M. F., Marinho, J. P., Dani, C., Funchal, C., & Coelho, J. C. (2015). Oxidative stress parameters of Gaucher disease type I patients. *Molecular Genetics and Metabolism Reports*, *4*, 1–5. https://doi.org/10.1016/j.ymgmr.2015.05.001

Miyagi, T., & Yamaguchi, K. (2012). Mammalian sialidases: Physiological and pathological roles in cellular functions. In *Glycobiology* (Vol. 22, Issue 7). https://doi.org/10.1093/glycob/cws057

Monti, E., Bonten, E., D'Azzo, A., Bresciani, R., Venerando, B., Borsani, G., Schauer, R., & Tettamanti, G. (2010). Sialidases in Vertebrates. A Family Of Enzymes Tailored For Several Cell Functions. *Advances in Carbohydrate Chemistry and Biochemistry*, *64*(C), 404–479. https://doi.org/10.1016/S0065-2318(10)64007-3

Moore, A. H., & O'Banion, M. K. (2002). Neuroinflammation and anti-inflammatory therapy for Alzheimer's disease. *Advanced Drug Delivery Reviews*, *54*(12). https://doi.org/10.1016/S0169-409X(02)00162-X

Mori, A., Chen, J. F., Uchida, S., Durlach, C., King, S. M., & Jenner, P. (2022). The Pharmacological Potential of Adenosine A2A Receptor Antagonists for Treating Parkinson's Disease. *Molecules*, *27*(7). https://doi.org/10.3390/molecules27072366

Morris, G., Gevezova, M., Sarafian, V., & Maes, M. (2022). Redox regulation of the immune response. In *Cellular and Molecular Immunology* (Vol. 19, Issue 10). https://doi.org/10.1038/s41423-022-00902-0

Mortada, I., Farah, R., Nabha, S., Ojcius, D. M., Fares, Y., Almawi, W. Y., & Sadier, N. S. (2021). Immunotherapies for Neurodegenerative Diseases. In *Frontiers in Neurology* (Vol. 12). https://doi.org/10.3389/fneur.2021.654739

Norden, D. M., Fenn, A. M., Dugan, A., & Godbout, J. P. (2014). TGFβ produced by IL-10 redirected astrocytes attenuates microglial activation. *GLIA*, *62*(6). https://doi.org/10.1002/glia.22647

O'Connor, T., Borsig, L., & Heikenwalder, M. (2015). CCL2-CCR2 Signaling in Disease Pathogenesis. *Endocrine, Metabolic & Immune Disorders-Drug Targets*, *15*(2). https://doi.org/10.2174/1871530315666150316120920

O'Dea, E. L., Barken, D., Peralta, R. Q., Tran, K. T., Werner, S. L., Kearns, J. D., Levchenko, A., & Hoffmann, A. (2007). A homeostatic model of IκB metabolism to control constitutive NF-κB activity. *Molecular Systems Biology*, *3*. https://doi.org/10.1038/msb4100148

Ogawa, Y., Furusawa, E., Saitoh, T., Sugimoto, H., Omori, T., Shimizu, S., Kondo, H., Yamazaki, M., Sakuraba, H., & Oishi, K. (2018). Inhibition of astrocytic adenosine receptor A2A attenuates microglial activation in a mouse model of Sandhoff disease. *Neurobiology of Disease*, *118*, 142–154. https://doi.org/10.1016/j.nbd.2018.07.014

Ohmi, K., Greenberg, D. S., Rajavel, K. S., Ryazantsev, S., Li, H. H., & Neufeld, E. F. (2003). Activated microglia in cortex of mouse models of mucopolysaccharidoses I and IIIB. *Proceedings of the National Academy of Sciences of the United States of America*, *100*(4). https://doi.org/10.1073/pnas.252784899

Ohmi, Y., Ohkawa, Y., Yamauchi, Y., Tajima, O., Furukawa, K., & Furukawa, K. (2012). Essential roles of gangliosides in the formation and maintenance of membrane microdomains in brain tissues. In *Neurochemical Research* (Vol. 37, Issue 6, pp. 1185–1191). https://doi.org/10.1007/s11064-012-0764-7

Okun, S., Peek, A., & Igdoura, S. A. (2023). Neuraminidase 4 (NEU4): new biological and physiological player. *Glycobiology*. https://doi.org/10.1093/glycob/cwad008

Orihuela, R., McPherson, C. A., & Harry, G. J. (2016). Microglial M1/M2 polarization and metabolic states. In *British Journal of Pharmacology* (Vol. 173, Issue 4). https://doi.org/10.1111/bph.13139

Osher, E., Fattal-Valevski, A., Sagie, L., Urshanski, N., Amir-Levi, Y., Katzburg, S., Peleg, L., Lerman-Sagie, T., Zimran, A., Elstein, D., Navon, R., Stern, N., & Valevski, A. (2011). Pyrimethamine increases β-hexosaminidase A activity in patients with Late Onset Tay Sachs. *Molecular Genetics and Metabolism*, *102*(3). https://doi.org/10.1016/j.ymgme.2010.11.163

Palmano, K., Rowan, A., Guillermo, R., Guan, J., & McJarrow, P. (2015). The role of gangliosides in neurodevelopment. In *Nutrients* (Vol. 7, Issue 5, pp. 3891–3913). https://doi.org/10.3390/nu7053891

Pará, C., Bose, P., & Pshezhetsky, A. V. (2020). Neuropathophysiology of lysosomal storage diseases: Synaptic dysfunction as a starting point for disease progression. In *Journal of Clinical Medicine* (Vol. 9, Issue 3). https://doi.org/10.3390/jcm9030616

Parenti, G., Andria, G., & Ballabio, A. (2015). Lysosomal storage diseases: From pathophysiology to therapy. *Annual Review of Medicine*, *66*. https://doi.org/10.1146/annurev-med-122313-085916

Phaneuf, D., Wakamatsu, N., Huang, J. Q., Borowski, A., Peterson, A. C., Fortunato, S. R., Ritter, G., Igdoura, S. A., Morales, C. R., Benoit, G., Akerman, B. R., Leclerc, D., Hanai, N., Marth, J. D., Trasler, J. M., & Gravel, R. A. (1996). Dramatically different phenotypes in mouse models of human Tay-Sachs and Sandhoff diseases. *Human Molecular Genetics*, *5*(1), 1–14. https://doi.org/10.1093/hmg/5.1.1

Picache, J. A., Zheng, W., & Chen, C. Z. (2022). Therapeutic Strategies For Tay-Sachs Disease. In *Frontiers in Pharmacology* (Vol. 13). https://doi.org/10.3389/fphar.2022.906647

Pinna, A., Serra, M., Marongiu, J., & Morelli, M. (2020). Pharmacological interactions between adenosine A2A receptor antagonists and different neurotransmitter systems. *Parkinsonism and Related Disorders*, *80*. https://doi.org/10.1016/j.parkreldis.2020.10.023

Pizzino, G., Irrera, N., Cucinotta, M., Pallio, G., Mannino, F., Arcoraci, V., Squadrito, F., Altavilla, D., & Bitto, A. (2017). Oxidative Stress: Harms and Benefits for Human Health. In *Oxidative Medicine and Cellular Longevity* (Vol. 2017). https://doi.org/10.1155/2017/8416763

Platt, F. M., Boland, B., & van der Spoel, A. C. (2012). Lysosomal storage disorders: The cellular impact of lysosomal dysfunction. *Journal of Cell Biology*, *199*(5), 723–734. https://doi.org/10.1083/jcb.201208152

Puri, V., Watanabe, R., Dominguez, M., Sun, X., Wheatley, C. L., Marks, D. L., & Pagano, R. E. (1999). Cholesterol modulates membrane traffic along the endocytic pathway in sphingolipid-storage diseases. *Nature Cell Biology*, *1*(6). https://doi.org/10.1038/14084

Quinville, B. M., Deschenes, N. M., Ryckman, A. E., & Walia, J. S. (2021). A comprehensive review: Sphingolipid metabolism and implications of disruption in sphingolipid homeostasis. In *International Journal of Molecular Sciences* (Vol. 22, Issue 11). https://doi.org/10.3390/ijms22115793

Rabbo, M. A., Khodour, Y., Kaguni, L. S., & Stiban, J. (2021). Sphingolipid lysosomal storage diseases: from bench to bedside. In *Lipids in Health and Disease* (Vol. 20, Issue 1). https://doi.org/10.1186/s12944-021-01466-0

Raivich, G. (2005). Like cops on the beat: The active role of resting microglia. In *Trends in Neurosciences* (Vol. 28, Issue 11). https://doi.org/10.1016/j.tins.2005.09.001

Ramesh, G., Maclean, A. G., & Philipp, M. T. (2013). Cytokines and chemokines at the crossroads of neuroinflammation, neurodegeneration, and neuropathic pain. *Mediators of Inflammation*, *2013*. https://doi.org/10.1155/2013/480739

Rees, D. A., Lewis, B. M., Lewis, M. D., Francis, K., Scanlon, M. F., & Ham, J. (2003). Adenosine-induced IL-6 expression in pituitary folliculostellate cells is mediated via A2b adenosine receptors coupled to PKC and p38 MAPK. *British Journal of Pharmacology*, *140*(4). https://doi.org/10.1038/sj.bjp.0705488

Rhee, S. G., Chang, T. S., Bae, Y. S., Lee, S. R., & Kang, S. W. (2003). Cellular regulation by hydrogen peroxide. *Journal of the American Society of Nephrology*, *14*(SUPPL. 3). https://doi.org/10.1097/01.asn.0000077404.45564.7e

Risher, W. C., Patel, S., Kim, I. H. wan, Uezu, A., Bhagat, S., Wilton, D. K., Pilaz, L. J., Singh Alvarado, J., Calhan, O. Y., Silver, D. L., Stevens, B., Calakos, N., Soderling, S. H., & Eroglu, C. (2014). Astrocytes refine cortical connectivity at dendritic spines. *ELife*, *3*, 1–24. https://doi.org/10.7554/eLife.04047

Rock, R. B., Gekker, G., Hu, S., Sheng, W. S., Cheeran, M., Lokensgard, J. R., & Peterson, P. K. (2004). Role of microglia in central nervous system infections. In *Clinical Microbiology Reviews* (Vol. 17, Issue 4). https://doi.org/10.1128/CMR.17.4.942-964.2004

Sandhoff, K., & Harzer, K. (2013). Gangliosides and gangliosidoses: Principles of molecular and metabolic pathogenesis. *Journal of Neuroscience*, *33*(25). https://doi.org/10.1523/JNEUROSCI.0822-13.2013

Sango, K., Yamanaka, S., Hoffmann, A., Okuda, Y., Grinberg, A., Westphal, H., McDonald, M. P., Crawley, J. N., Sandhoff, K., Suzuki, K., & Proia, R. L. (1995). Mouse models of Tay–Sachs and Sandhoff diseases differ in neurologic phenotype and ganglioside metabolism. *Nature Genetics*, *11*(2), 170–176. https://doi.org/10.1038/ng1095-170

Scerra, G., De Pasquale, V., Scarcella, M., Caporaso, M. G., Pavone, L. M., & D'Agostino, M. (2022). Lysosomal positioning diseases: Beyond substrate storage. In *Open Biology* (Vol. 12, Issue 10). https://doi.org/10.1098/rsob.220155

Schnaar, R. L. (2010). Brain gangliosides in axon-myelin stability and axon regeneration. In *FEBS Letters* (Vol. 584, Issue 9, pp. 1741–1747). https://doi.org/10.1016/j.febslet.2009.10.011

Schnaar, R. L., Gerardy-Schahn, R., & Hildebrandt, H. (2014). Sialic acids in the brain: Gangliosides and polysialic acid in nervous system development, stability, disease, and regeneration. *Physiological Reviews*, *94*(2). https://doi.org/10.1152/physrev.00033.2013

Schneider Gasser, E. M., Straub, C. J., Panzanelli, P., Weinmann, O., Sassoè-Pognetto, M., & Fritschy, J.-M. (2006). Immunofluorescence in brain sections: simultaneous detection of presynaptic and postsynaptic proteins in identified neurons. *Nature Protocols*, *1*(4), 1887–1897. https://doi.org/10.1038/nprot.2006.265

Schultz, M. L., Tecedor, L., Chang, M., & Davidson, B. L. (2011). Clarifying lysosomal storage diseases. In *Trends in Neurosciences* (Vol. 34, Issue 8). https://doi.org/10.1016/j.tins.2011.05.006

Schwaninger, M., Neher, M., Viegas, E., Schneider, A., & Spranger, M. (1997). Stimulation of interleukin-6 secretion and gene transcription in primary astrocytes by adenosine. *Journal of Neurochemistry*, *69*(3). https://doi.org/10.1046/j.1471-4159.1997.69031145.x

Sedger, L. M., & McDermott, M. F. (2014). TNF and TNF-receptors: From mediators of cell death and inflammation to therapeutic giants - past, present and future. In *Cytokine and Growth Factor Reviews* (Vol. 25, Issue 4). https://doi.org/10.1016/j.cytogfr.2014.07.016

Seyrantepe, V., Demir, S. A., Timur, Z. K., Gerichten, J. Von, Marsching, C., Erdemli, E., Oztas, E., Takahashi, K., Yamaguchi, K., Ates, N., Demir, B. D., Dalkara, T., Erich, K., Hopf, C., Sandhoff, R., & Miyagi, T. (2018). Murine Sialidase Neu3

facilitates GM2 degradation and bypass in mouse model of Tay-Sachs disease. *Experimental Neurology*, *299*(July 2017), 26–41. https://doi.org/10.1016/j.expneurol.2017.09.012

Seyrantepe, V., Demir, S. A., Timur, Z. K., Von Gerichten, J., Marsching, C., Erdemli, E., Oztas, E., Takahashi, K., Yamaguchi, K., Ates, N., Demir, B. D., Dalkara, T., Erich, K., Hopf, C., Sandhoff, R., & Miyagi, T. (2018). Murine Sialidase Neu3 facilitates GM2 degradation and bypass in mouse model of Tay-Sachs disease. *Experimental Neurology*, *299*(July 2017), 26–41. https://doi.org/10.1016/j.expneurol.2017.09.012

Seyrantepe, V., Lema, P., Caqueret, A., Dridi, L., Hadj, S. B., Carpentier, S., Boucher, F., Levade, T., Carmant, L., Gravel, R. A., Hamel, E., Vachon, P., Cristo, G. Di, Michaud, J. L., Morales, C. R., & Pshezhetsky, A. V. (2010). Mice Doubly-deficient in lysosomal hexosaminidase a and neuraminidase 4 show epileptic crises and rapid neuronal loss. *PLoS Genetics*, *6*(9). https://doi.org/10.1371/journal.pgen.1001118

Shih, R. H., Wang, C. Y., & Yang, C. M. (2015). NF-kappaB signaling pathways in neurological inflammation: A mini review. In *Frontiers in Molecular Neuroscience* (Vol. 8, Issue DEC). https://doi.org/10.3389/fnmol.2015.00077

Singh, D. (2022). Astrocytic and microglial cells as the modulators of neuroinflammation in Alzheimer's disease. In *Journal of Neuroinflammation* (Vol. 19, Issue 1). https://doi.org/10.1186/s12974-022-02565-0

Sipione, S., Monyror, J., Galleguillos, D., Steinberg, N., & Kadam, V. (2020). Gangliosides in the Brain: Physiology, Pathophysiology and Therapeutic Applications. In *Frontiers in Neuroscience* (Vol. 14). https://doi.org/10.3389/fnins.2020.572965

Sivandzade, F., & Cucullo, L. (2021). Regenerative stem cell therapy for neurodegenerative diseases: An overview. In *International Journal of Molecular Sciences* (Vol. 22, Issue 4). https://doi.org/10.3390/ijms22042153

Smutova, V., Albohy, A., Pan, X., Korchagina, E., Miyagi, T., Bovin, N., Cairo, C. W., & Pshezhetsky, A. V. (2014). Structural basis for substrate specificity of mammalian neuraminidases. *PLoS ONE*, *9*(9). https://doi.org/10.1371/journal.pone.0106320

Sofroniew, M. V. (2009). Molecular dissection of reactive astrogliosis and glial scar formation. In *Trends in Neurosciences* (Vol. 32, Issue 12). https://doi.org/10.1016/j.tins.2009.08.002

Sonnino, S., Mauri, L., Chigorno, V., & Prinetti, A. (2007). Gangliosides as components of lipid membrane domains. In *Glycobiology* (Vol. 17, Issue 1). https://doi.org/10.1093/glycob/cwl052

Staretz-Chacham, O., Lang, T. C., Lamarca, M. E., Krasnewich, D., & Sidransky, E. (2009). Lysosomal storage disorders in the newborn. In *Pediatrics* (Vol. 123, Issue 4). https://doi.org/10.1542/peds.2008-0635

Stepien, K. M., Roncaroli, F., Turton, N., Hendriksz, C. J., Roberts, M., Heaton, R. A., & Hargreaves, I. (2020). Mechanisms of mitochondrial dysfunction in lysosomal storage disorders: A review. In *Journal of Clinical Medicine* (Vol. 9, Issue 8). https://doi.org/10.3390/jcm9082596

Stockwell, J., Jakova, E., & Cayabyab, F. S. (2017). Adenosine A1 and A2A receptors in the brain: Current research and their role in neurodegeneration. In *Molecules* (Vol. 22, Issue 4). https://doi.org/10.3390/molecules22040676

Strzelec, M., Detka, J., Mieszczak, P., Sobocińska, M. K., & Majka, M. (2023). Immunomodulation—a general review of the current state-of-the-art and new therapeutic strategies for targeting the immune system. In *Frontiers in Immunology* (Vol. 14). https://doi.org/10.3389/fimmu.2023.1127704

Sun, A. (2018). Lysosomal storage disease overview. *Annals of Translational Medicine*, *6*(24). https://doi.org/10.21037/atm.2018.11.39

Suzuki, K., Yamaguchi, A., Yamanaka, S., Kanzaki, S., Kawashima, M., Togo, T., Katsuse, O., Koumitsu, N., Aoki, N., Iseki, E., Kosaka, K., Yamaguchi, K., Hashimoto, M., Aoki, I., & Hirayasu, Y. (2016). Accumulated α-synuclein affects the progression of GM2 gangliosidoses. *Experimental Neurology*, *284*, 38–49. https://doi.org/10.1016/j.expneurol.2016.07.011

Tang, Y., & Le, W. (2016). Differential Roles of M1 and M2 Microglia in Neurodegenerative Diseases. In *Molecular Neurobiology* (Vol. 53, Issue 2). https://doi.org/10.1007/s12035-014-9070-5

Tettamanti, G. (2003). Ganglioside/glycosphingolipid turnover: New concepts. In *Glycoconjugate Journal* (Vol. 20, Issue 5). https://doi.org/10.1023/B:GLYC.0000033627.02765.cc

Thundyil, J., & Lim, K. L. (2015). DAMPs and neurodegeneration. In *Ageing Research Reviews* (Vol. 24). https://doi.org/10.1016/j.arr.2014.11.003

Tjalkens, R. B., Popichak, K. A., & Kirkley, K. A. (2017). Inflammatory Activation of Microglia and Astrocytes in Manganese Neurotoxicity. In *Advances in Neurobiology* (Vol. 18). https://doi.org/10.1007/978-3-319-60189-2_8

Toro, C., Zainab, M., & Tifft, C. J. (2021). The GM2 gangliosidoses: Unlocking the mysteries of pathogenesis and treatment. *Neuroscience Letters*, *764*. https://doi.org/10.1016/j.neulet.2021.136195

Tsakiri, N., Kimber, I., Rothwell, N. J., & Pinteaux, E. (2008). Interleukin-1-induced interleukin-6 synthesis is mediated by the neutral sphingomyelinase/Src kinase pathway in neurones. *British Journal of Pharmacology*, *153*(4). https://doi.org/10.1038/sj.bjp.0707610

Varki, A. (2011). Evolutionary forces shaping the Golgi glycosylation machinery: Why cell surface glycans are universal to living cells. *Cold Spring Harbor Perspectives in Biology*, *3*(6). https://doi.org/10.1101/cshperspect.a005462

Vidal-Donet, J. M., Cárcel-Trullols, J., Casanova, B., Aguado, C., & Knecht, E. (2013). Alterations in ROS Activity and Lysosomal pH Account for Distinct Patterns of Macroautophagy in LINCL and JNCL Fibroblasts. *PLoS ONE*, *8*(2). https://doi.org/10.1371/journal.pone.0055526

von Lubitz, D. K. (1999). Adenosine and cerebral ischemia: therapeutic future or death of a brave concept? *European Journal of Pharmacology*, *371*(1). https://doi.org/10.1016/S0014-2999(99)00135-1

Walsh, R. N., & Cummins, R. A. (1976). The open-field test: A critical review. *Psychological Bulletin*, *83*(3). https://doi.org/10.1037/0033-2909.83.3.482

Wang, G., & Bieberich, E. (2018). Sphingolipids in neurodegeneration (with focus on ceramide and S1P). In *Advances in Biological Regulation* (Vol. 70). https://doi.org/10.1016/j.jbior.2018.09.013

Wang, J. N., Fan, H., & Song, J. T. (2023). Targeting purinergic receptors to attenuate inflammation of dry eye. In *Purinergic Signalling* (Vol. 19, Issue 1). https://doi.org/10.1007/s11302-022-09851-9

Wang, P., Rothwell, N. J., Pinteaux, E., & Brough, D. (2008). Neuronal injury induces the release of pro-interleukin-1β from activated microglia in vitro. *Brain Research*, *1236*. https://doi.org/10.1016/j.brainres.2008.08.001

Wang, Q., Liu, Y., & Zhou, J. (2015). Neuroinflammation in Parkinson's disease and its potential as therapeutic target. In *Translational Neurodegeneration* (Vol. 4, Issue 1). https://doi.org/10.1186/s40035-015-0042-0

Wang, W. Y., Tan, M. S., Yu, J. T., & Tan, L. (2015). Role of pro-inflammatory cytokines released from microglia in Alzheimer's disease. In *Annals of Translational Medicine* (Vol. 3, Issue 10). https://doi.org/10.3978/j.issn.2305-5839.2015.03.49

Wei, H., Kim, S. J., Zhang, Z., Tsai, P. C., Wisniewski, K. R., & Mukherjee, A. B. (2008). ER and oxidative stresses are common mediators of apoptosis in both neurodegenerative and non-neurodegenerative lysosomal storage disorders and are alleviated by chemical chaperones. *Human Molecular Genetics*, *17*(4). https://doi.org/10.1093/hmg/ddm324

Wendeler, M., Werth, N., Maier, T., Schwarzmann, G., Kolter, T., Schoeniger, M., Hoffmann, D., Lemm, T., Saenger, W., & Sandhoff, K. (2006). The enzyme-binding region of human GM2-activator protein. *FEBS Journal*, *273*(5). https://doi.org/10.1111/j.1742-4658.2006.05126.x

Wendimu, M. Y., & Hooks, S. B. (2022). Microglia Phenotypes in Aging and Neurodegenerative Diseases. In *Cells* (Vol. 11, Issue 13). https://doi.org/10.3390/cells11132091

Woš, M., Szczepanowska, J., Pikuła, S., Tylki-Szymańska, A., Zabłocki, K., & Bandorowicz-Pikuła, J. (2016). Mitochondrial dysfunction in fibroblasts derived

from patients with Niemann-Pick type C disease. *Archives of Biochemistry and Biophysics*, *593*, 50–59. https://doi.org/10.1016/j.abb.2016.02.012

Wydra, K., Gawliński, D., Gawlińska, K., Frankowska, M., Borroto-Escuela, D. O., Fuxe, K., & Filip, M. (2020). Adenosine A2AReceptors in Substance Use Disorders: A Focus on Cocaine. In *Cells* (Vol. 9, Issue 6). https://doi.org/10.3390/cells9061372

Wyss-Coray, T., & Mucke, L. (2002). Inflammation in neurodegenerative disease - A double-edged sword. In *Neuron* (Vol. 35, Issue 3). https://doi.org/10.1016/S0896-6273(02)00794-8

Yamanaka, S., Johnsont, M. D., Grinbergt, A., Westphalt, H., Crawleyt, J. N., Taniike, M., Suzuki, K., & Proia, R. L. (1994). Targeted disruption of the Hexa gene results in mice with biochemical and pathologic features of Tay-Sachs disease (animal model/GM2 ganglioudosis/homologous recombination/lysosomal storage disease). *Medical Sciences*, *91*, 9975–9979. https://doi.org/10.1073/pnas.91.21.9975

Yang, D., Elner, S. G., Bian, Z. M., Till, G. O., Petty, H. R., & Elner, V. M. (2007). Pro-inflammatory cytokines increase reactive oxygen species through mitochondria and NADPH oxidase in cultured RPE cells. *Experimental Eye Research*, *85*(4). https://doi.org/10.1016/j.exer.2007.06.013

Yu, R. K., Tsai, Y.-T., Ariga, T., & Yanagisawa, M. (2011). Structures, Biosynthesis, and Functions of Gangliosides-an Overview. *Journal of Oleo Science*, *60*(10), 537–544. https://doi.org/10.5650/jos.60.537

Yuziuk, J. A., Bertoni, C., Beccari, T., Orlacchio, A., Wu, Y. Y., Li, S. C., & Li, Y. T. (1998). Specificity of mouse G(M2) activator protein and β-N-acetylhexosaminidases A and B. Similarities and differences with their human counterparts in the catabolism of G(M2). *Journal of Biological Chemistry*, *273*(1), 66–72. https://doi.org/10.1074/jbc.273.1.66

Yuzlenko, O., & Kiec-Kononowicz, K. (2006). Potent Adenosine A1 and A2A Receptors Antagonists: Recent Developments. *Current Medicinal Chemistry*, *13*(30). https://doi.org/10.2174/092986706779026093

Zhang, W., Xiao, D., Mao, Q., & Xia, H. (2023). Role of neuroinflammation in neurodegeneration development. In *Signal Transduction and Targeted Therapy* (Vol. 8, Issue 1). https://doi.org/10.1038/s41392-023-01486-5

VITA

EDUCATIONAL INFORMATION

- February 2019 – November 2023 Izmir Institute of Technology, Turkey
PhD. Department of Molecular Biology and Genetics, Faculty of Science
- June 2016 – December 2018 Izmir Institute of Technology, Turkey
M.Sc. Department of Molecular Biology and Genetics, Faculty of Science
- September 2010 – February 2016 Izmir Institute of Technology, Turkey
B.Sc. Department of Molecular Biology and Genetics, Faculty of Science

AWARDS

9 October 2022 FEBS Advanced Lecture Course: 360° Lysosome
Nurselin Ates, Volkan Seyrantepe "Small Molecule Treatment Induces Exocytosis in Tay-Sachs Disease Cells" (Oral Presentation)

4 November 2018 2nd International Cell Death Research Congress
Nurselin Ates, Ayten Nalbant , Volkan Seyrantepe "Investigation of Redox Homeostasis in Early-Onset Tay-Sachs Mouse Model" (Oral Presentation)

PUBLICATIONS

Sengul, T., Can, M., Ateş, N., & Seyrantepe, V. (2023). Autophagic flux is impaired in the brain tissue of Tay-Sachs disease mouse model. Plos one, 18(3), e0280650.

Demir, S. A., Timur, Z. K., Ateş, N., Martínez, L. A., & Seyrantepe, V. (2020). GM2 ganglioside accumulation causes neuroinflammation and behavioral alterations in a mouse model of early onset Tay-Sachs disease. Journal of Neuroinflammation, 17(1). https://doi.org/10.1186/s12974-020-01947-6

Seyrantepe, V., Demir, S. A., Timur, Z. K., Von Gerichten, J., Marsching, C., Erdemli, E., … Miyagi, T. (2018). Murine Sialidase Neu3 facilitates GM2 degradation and bypass in mouse model of Tay-Sachs disease. Experimental Neurology, 299(July 2017), 26–41. https://doi.org/10.1016/j.expneurol.2017.09.012

SCHOLARSHIPS

- TUBITAK BIDEB National Scholarship Program for Ph.D. students 2211A
- Turkish Higher Education Council's 100/2000 Ph.D. Fellowship Program